Winter 2005

Brittle Deformation in an Ancient Accretionary Prism Setting: Lopez Structural Complex, San Juan Islands, NW Washington

John R. (John Rhea) Gillaspy
Western Washington University

BRITTLE DEFORMATION IN AN ANCIENT ACCRETIONARY PRISM SETTING: LOPEZ STRUCTURAL COMPLEX, SAN JUAN ISLANDS, NW WASHINGTON

BY

JOHN R. GILLASPY

Accepted in Partial Completion

of the Requirements for the Degree

Master of Science
Geology

Moheb A. Ghali, Dean of Graduate School

ADVISORY COMMITTEE

Chair, Dr. Elizabeth R. Schermer

Dr. Russell F. Burmester

Dr. David M. Hirsch

MASTER'S THESIS

In presenting this thesis in partial fulfillment of the requirements for a master's degree at Western Washington University, I agree that the Library shall make its copies freely available for inspection. I further agree that copying of this thesis in whole or in part is allowable only for scholarly purposes. It is understood, however, that any copying or publication of this thesis for commercial purposes, or for financial gain, shall not be allowed without my written permission.

Signature _____

Date 3-22-05

MASTER'S THESIS

In presenting this thesis in partial fulfillment of the requirements for a master's degree at Western Washington University, I grant to Western Washington University the non-exclusive royalty-free right to archive, reproduce, distribute, and display the thesis in any and all forms, including electronic format, via any digital library mechanisms maintained by WWU.

I represent and warrant this is my original work and does not infringe or violate any rights of others. I warrant that I have obtained written permissions from the owner of any third party copyrighted material included in these files.

I acknowledge that I retain ownership rights to the copyright of this work, including but not limited to the right to use all or part of this work in future works, such as articles or books.

Library users are granted permission for individual, research and non-commercial reproduction of this work for educational purposes only. Any further digital posting of this document requires specific permission from the author.

Any copying or publication of this thesis for commercial purposes, or for financial gain, is not allowed without my written permission.

Name: John Gillaspy

Signature: _____

Date: 5-30-2018

BRITTLE DEFORMATION IN AN ANCIENT ACCRETIONARY PRISM SETTING: LOPEZ STRUCTURAL COMPLEX, SAN JUAN ISLANDS, NW WASHINGTON

A Thesis
Presented to
The Faculty of
Western Washington University

In Partial Fulfillment
of the Requirements for the Degree
Master of Science

by
John R. Gillaspy
March 2005

Abstract

Fault-bounded slices of allochthonous Paleozoic to Mesozoic bedrock of the San Juan Islands in northwest Washington provide a locality in which to study terrane translation and ductile and brittle deformation in an accretionary wedge setting, as well as the factors involved in preservation of blueschist-facies terranes. This study contributes to understanding of the tectonic evolution of the Lopez Structural Complex, a major Late Cretaceous terrane-bounding fault zone in the San Juan Thrust System. Structural study is combined with X-ray diffraction and fluid inclusion analysis to constrain the relative timing, kinematics, and P-T conditions of fabric formation and post-fabric brittle deformation in the Lopez Structural Complex.

Deformation is characterized by multiple generations of ductile and brittle structures. After formation of a regional flattening fabric by two processes, pressure solution and localized bi-directional shearing, the area was crosscut by brittle structures including: 1) early strike-slip structures related to bi-directional northwest/southeast shear, 2) southwest-vergent thrusts, 3) extension veins and normal faults related to northwest/southeast extension, and 4) conjugate strike-slip structures also related to northwest/southeast extension. The presence of comparable structures in the eastern San Juan Islands (Lamb and Schermer, 2003) and adjacent to the Lopez Structural Complex indicates this sequence of brittle deformation is widespread in the San Juan nappes.

X-ray diffraction and petrographic observations of vein material identify aragonite- and prehnite-bearing veins associated with thrust, normal, and strike-slip structures, although most of the latest strike-slip faults contain only prehnite and calcite.

High pressure minerals constrain brittle deformation to have occurred at greater than ~ 20 km depth and at most ~ 200° C. Fluid inclusion analyses of aqueous and methane-bearing inclusions in vein quartz are in agreement with low temperature conditions after vein formation and tentatively suggest rapid exhumation to shallow depths under near isothermal conditions.

Sustained high-pressure – low-temperature conditions and the preservation of widespread aragonite are possible only if structures formed in an accretionary prism during active subduction. Therefore, meter-scale brittle structures in rocks of the Lopez Structural Complex record a pattern of internal wedge deformation at depth or early during uplift of the San Juan nappes. The sequence observed is generally consistent with internal orogen-normal contraction and vertical thickening followed by vertical thinning and lateral along-strike extension. Possible mechanisms for brittle deformation include a change in the angle or magnitude of plate convergence vectors, a large underplating or accretion event, or the collision of the Cretaceous prism with the margin of Wrangellia.

Acknowledgments

This thesis benefited from the advice and technical help of many fellow geologists. First, my committee deserves much recognition. Liz Schermer has been an excellent advisor and her passion for geology (even for low grade rocks!) is contagious. She shared countless hours of discussion and, although she trusted me to work independently and make my own mistakes, was always there to keep me on track. Russ Burmester helped me to define this thesis in its initial stages, greatly contributed to the refinement of this manuscript, and encouraged me to keep an open mind. Dave Hirsch aided in petrographic study and gave valuable suggestions that improved the interpretation of my P-T data.

I thank other WWU faculty who unselfishly contributed to this work. Ned Brown and Clark Blake provided unpublished manuscripts and enlightening discussion on numerous occasions. Ned Brown was especially helpful in narrowing the scope of this thesis and lending advice for successful field and laboratory work. Bernie Housen and Dave Engebretsen also provided advice. George Mustoe gave technical help during laboratory work. Dan Marshall at Simon Fraser University graciously volunteered his laboratory and assistance towards the fluid inclusion portion of this thesis.

Friends and coworkers donated their time and ideas in the field. For their generosity and company, I would like to thank Liz Schermer, Craig Martodam, Mary Beth Cheversia, Amy Fluette, Troy Baggerman, Chris and Karen Houck, Aaron Clark, Todd Belanger, and Justin Brooks.

Finally, I am indebted to the support of friends and family. Thank you to all of my fellow students at WWU who have made graduate school a very enjoyable experience, to my roommates for everything, and to my parents, Tom and Cathy Gillaspy, whose unwavering support and encouragement have always guided me.

Funding for this project was provided by a Geological Society of America student research grant, an advance for field work from the Geology Department at WWU, and a graduate research grant from the Bureau for Faculty Research at WWU. Travel to the Geological Society of America 2004 Annual Conference was funded by a Ross Travel Grant through WWU.

Table of Contents

List of Figures

List of Tables

I. Introduction

Long-lived subduction and terrane accretion along the western margin of North America have emplaced a melange of tectonic elements in much of Washington, Oregon, and California. Two processes in particular related to this subduction may have played a significant role in modifying terranes and their locations during westward growth of the continental margin: terrane translation and accretionary wedge tectonics. Some Cordilleran geologists propose 'fixist' models that state terranes have moved only tens to hundreds of kilometers following accretion (Monger and Price, 1996; Mahoney et al., 1999; Butler et al., 2001), while others debate a translational history in which many terranes have traveled northward thousands of kilometers along the Cordilleran margin during periods of oblique subduction (Irving et al., 1996; Housen and Beck, 1999). While paleomagnetic evidence has lent much support to translation, geologic evidence for this translation is sparse and thus it becomes increasingly important to include structural evidence in tests of translation hypotheses.

To identify the structures within an accretionary setting that may accommodate terrane translation during oblique subduction, an understanding of all ductile and brittle deformation episodes is crucial. Accretion of tectonic elements in an accretionary prism can result in several deformation events, multiple metamorphic fabrics, and complex structural patterns. Models of accretionary prism processes generally support a period of large-scale faulting, fabric formation, and ductile flattening during and after underplating, followed by intrawedge deformation and finally exhumation (e.g., Platt, 1986; Feehan and Brandon, 1999). In this way, high pressure-low temperature metamorphosed rocks

such as those in the San Juan Islands are created and can be emplaced near the surface and preserved in ancient prism settings.

One particular debate regarding accretionary processes involves the relative importance of uplift mechanisms for underplated and high pressure metamorphosed terranes in ancient prism settings. Brittle uplift by large scale listric normal faulting or late, out-of-sequence thrusting during continued subduction have long been discussed as likely mechanisms for the juxtaposition of high pressure rocks with shallow assemblages (Platt, 1986, 1987, 1993; Dewey, 1988; Harms et al., 1992; Fassoulas et al., 1994). More recently, some workers have stressed ductile thinning by pressure solution and volume loss as an important steady-state process facilitating exhumation in low temperature environments (Feehan and Brandon, 1999; Ring and Brandon, 1999). If the fore-arc of an orogen becomes subaerially exposed, erosion may also contribute significantly to removal of material from the crest of the prism and exhumation of deep rocks (Brandon et al., 1998). Of course, evidence for multiple processes can exist in a preserved prism. It becomes an interesting challenge to determine which of these mechanisms is active at what P-T conditions, as well as what effect plate-scale external changes can have on the kinematics, timing, and operation of a given deformational style.

Project Introduction

The fault-bounded slices of Paleozoic to Mesozoic bedrock of the San Juan Islands, situated along the North American margin in northwest Washington State, provide a locality in which to study terrane translation, deformation in an accretionary wedge setting, and the factors contributing to uplift of blueschist-facies metamorphosed

rocks. However, the geologic history of the San Juan Islands is complex and remains controversial. Three main tectonic interpretations have been published, two of which involve some amount of coastwise translation during periods of oblique subduction (Brandon et al., 1988; Maekawa and Brown, 1991; Bergh, 2002). Other workers have documented several post-metamorphic deformational events that may have reactivated faults and reoriented rocks in the region, but uncertainty in the ages and magnitudes of these events leaves the effect on orientations of older structures unknown (Burmester et al., 2000; Lamb, 2000; Lamb and Schermer, 2003). The relative and absolute timing of high pressure metamorphism, large-scale faulting and terrane assembly, and brittle deformation has been studied (Brandon et al., 1988; Brown et al., in press; Lamb and Schermer, 2003) but results are controversial so more data are required to constrain the relative ages of events and P-T conditions, especially regarding late deformation. Apart from fission track data (Johnson et al., 1986), very little post-fabric pressure and temperature information is available. Consequently, more study is necessary in order to better understand the complicated tectonic evolution of rocks in the San Juan Islands.

This study investigates the late-stage tectonic evolution of the Lopez Structural Complex in the San Juan Islands by studying the kinematics, relative timing, and P-T conditions of brittle deformation. Traditional field methods were used to gather structural data throughout the study area. Mineralogical data on vein material collected by x-ray diffraction and supported by petrographic observations help determine pressure and temperature conditions for specific deformational events. Reconnaissance fluid inclusion research on inclusion assemblages in two vein sets provides additional information on late brittle P-T conditions. Hypotheses on the deformation of rocks in the

San Juan Islands presented by previous workers are evaluated in light of these new kinematic, geochronologic, and thermobarometric data. Finally, the information gathered in this study leads to a better understanding of the complex geologic history of the San Juan Islands and contributes data to further the study of accretionary wedge processes and Cordilleran tectonics.

II. Geologic Setting and Previous Work

Regional Geology

The San Juan Islands are located along the northwest coast of Washington State (Figure 1). To the north is the Coast Plutonic Complex in British Columbia, which intrudes Mesozoic accreted terranes and is part of the Cretaceous Cordilleran magmatic arc (Armstrong, 1988). East of the Straight Creek fault in the North Cascades range are the plutonic and high grade metamorphic rocks of the Late Cretaceous to Tertiary magmatic arc (Misch, 1988; Haugerud, 1989). In the lower elevations west of the Straight Creek fault and stretching out towards the Puget Sound lies the Northwest Cascades System (NWCS; Brown, 1987), which is probably part of the Cretaceous Cordilleran accretionary complex. The NWCS is described by Brown (1987) as a thrust stack composed of Paleozoic to Mesozoic accreted terranes that experienced low grade, high pressure metamorphism in Cretaceous time. Because of broad similarities in rock types and timing of metamorphism, the NWCS has been linked to terranes in the Klamath Mountains (Brown, submitted). Bedrock of Vancouver Island to the northwest belongs to Wrangellia (Jones et al., 1977), a large terrane of island arc affinity accreted in Jurassic or Cretaceous time. The Olympic Mountains to the southwest expose exhumed accretionary wedge material and ocean floor rocks that were accreted in the early Cenozoic (Brandon et al., 1998).

Basement rocks of the San Juan Islands (Figure 2) are a complex of accreted oceanic metasedimentary and metavolcanic terranes named the San Juan Thrust System

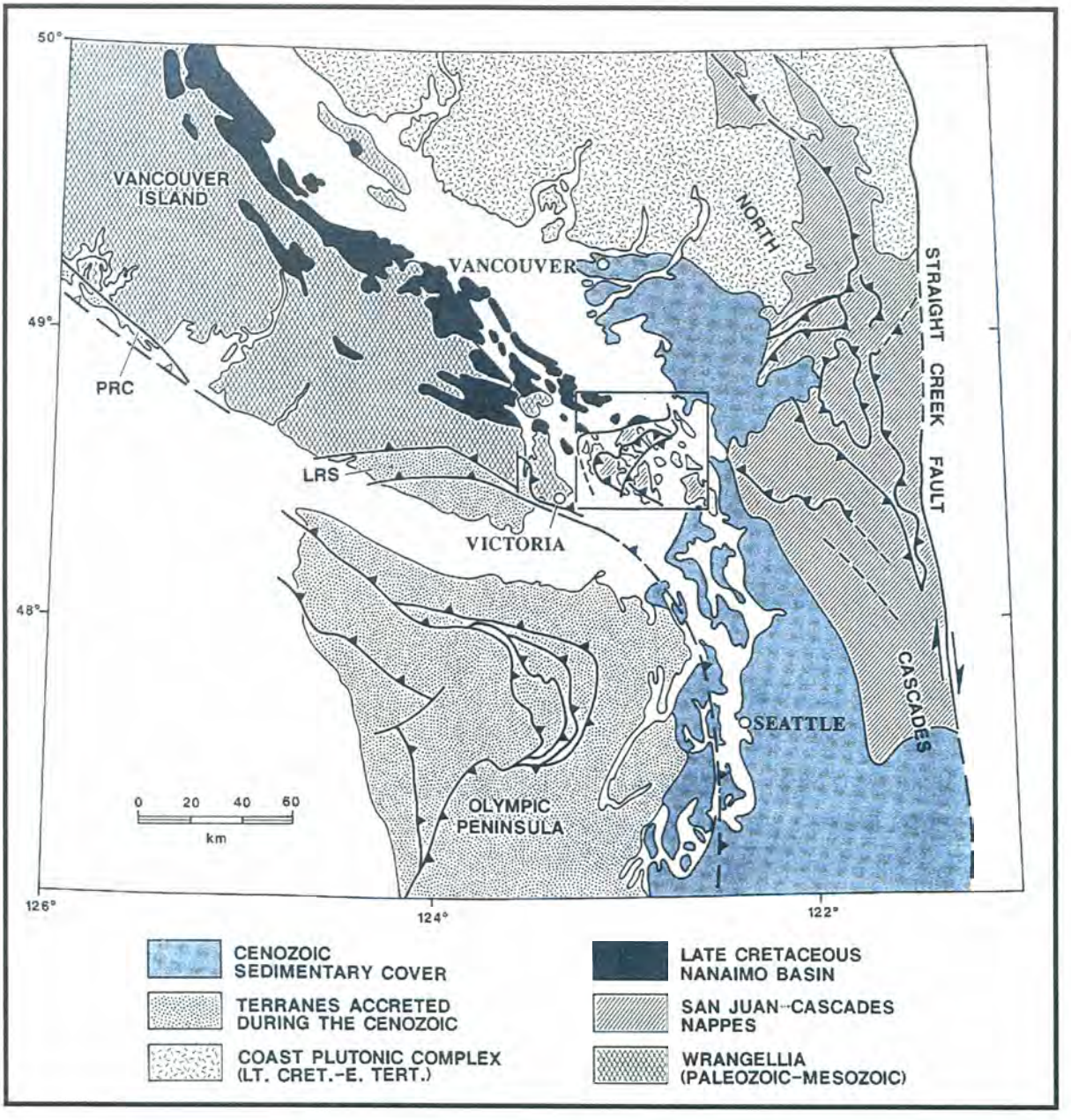

Figure 1: Regional tectonic map of western Washington and southwest British Columbia. The San Juan Islands lie within the boxed area (Figures 2a, 3). PRC = Pacific Rim Complex. LRS = Leech River Schist. From Brandon et al. (1988).

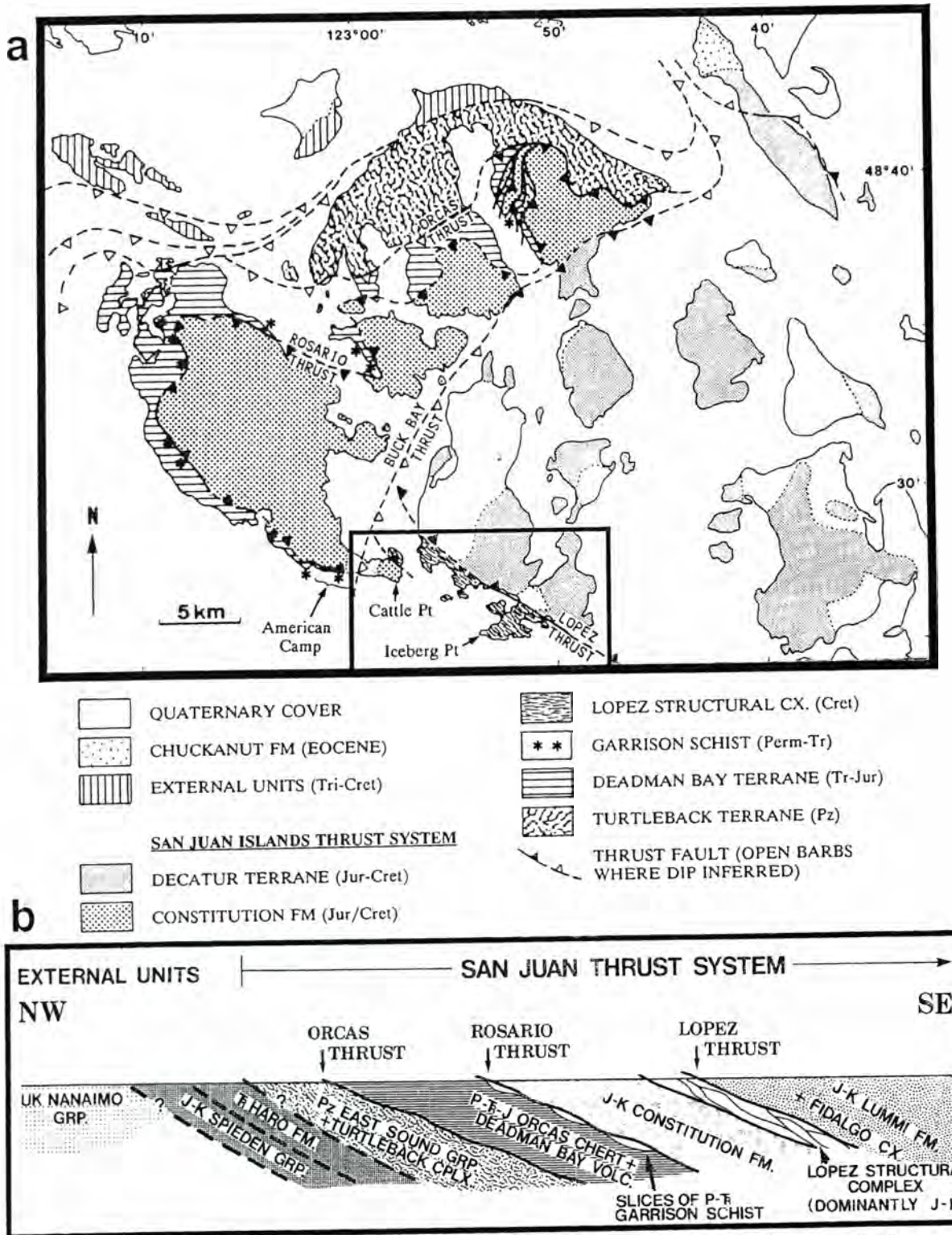

Figure 2: (a) Bedrock geologic map of the San Juan Islands. The study area, the Lopez Structural Complex, is boxed (Figure 4). From Maekawa and Brown (1991). (b) Schematic cross-section through the San Juan nappes showing approximate terrane stratigraphy and age relations. From Brandon et al. (1988).

(SJTS; Brandon et al., 1988). The SJTS is possibly part of the larger NWCS, or is correlative (Brown, 1987). Most of the terranes in the San Juan Islands are known to have experienced high pressure, low temperature metamorphism sometime in the Cretaceous. The geology of the San Juan Islands is discussed in detail below. Along the northern edge of the islands, the metamorphosed terranes are in fault contact with unmetamorphosed rocks of the Upper Cretaceous Nanaimo Group, a syn-orogenic clastic sequence that lies unconformably on basement rocks of Wrangellia on Vancouver Island (Brandon et al., 1988).

Geology of the San Juan Islands

Terranes of the San Juan Islands are thin nappes that are stacked along major bounding faults that presently dip gently or moderately southeastward (Brandon et al., 1988). Rocks range in age from Paleozoic to mid-Cretaceous and the rocks young structurally upwards and to the east (Brandon et al., 1988). Within the area of interest, at least four distinct terrane assemblages exist (Figure 2).

Paleozoic Terranes

The oldest and structurally lowest nappe is the Turtleback terrane, a suite of arc plutonic and volcanic rocks of Ordovician to Permian age (Brandon et al., 1988). This is separated by a faulted contact interpreted as the Orcas thrust (Vance, 1977) from Permian to Jurassic pillow basalt with interbedded limestone of the Deadman Bay volcanics and the Triassic to Jurassic Orcas chert. Together these units form the discontinuous stratigraphy of the Deadman Bay terrane (Brandon et al., 1988). The Rosario Thrust

(Brandon, 1980) defines the upper boundary of the Deadman Bay terrane (Figure 2b). It is a thin, 100 to 200 meter wide imbricate fault zone that contains small slices of Permo-Triassic exotic mafic material of the Garrison Schist (Vance, 1975; Brandon, 1980). The Garrison Schist is not equivalent in metamorphic grade or composition to other rocks in the San Juan Islands and therefore provides evidence for offset of at least 30 kilometers along the Rosario fault zone (Brandon et al., 1988).

Mesozoic Terranes

East and south of the Rosario fault zone is the Jura-Cretaceous Constitution terrane, an arc-related clastic sequence of massive sandstone interbedded with mudstone, ribbon chert, and pillow basalt (Brandon et al., 1988). The Lopez Structural Complex has been interpreted by most workers as a thrust system (Brandon et al., 1988; Maekawa and Brown, 1991) that defines the upper boundary of the Constitution terrane (Figure 2b), although the contact is not exposed. However, the Buck Bay fault (Figure 2a), which strikes northeast through the islands and bounds the southeastern extent of the Constitution Formation in map view, may be this contact (Burmester et al., 2000). The Lopez Structural Complex is the focus of this study and is discussed in detail below.

Bedrock in the eastern San Juan Islands was previously assigned to the structurally highest Decatur terrane (Brandon et al., 1988), which is divided into an ophiolitic sequence called the Fidalgo Igneous Complex (Brown, 1977) and the unconformable clastic and volcanic Lummi Formation (Vance, 1975). However, recent work suggests that the Lummi Formation and other associated packages are unrelated to the Fidalgo Complex because contacts between the components are faulted and

differences in chemistry and metamorphic history exist (Figure 3; Burmester et al., 2000). The Jurassic Fidalgo Igneous Complex includes mafic and ultramafic rocks succeeded by island arc-related quartz diorite, volcanic rocks, and turbidite deposits (Brandon et al., 1988), while the other Jurassic to Early Cretaceous clastic and volcanic packages are composed of high-pressure metamorphosed metagreywacke, MORB-type pillow basalt, and ribbon chert of ocean floor affinity (Burmester et al., 2000; Blake et al., in preparation). For the purpose of clarity and because no official terrane name has been assigned, rocks of ocean floor origin once belonging to the Decatur terrane will be referred to in this study as the Ocean Floor Complex after unpublished maps by Blake et al. (in preparation). Although Brandon et al. (1988) show the Lummi Formation in unconformable depositional contact with the Fidalgo Igneous Complex, Lamb (2000) proposed that Ocean Floor Complex rocks lay structurally beneath the overthrust ophiolite.

The Lopez Structural Complex

The Lopez Structural Complex (LSC), exposed along the southern edge of Lopez Island and the southeastern peninsula of San Juan Island (Figures 2, 4), separates the Constitution terrane from the structurally higher Fidalgo Complex and the Ocean Floor Complex (Brandon, 1980). The LSC is a 2.5 km wide imbricate zone composed of large coherent blocks of Ocean Floor Complex clastic and volcanic rocks, Constitution terrane sandstone and disrupted mudstone sequences, and exotic material. One important exotic slice called the Richardson complex is composed of middle Cretaceous pillow lava, volcanic breccia, and associated argillite (Brandon et al., 1988). Minor components of

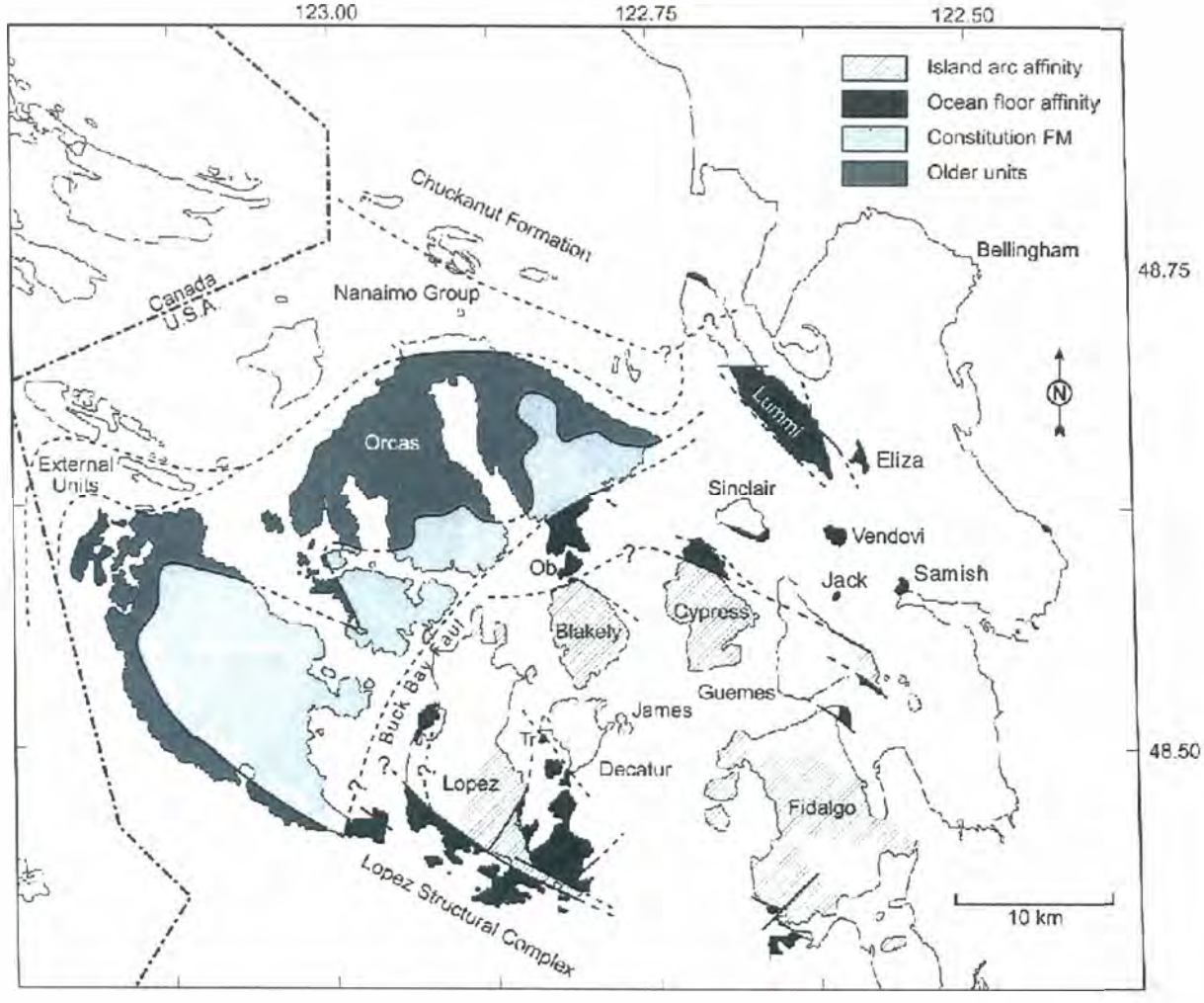

Figure 3: Revised terrane map of the San Juan Islands. The structurally highest and most eastern Decatur terrane is now considered to be two distinct suites of rocks based on formation in an ocean floor or island arc setting. Basalts in the Lopez Structural Complex are only consistent with ocean floor geochemistry. From Burmester et al. (2000).

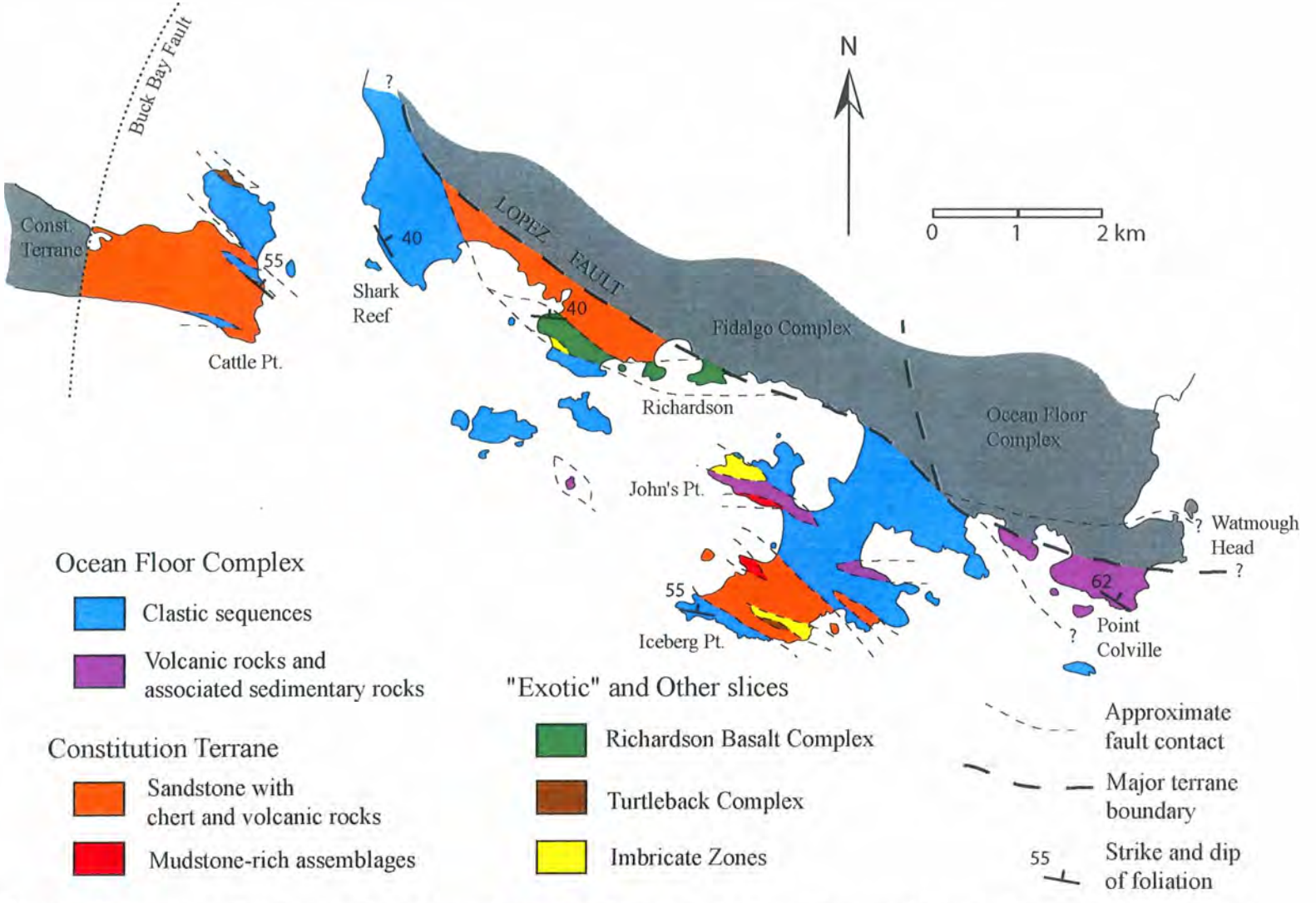

Figure 4: Terrane affinity map of the Lopez Structural Complex. Adjacent terranes in grey. See text for discussion. Modified from Brandon et al. (1988), Burmester et al. (2000), and Blake et al. (in preparation) to reflect recently proposed terrane definitions.

the LSC include highly imbricated mudstone and a small slice of the Turtleback Complex. Foliation and fault contacts in the LSC dip moderately or steeply to the northeast, and terrane lenses are generally elongate northwest-southeast (Figure 4). These structural features approximately parallel the northern boundary of the zone, named the Lopez Thrust by Brandon (1980), where most of the offset in the zone is thought to have occurred (Brandon et al., 1988). The upper boundary of the LSC is the fault contact with the Fidalgo Complex and the Ocean Floor Complex (Burmester et al., 2000).

The age of faulting and terrane juxtaposition along the LSC is constrained to 112-84 Ma. The youngest known rock in the LSC is an argillite containing 112 Ma foraminifera found within the Richardson complex (Brown et al., in press). Thus, faulting must have occurred after 112 Ma. Uplift of these terranes occurred by at least 84 Ma, constrained by the presence of blueschist detritus from the SJTS in 84 Ma fossil-dated beds of the Nanaimo group (Ward, 1978; Brandon et al., 1988).

Geologic History of the SJTS

Controversial Tectonic Interpretations

Although much of the San Juan Islands has been extensively mapped, controversy surrounds interpretation of the Cretaceous accretionary events. This disagreement is due in part to the complexity of fault zone structures as well as uncertainty in the relative and absolute timing of peak metamorphism and major faulting. Three main published tectonic interpretations exist: a contraction model, a translation model, and a linked faulting model. All three models are based on field mapping, fault zone kinematics,

metamorphic assemblages, and geochronology, and all assume that burial by thrust stacking caused the high pressure, low temperature metamorphism. In the contraction model (Figure 5a), the entire SJTS was accreted and thrust to the southwest over the present Cascade crystalline core during orogen-normal contraction related to the collision of Wrangellia at approximately 100 Ma (Brandon et al., 1988). This produced major southwest-vergent thrusts and caused northeast/southwest shortening of the terranes. The apparent southwest-vergent asymmetry of folds and shears within the Rosario and Lopez fault zones supports a top-to-the-southwest transport direction for the SJTS (Cowan and Brandon, 1994). After burial and blueschist facies metamorphism, a prevalent northeast-dipping solution mass transfer (SMT) flattening cleavage was imposed on the terranes and fault zones during rapid uplift (Feehan and Brandon, 1999).

In the translation model (Figure 5b), the terranes, following accretion, juxtaposition, and possibly partial subduction farther south along the Cordilleran margin, were emplaced into their present position by orogen-parallel dextral motion (Maekawa and Brown, 1991). Convergence with the previously accreted Wrangellia resulted in northwest-vergent thrusting and right-lateral shearing, which produced a northwest/southeast lineation in the fault zones and synchronous high pressure metamorphism. The linked faulting model (Figure 6; Bergh, 2002) suggests a link between thrusting and translation. In this hypothesis, the onset of orogen-normal accretion caused southwest-vergent thrusting and large-scale folding. Both the thrusts and the axial planar cleavage steepen landward so that these structures are nearly vertical in the LSC. Bergh (2002) hypothesized that a change to oblique subduction initiated left-lateral strike-slip motion within the steep LSC and northwest-directed thrusting within

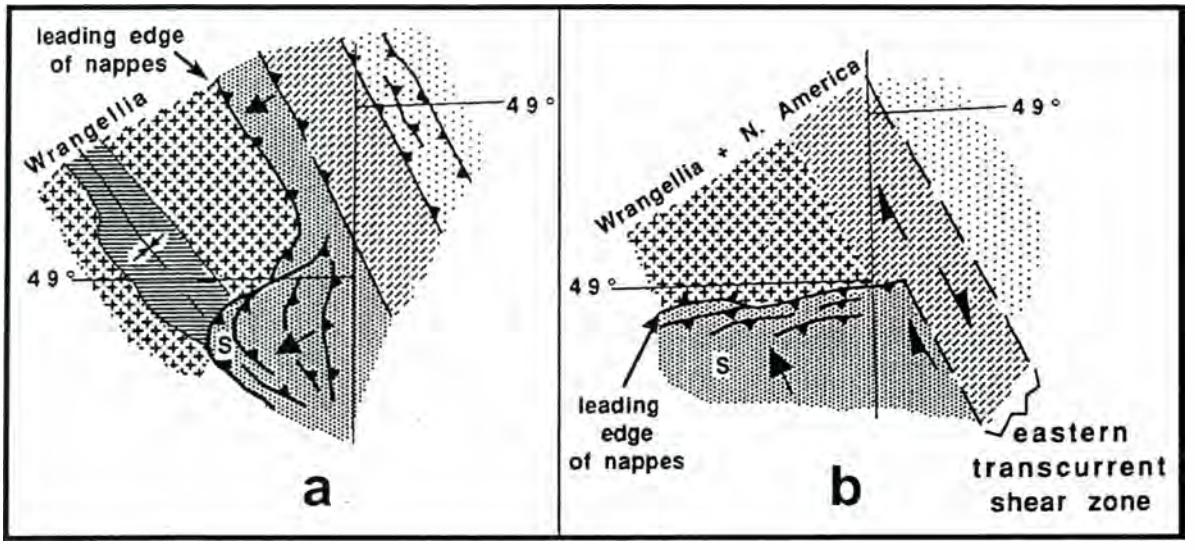

Figure 5: Schematic maps of two competing models of Late Cretaceous orogeny. S = San Juan nappes. (a) Illustration of the contraction model showing orogen-normal contraction and southwest-vergent thrusting. (b) Illustration of the translation model showing orogen-parallel dextral translation and northwest-vergent thrusting of the San Juan nappes. From Cowan and Brandon (1994).

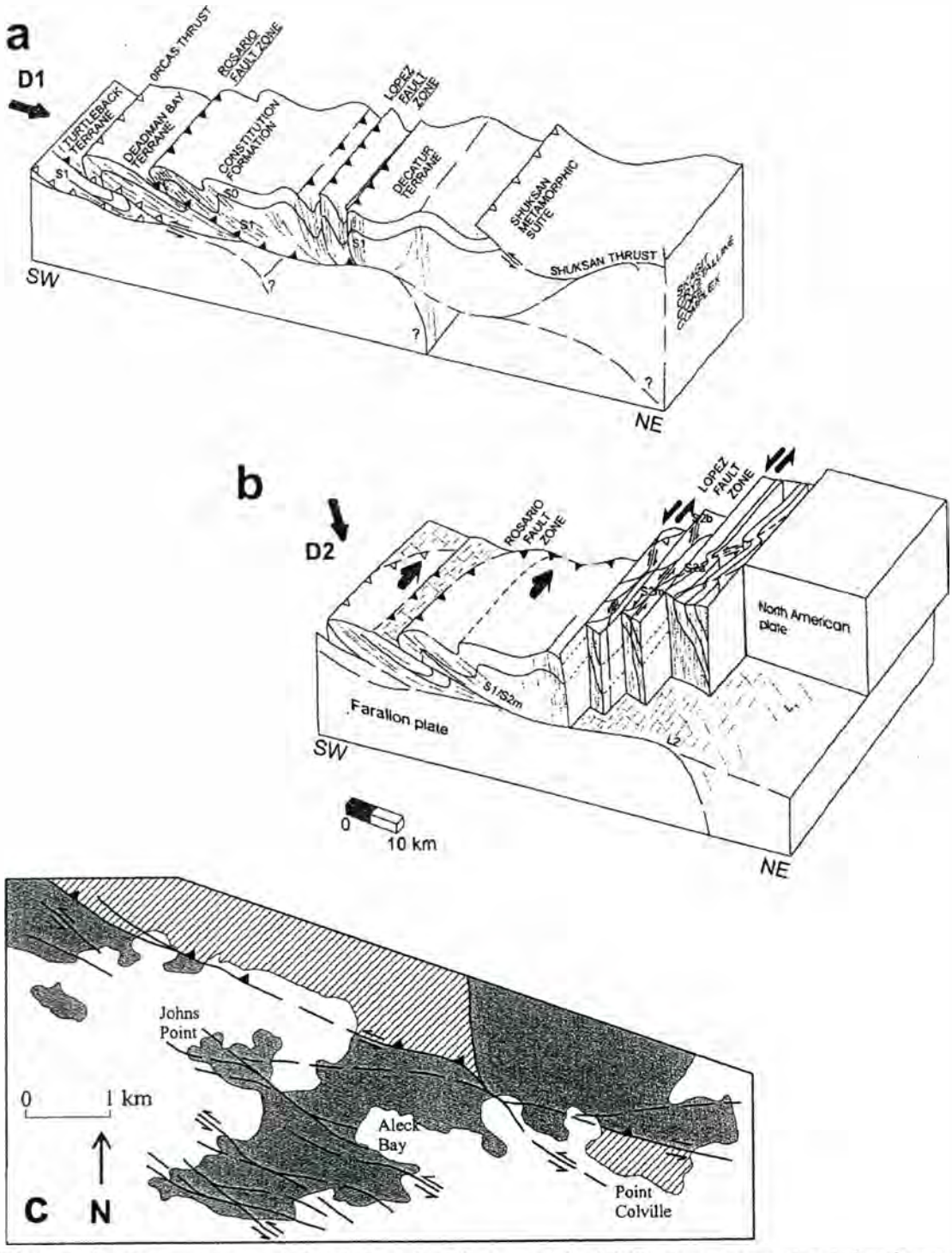

Figure 6: Illustrations of the linked faulting model. (a) Orogen-normal subduction results in southwest-vergent thrusting and large scale folding. (b) A shift to oblique subduction results in reactivation of fault zones: northwest-vergent thrusting occurs in the shallowly dipping Rosario fault zone, while sinistral strike-slip faulting occurs in the steeply dipping Lopez fault zone. (c) Map view of the Lopez Structural Complex, dissected by anastomosing sinistral faults. From Bergh (2002).

the Rosario fault zone. Slip along reactivated foliation and faults concentrated in high strain zones formed a northwest trending, gently plunging L2 lineation. As a result of the D2 deformation, the LSC was dissected by anastomosing left-lateral faults subparallel to the regional fabric (Figure 6b, c; Bergh, 2002).

Ages of Deformation

The relative and absolute timing of deformational events in the San Juan Islands is uncertain. Previous work determined that the major faulting along the Lopez and Rosario thrusts occurred between 112 and 84 Ma in the Late Cretaceous (Brandon et al., 1988; Brown et al., in press). However, a recent Ar/Ar date from LSC fault rocks associated with major faulting revealed that the onset of blueschist facies metamorphism may be significantly older than the 112 Ma faulting constraint. Phengite, high-pressure mica found in metamorphic fabric of the exotic Richardson basalt unit, was dated at 125 Ma (Brown and Lapen, 2003; Brown et al., in press). Additionally, two Ar/Ar dates from mica in the fabric of Ocean Floor Complex metagreywacke in the northeast San Juan Islands yield Late Jurassic metamorphic ages of 154 Ma and 137 Ma (Lamb, 2000; Lamb and Schermer, 2003).

Thus, blueschist metamorphism of terranes in the San Juan Islands probably began prior to formation of the LSC during Late Cretaceous fault juxtaposition. Brown et al. (in press) revise the translation model to account for this age discrepancy. Terranes may have been accreted and metamorphosed separately to the south in a prism setting, then juxtaposed after 112 Ma, translated northward as a fore-arc sliver, and finally thrust to the northwest atop Wrangellia. Recent Ar-Ar results suggest a possible Ar-loss event

in the Late Cretaceous around 100 Ma, which correlates loosely in time with juxtaposition and/or final emplacement (Lamb, 2000). Fission-track dating of the Nanaimo Group, which overlaps Wrangellia yet contains detritus attributed to unroofing of the San Juan terranes, revealed evidence suggesting partial annealing of apatite grains at approximately 60 to 70 Ma (Johnson et al., 1986). Although not well constrained, this Early Tertiary date may be the age of low temperature post-emplacement deformation or the age of exhumation to near-surface conditions.

Other Relevant Work

There is evidence for appreciable post-assembly deformation in rocks of the San Juan Islands. A recent paleomagnetic study by Burmester et al. (2000) demonstrated that Late Cretaceous structures have been reoriented sometime after terrane juxtaposition. Rocks in the San Juan Islands were remagnetized in a normal polarity paleomagnetic field by low temperature, hydrothermal processes (Burmester et al., 2000). This most likely occurred during the Cretaceous normal superchron, from 118-83 Ma, and was probably associated with terrane accretion or juxtaposition. Since that event, the magnetic directions have been scattered and now show virtually no large-scale consistency across the San Juan Islands (Figure 7). Mechanisms to account for the scatter include folding, listric block faulting, vertical axis block rotation, and coastwise translation, all of which are possibilities for terranes of the San Juan Islands (Burmester et al., 2000). However, consistency within the LSC (Figure 7: boxed) suggests that rocks in the complex, while paleomagnetically different from elsewhere in the San Juan Islands, were not locally reoriented with respect to one another. A major problem that

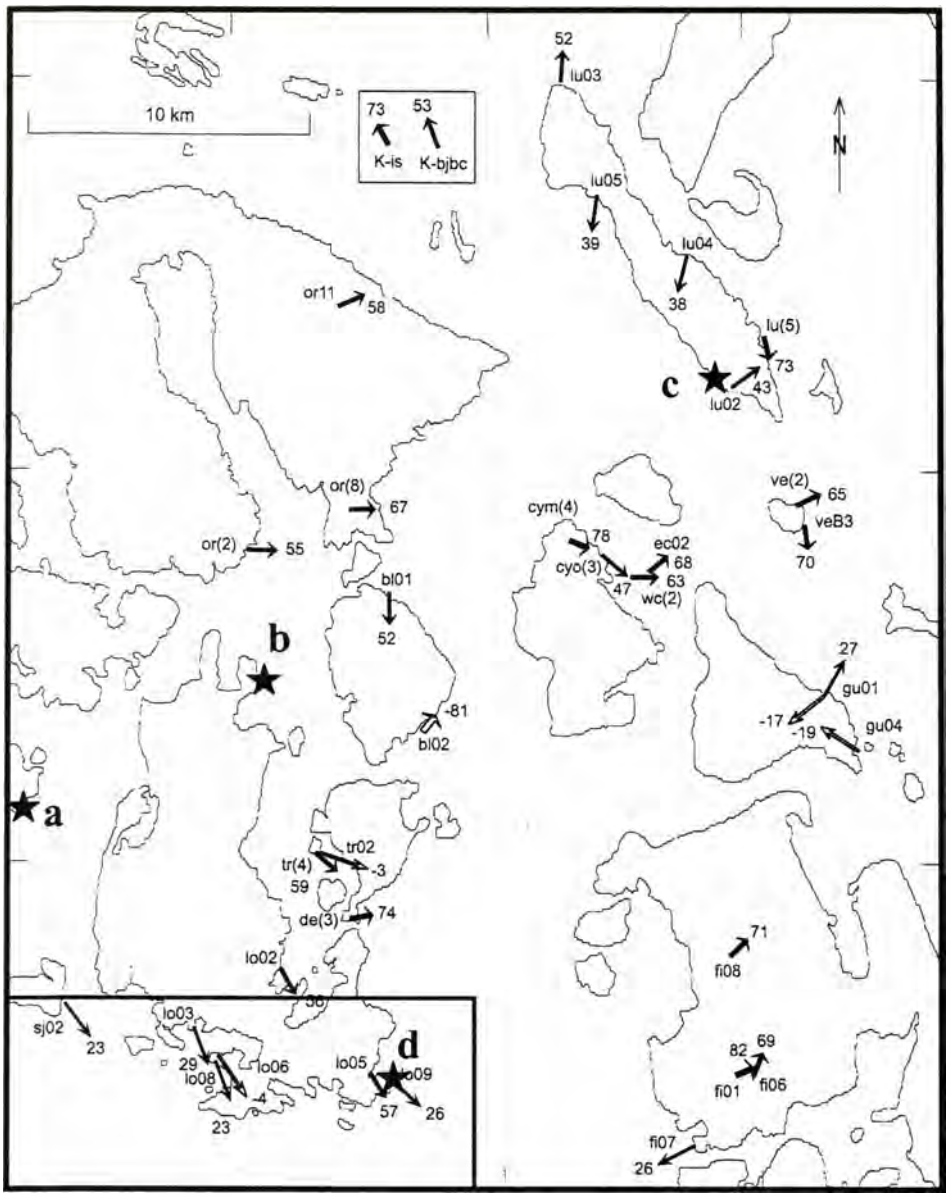

Figure 7: Map of the eastern San Juan Islands shown with paleomagnetic directions. Shorter arrows indicate steeper inclination. Magnetic directions show significant scatter across the region, but are locally consistent, e.g., in the LSC (boxed). The four black stars show the locations of field sites outside the LSC: (a) Constitution Terrane, (b) Fidalgo Complex, (c) Lummi Formation – Ocean Floor Complex, (d) Obstruction Formation – Ocean Floor Complex. Modified from Burmester et al. (2000).

arises from evidence of differential rotation by independent rotation axes is that all orientations of structures are inherently suspect and may not be characteristic of original orientations. All compass directions that describe structural orientations in the San Juan Islands, including those used in this study, represent present orientations that are not directly applicable to Cretaceous orientations without better understanding of the causes and amount of rotation. This limits our ability to fully interpret the tectonic history of the San Juan Islands, so it is important to examine late structures that may be responsible for local and regional rotation in the attempt to restore all structures to their original orientations.

The existence and prevalence of late structures was noted previously by Maekawa and Brown (1991), although until recently very little was known about their kinematics. Lamb and Schermer (2003) documented three stages of brittle deformation in the eastern San Juan Islands that post-date Late Jurassic to Early Cretaceous blueschist metamorphism. After terrane juxtaposition and mostly north to northeast-vergent thrust faulting, a period of generally top to the south and west extension by normal faulting occurred. Next followed conjugate strike-slip deformation associated with approximately north/south extension. Each of these post-fabric events has associated faulting and veining. The latest documented deformational event caused km-scale broad folding of the region around a shallowly southeast-plunging fold axis (Feehan and Brandon, 1999; Lamb, 2000). Brittle structures could partly be the cause of the magnetic direction scatter found by Burmester et al. (2000). However, Lamb (2000) found considerable differences in orientations of even these structures across the eastern San Juan Islands. Therefore, the late regional folding, and possibly other as of yet unknown mechanisms, may have

played a significant role in reorienting rocks of the region. It is unclear, though, what effect late structures have had in total on the orientations of Late Cretaceous structures in the San Juan Islands.

III. Structural Descriptions and Kinematics

Introduction

Rocks of the Lopez Structural Complex have been deformed by multiple generations of both ductile and brittle events. This study describes the relative ages and characteristics of the several stages in development of brittle structures in order to better understand the later stages of structural and tectonic evolution experienced by terranes in the San Juan Islands. Meter-scale structures were studied in representative rocks across the entirety of the LSC on Lopez and San Juan Islands, both within coherent terrane blocks and near terrane contacts. Sites were selected based on bedrock terrane affiliation and rock type as well as geographic location within the complex and proximity to previously mapped thrusts and strike-slip faults. The distribution of terrane slices and location of major faulted contacts was determined using the revised terrane map of the Lopez Structural Complex (Figure 4), structural maps by Bergh (2002), and petrologic maps by Blake et al. (in preparation). Preliminary structural data were also collected in adjacent terranes for comparison with the timing and kinematics of deformation in the LSC.

Structural analysis for each site included measuring fabric and post-fabric brittle structures as well as determining relative ages using cross-cutting relationships. The slip sense of faults was determined by offset of rock types or drag folding of nearby fabric. Where these were not present, other features such as the asymmetry of slickenside steps and the orientation of subsidiary fractures were used as described in Petit (1987). See

Appendix A for details on the methods of data collection. Cross-cutting relationships were used to divide observed structures into several major groups. Faults and veins in each group were analyzed kinematically. Plotting of fault and shear zone data and kinematic analysis were completed using StereoWin v 1.2.0 and FaultKinWin v 1.2.2 (Allmendinger, 2003). FaultKinWin v 1.2.2 calculates principal strain axes for each fault, which takes into consideration the orientation of the fault or shear plane and striae, as well as the slip sense. After analysis, faults are represented by P and T axes. The P axis (closed circle) corresponds to the maximum contraction direction for a fault. The T axis (open square) corresponds to the maximum extension direction. Consistency in the relative timing of structures and visible clustering of P and T axes within a group allows for broad kinematic interpretation of the principal strain axes for the entire group. Details of data analysis are provided in Appendix A.

Ductile and brittle structures are divided into several major groups based on relative age and structure type. Early structures such as folded bedding and folded vein sets predate fabric formation. Multiple types of fabric are present in the LSC, including a regional pressure solution foliation, a localized non-coaxial foliation and lineation, and a cataclastic foliation. Evidence exists for four stages of brittle structures. Early strike-slip deformation was followed by meter-scale southwest-vergent thrusting. After contraction, extension was accomplished first by veining and normal faulting, then later by conjugate strike-slip deformation. Structures are discussed in order of relative age below. All of the following references to compass directions correspond to present coordinates and may not accurately reflect Cretaceous orientations.

Early Structures

Early structures are defined here as structures that predate and are overprinted by the regional pressure solution foliation. These include disrupted and folded sedimentary and volcanic layering as well as deformed vein sets. In terranes dominated by clastic sequences, bedding is locally well preserved. Layers are generally subparallel to the regional foliation, dipping to the northeast (Figure 8). Graded bedding in metagreywacke units indicates some bedding is overturned, but because of limited outcrop and extensive faulting it is difficult to follow layers and observe fold characteristics. Smaller, meter-scale folding is best seen in turbidite sequences in rocks affiliated with the Ocean Floor Complex. These folds are generally tight to isoclinal and reclined, with axial planes that approximately parallel local fabric (Figure 9).

In mudstone-rich assemblages, metagreywacke, chert, and greenstone lenses are discontinuous and boudined on a centimeter to meter scale within an argillaceous matrix (Figure 10a). Lithologic layering in argillaceous rocks is best seen in thin section, although it is typically disrupted by deformation. Siltstone and shale layer contacts mostly parallel the anastomosing foliation. Coarser material occurs within lenses bound by selvage zones or mudstone-rich layers. Detached tight or isoclinal fold hinges of thin beds are common (Figure 10b). The foliation is axial planar to mm-scale folds.

Early vein sets are deformed by the regional foliation (Figure 11). Field observations indicate that deformed veins are composed primarily of quartz and/or carbonate. Sets are of similar size and amount of vein material to later cm-scale vein sets, but are obviously folded or boudined into parallelism with the foliation. Foliation is

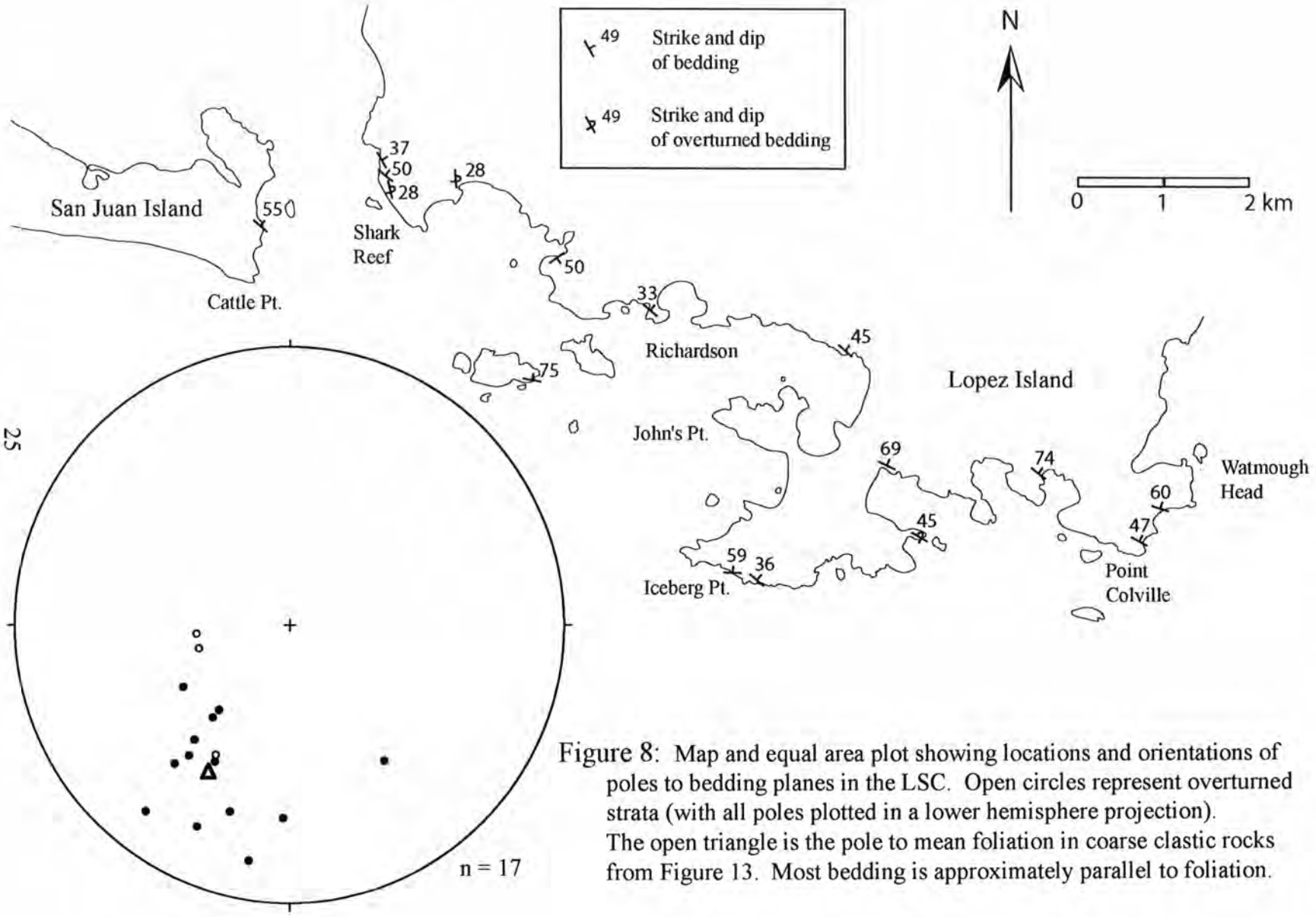

Figure 8: Map and equal area plot showing locations and orientations of poles to bedding planes in the LSC. Open circles represent overturned strata (with all poles plotted in a lower hemisphere projection). The open triangle is the pole to mean foliation in coarse clastic rocks from Figure 13. Most bedding is approximately parallel to foliation.

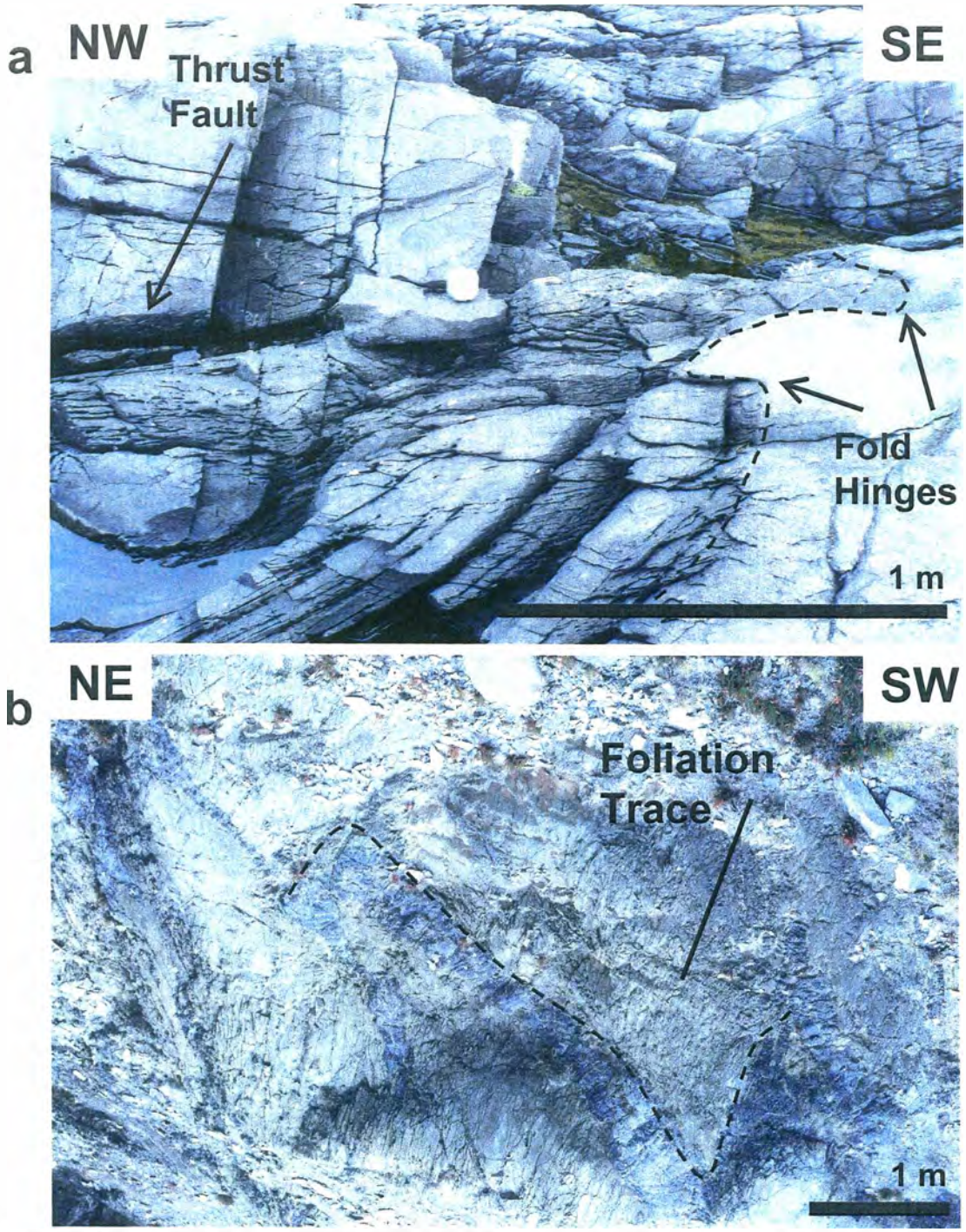

Figure 9: (a) Tight, reclined folds of bedding in graded metagreywacke at Shark Reef. Limbs are subparallel to foliation. A folded contact is traced by the dashed line. This fold is crosscut by a meter-scale thrust fault and offset top-to-the-south out of view. Taken looking down to the northeast. (b) A tightly folded black shale layer in turbidite layering on Iceberg Point. The upper shale boundary is traced. Foliation in the area is generally axial planar to folds of bedding but local variations exist. Taken looking down to the southeast.

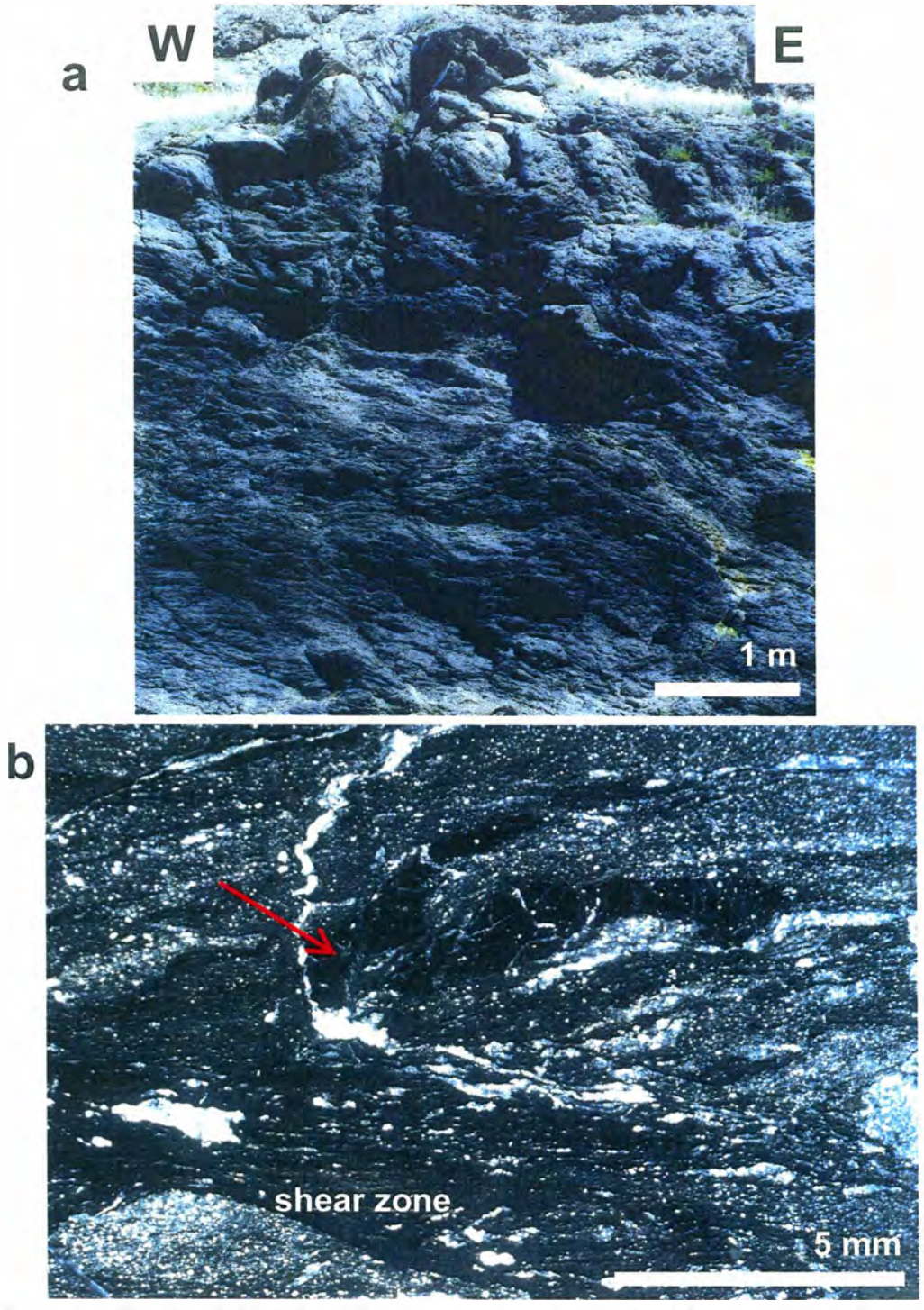

Figure 10: (a) Original bedding in argillite-rich zones is highly disrupted. Boudins of chert, sandstone, and basalt stand out from the fine matrix. (b) Photomicrograph of a detached isoclinal fold hinge of shale (marked by the red arrow) surrounded by siltstone. Foliation runs approximately horizontal across the picture. An argillaceous shear zone, shown in greater detail in Figure 16, runs subparallel to the siltstone foliation near the bottom of the photograph.

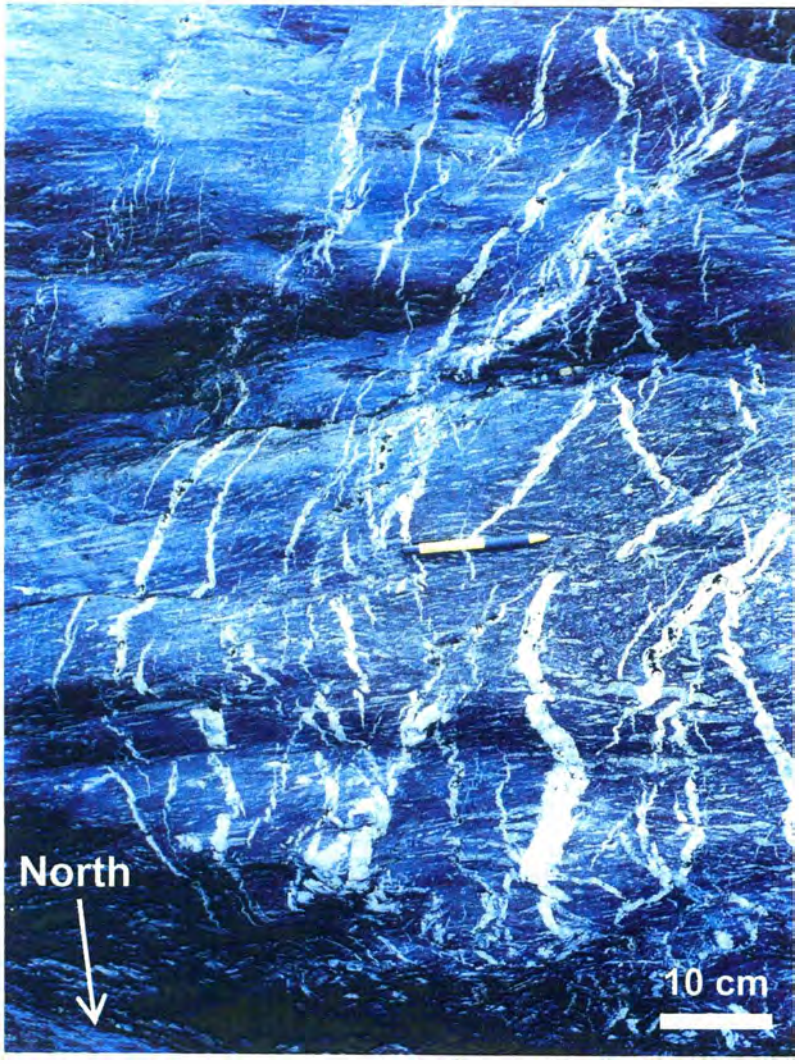

Figure 11: An early vein set in an argillite-rich outcrop at Cattle Point. Veins display mm-scale open to close folds and foliation is approximately axial planar to the folds. Yellow pencil for scale is aligned with trace of foliation. Outcrop surface is subhorizontal.

approximately axial planar to the folds. Because data on folds of bedding and early vein sets are very sparse, no kinematic interpretation has been attempted.

Regional Fabrics

Three types of fabrics exist within the LSC. A pressure solution foliation of varied intensity is seen in zones of coarse grained rocks. A localized shear fabric is found in zones of fine grained rocks. Cataclastic zones are found at several terrane boundaries within the LSC.

Fabric in Coarse Clastic Rocks

The pervasive fabric within the LSC is a pressure solution foliation of varied intensity. In outcrop, it is seen most easily in the generally coherent metagreywacke units (Figure 12a) and within pods of coarse material in argillaceous units. The foliation dips moderately to the northeast and its orientation is fairly consistent across the LSC (Figure 13). No prevalent lineation is observed in outcrop. Pressure solution at the grain scale was the dominant mechanism of foliation formation. In thin section, dark selvage zones anastomose between coarse grains of primarily quartz, chert, and feldspar (Figure 12b). Grain edges parallel to foliation are truncated by the selvage zones. Some quartz grains show evidence for grain boundary dissolution and recrystallization along jagged surfaces perpendicular to foliation. Reprecipitated fibrous quartz extends from these boundaries in the plane of foliation (Figure 14). Thus, grains are typically asymmetrical and show a preferred shape orientation parallel to the selvages. However, they are not significantly internally strained. Some quartz grains show evidence of undulatory extinction but

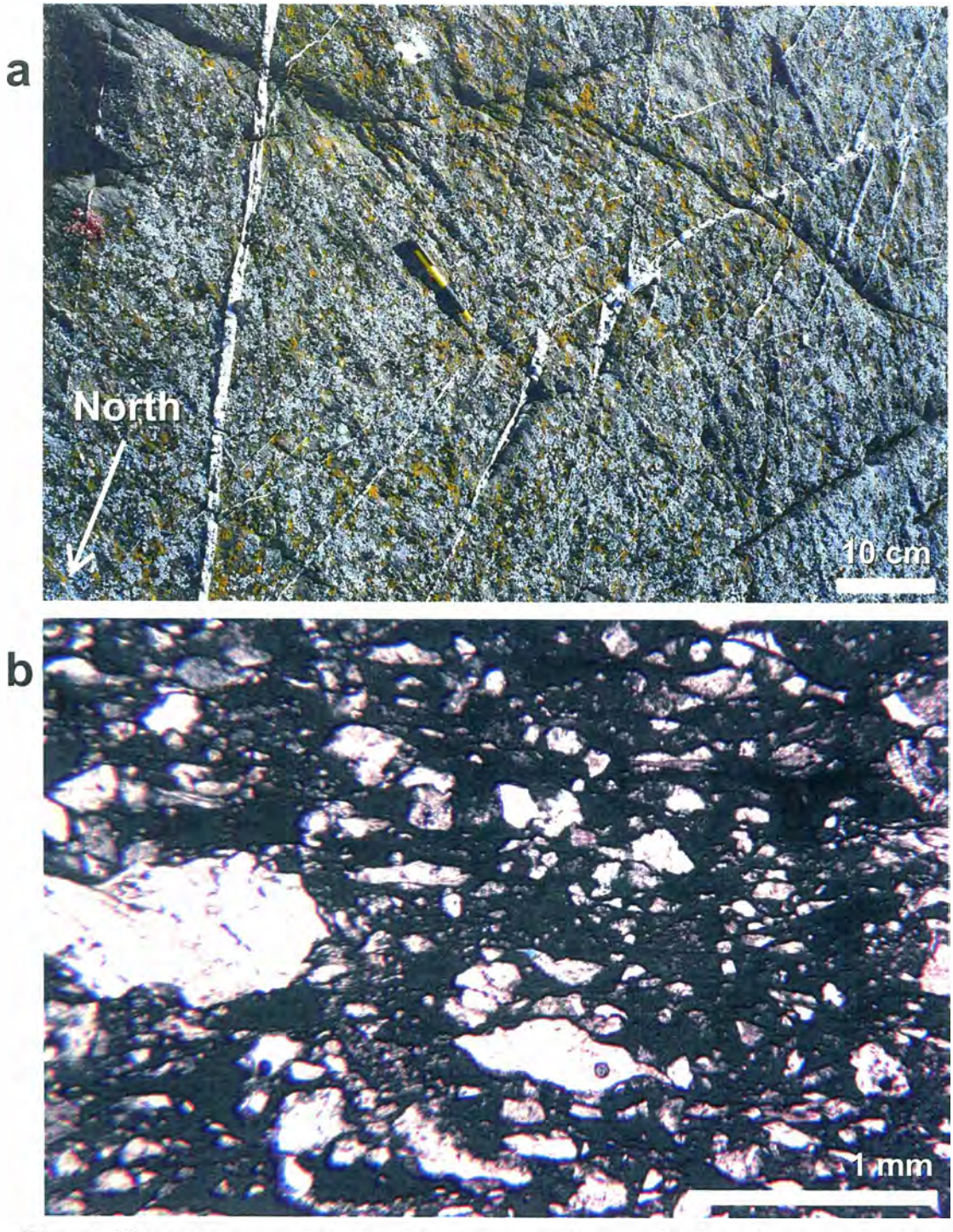

Figure 12: (a) Pressure solution foliation in medium grained sandstone at Cattle Point. Pencil points to the WNW and is aligned with the trace of fabric. Taken looking down to the southwest. (b) Pressure solution foliation in thin section from a medium grained sandstone sample. Large grains show a shape preferred orientation and dark selvages anastomose between grains.

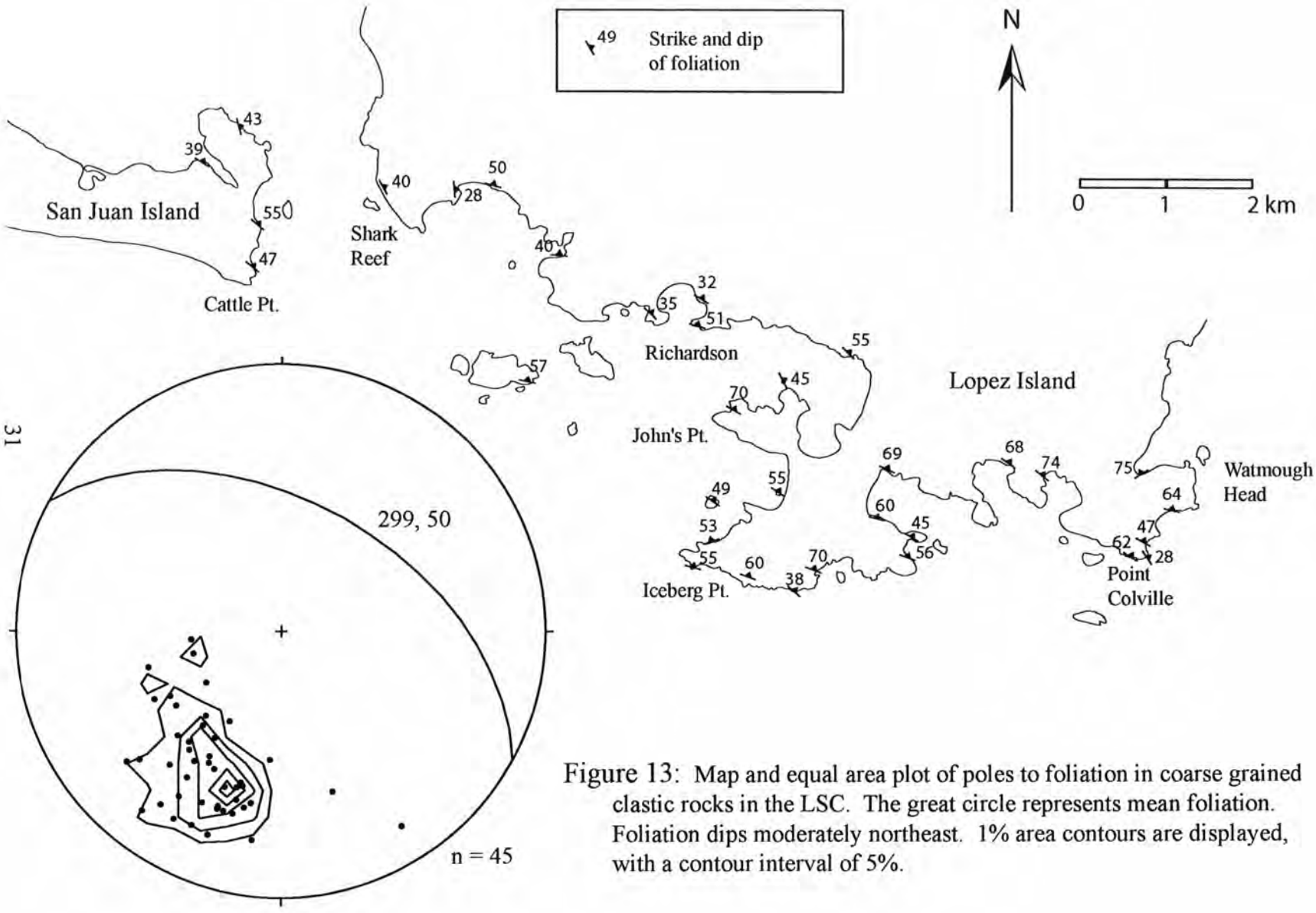

Figure 13: Map and equal area plot of poles to foliation in coarse grained clastic rocks in the LSC. The great circle represents mean foliation. Foliation dips moderately northeast. 1% area contours are displayed, with a contour interval of 5%.

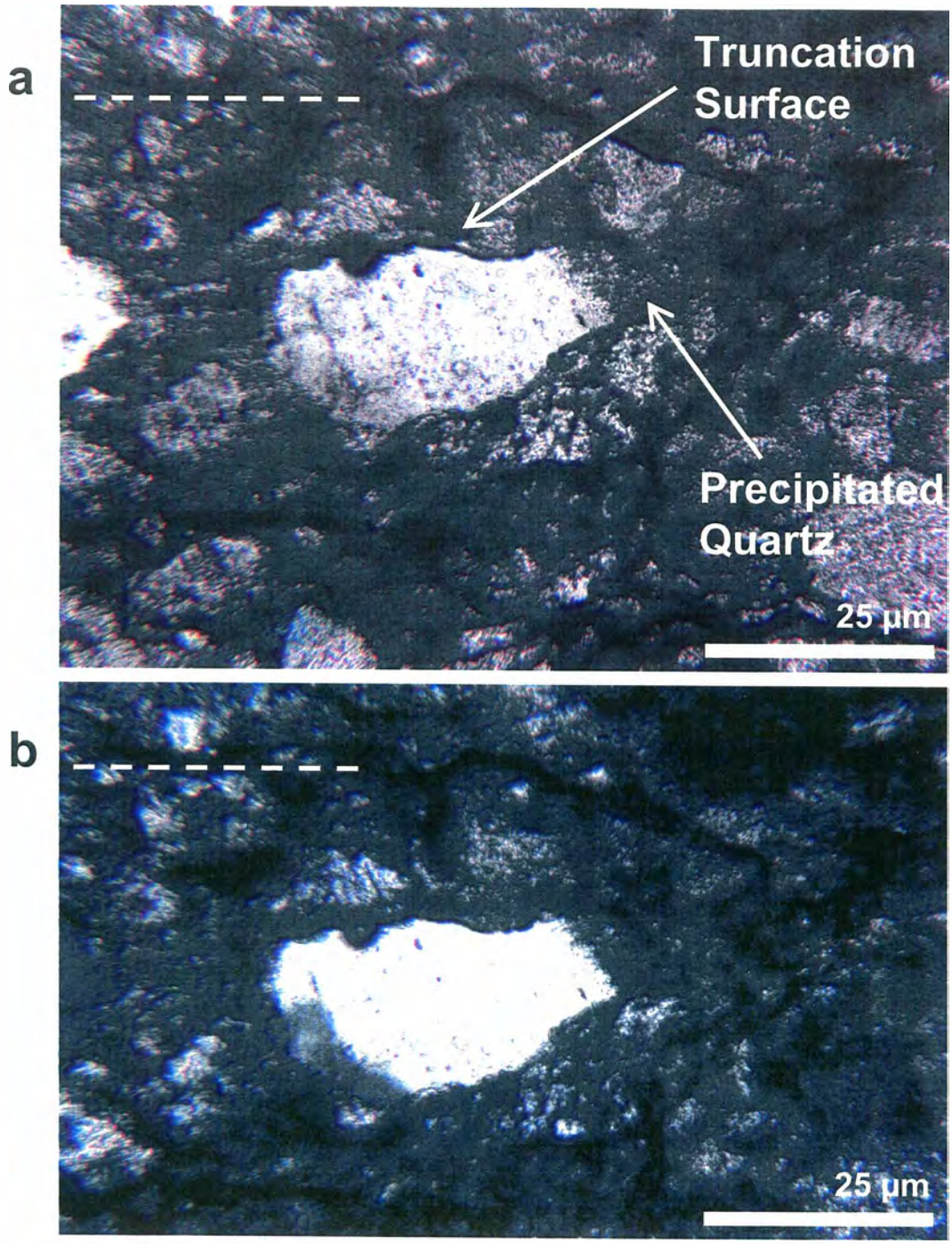

Figure 14: Evidence of pressure solution processes acting on an individual quartz grain within a coarse sandstone. Surfaces parallel to foliation are truncated unevenly and the grain is lengthened by precipitation parallel to foliation. Under cross polarized light, quartz grains show little or no evidence of internal deformation. Dashed line aligned with trace of fabric. Taken in plane polarized (a) and cross polarized (b) light at 100x magnification.

subgrains are generally not developed, and many grains are not visibly internally deformed.

Fabric in Fine Grained Rocks

Argillaceous rocks are typically more strongly foliated in outcrop than are coarse-grained rocks, and evidence suggests that the fabric in these finer zones may be partly non-coaxial in nature. Foliation within argillaceous zones dips steeply to the north-northeast (Figure 15), and is generally slightly steeper than the pressure solution foliation prevalent in coarse clastic zones. In outcrop, inclusions of metagreywacke exhibit pressure solution foliation subparallel to foliation in the surrounding matrix. However, pressure solution foliation does not appear to continue directly from metagreywacke lenses into the argillite. Subhorizontal slickenlines oriented approximately west-northwest/east-southeast are found on some chert and metagreywacke inclusion-matrix contacts, along slip planes which parallel the argillaceous fabric (Figure 15). Evidence of a shear component of fabric formation is also seen locally in thin section. Shear zones are distributed within some mm-scale mudstone-rich layers, while pressure solution foliation is preserved within more coarse grained lenses (Figures 10b, 16a). Scattered silt- and sand-sized particles within fine zones are generally aligned within the foliation and many have asymmetric tails (Figure 16b), but no consistent shear sense is observed. As noted in outcrop, pressure solution foliation is not observed to continue into these shear zones. Thus, while evidence of pressure solution processes exists within coarse clasts in argillaceous zones, macroscopic and mesoscopic indications of localized layer-parallel shearing along discrete planes are also present.

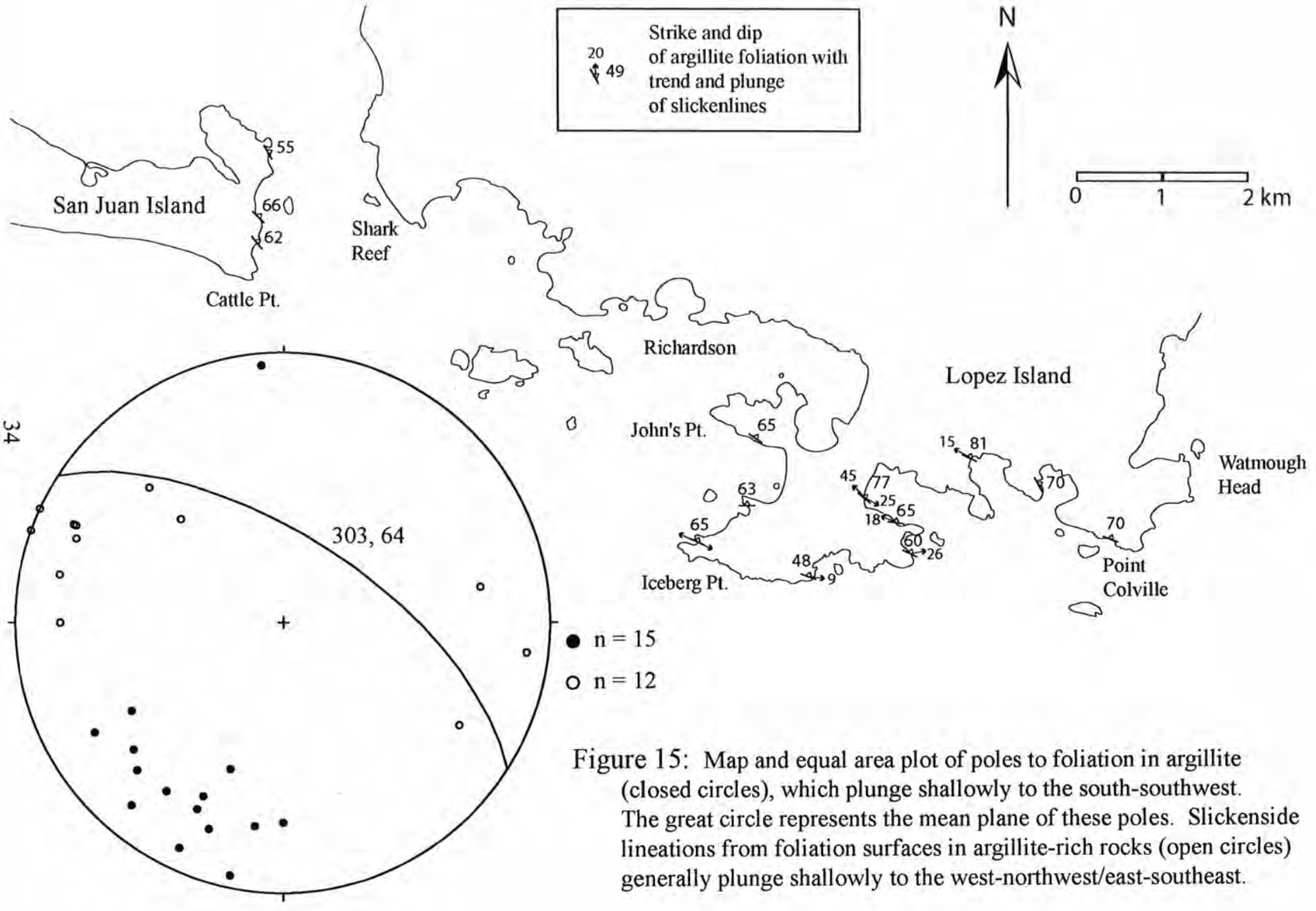

Figure 15: Map and equal area plot of poles to foliation in argillite (closed circles), which plunge shallowly to the south-southwest. The great circle represents the mean plane of these poles. Slickenside lineations from foliation surfaces in argillite-rich rocks (open circles) generally plunge shallowly to the west-northwest/east-southeast.

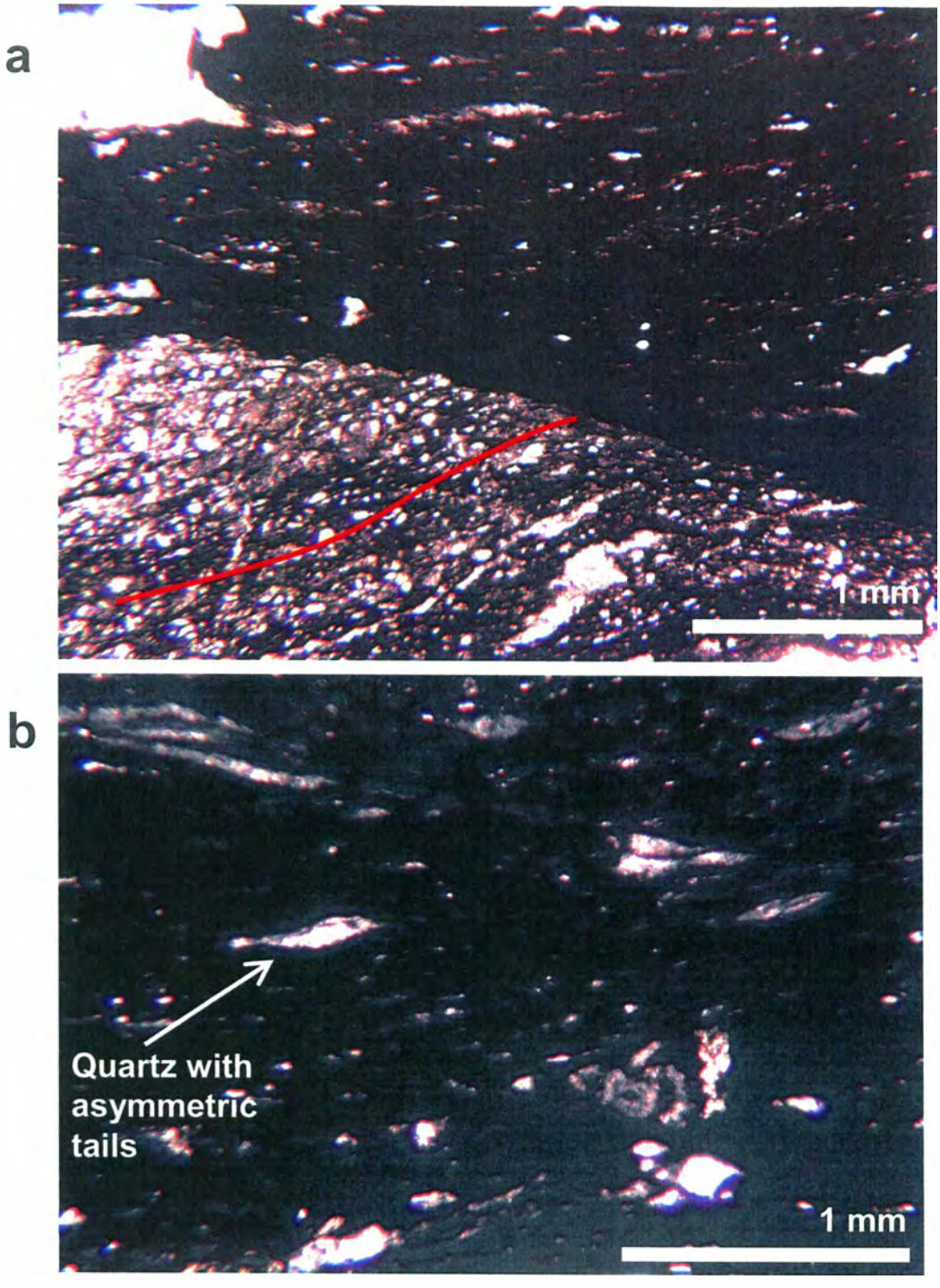

Figure 16: Evidence in thin section of lateral shearing in a mudstone-rich zone. (a) Pressure solution foliation (red line) is present in the silty lens at the bottom of the photograph but does not continue directly into the mudstone-rich zone. At this contact, the siltstone foliation is truncated and dragged by shearing. (b) Many quartz grains within the fine zone have asymmetric tails indicative of shearing, but no consistent shear sense is observed.

The Relative Timing of Fabrics

The relative timing of pressure solution foliation and localized shear fabric is typically ambiguous, but at some contacts seen in thin section shearing appears to have continued after the cessation of pressure solution processes. Foliation in mm-scale mudstone-rich zones is generally not parallel to foliation in neighboring coarse-grained pods, and foliation is not continuous across shear zone contacts. Additionally, shear zones truncate and drag pressure solution foliation at some layer contacts (Figures 10b, 16a). To deform pressure solution foliation, some localized shearing must have occurred after pressure solution ceased, although the lack of clear crosscutting relations at many contacts seen in thin section suggests the pervasive pressure solution fabric and localized shear-related fabric may have formed during the same episode of deformation.

Cataclastic Fabric

Cataclastic zones generally upwards of 1 meter thick occur at several of the terrane boundaries previously mapped by Brandon et al. (1988). The strong fabric in cataclasites dips moderately to the north (Figure 17), which is roughly equivalent in orientation to regional pressure solution fabric. Dip-slip slickenfibers are found on foliation-parallel vein material in the fault zone at Davis Head, and an oblique stretched clast lineation is seen on cataclastic foliation surfaces at Iceberg Point. From field observations, it is unclear whether formation of the cataclastic zones postdates or precedes and is overprinted by pressure solution foliation. However, cataclastic foliation and pressure solution foliation display similar timing constraints relative to brittle structures in outcrop. Early veins are boudined and nearly parallel to fabric, while

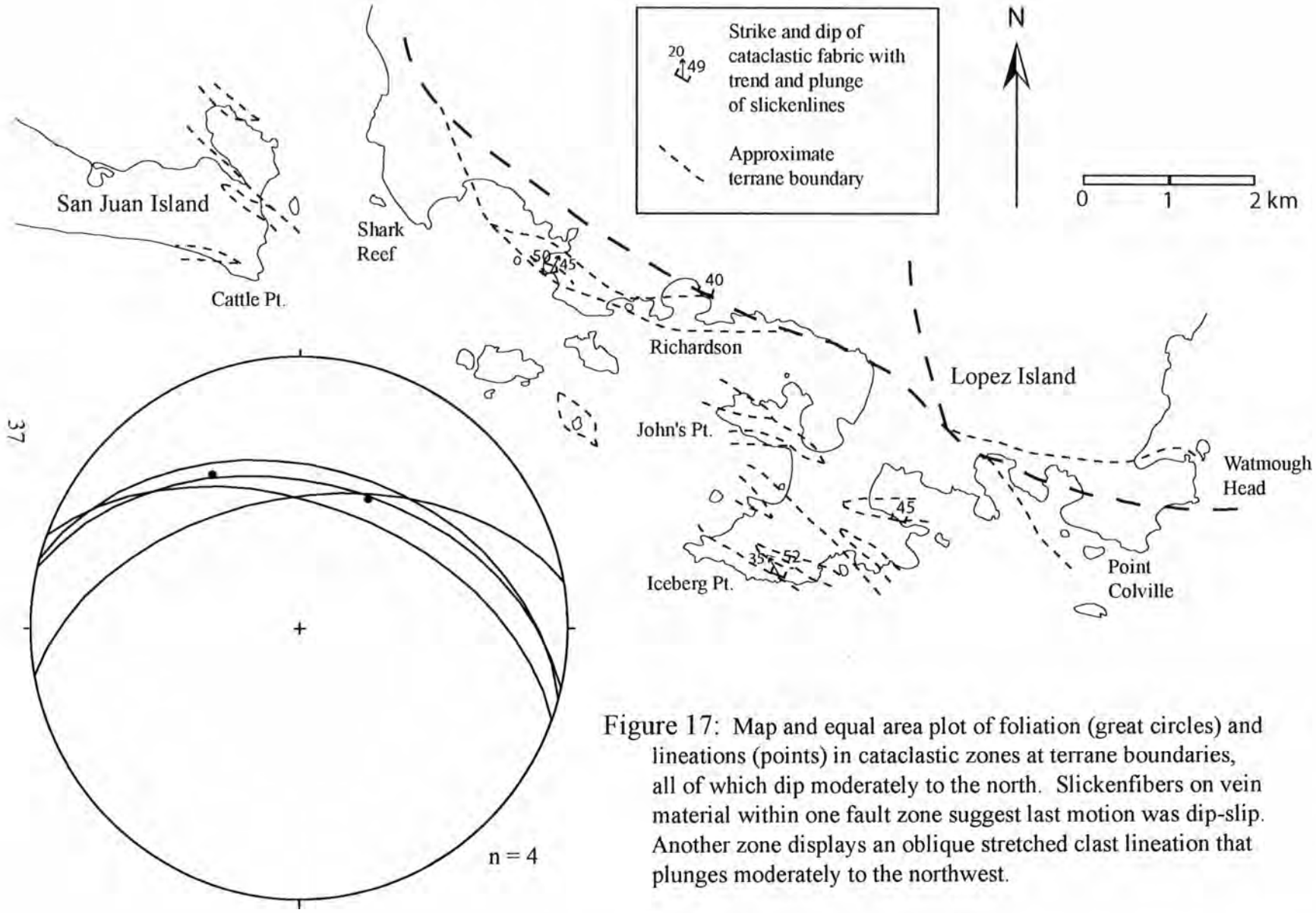

Figure 17: Map and equal area plot of foliation (great circles) and lineations (points) in cataclastic zones at terrane boundaries, all of which dip moderately to the north. Slickenfibers on vein material within one fault zone suggest last motion was dip-slip. Another zone displays an oblique stretched clast lineation that plunges moderately to the northwest.

several generations of late veins and faults crosscut the cataclastic zones (Figure 18). So, although field observations in cataclastic zones provide no new clarity on the relative timing of major faulting and fabric formation debated by previous authors, both episodes of deformation are known to precede the brittle structural sequence discussed below.

The Kinematics of Fabric Formation

Information on the kinematics of deformation during fabric formation can be derived from the orientation and type of fabric present. The regional pressure solution foliation is interpreted as a flattening foliation: grains display a consistent long axis orientation in the plane of the foliation, but they form no observable lineation to signify a preferred stretching direction. Therefore, the mean orientation of poles to foliation is the maximum shortening direction (Price and Cosgrove, 1990). In the LSC, poles to pressure solution foliation on average plunge moderately to the SW (Figure 13).

Argillaceous fabric displays three key features for interpretation: large grains are oriented approximately parallel to the surrounding foliation as they are in coarse-grained rocks, striations occur on some clasts in outcrop within the plane of foliation, and there is no consistency to shear sense within this fabric. Because of the evidence for flattening of large grains and lack of a consistent shear sense, poles to argillaceous foliation are also interpreted to represent the maximum coaxial shortening direction. Poles plot shallowly to the SW (Figure 15), which is roughly equivalent to the poles of pressure solution foliation in metagreywacke rocks. The lineation on clasts constrains the slip vector of localized shearing in argillite-rich rocks as subhorizontal to the northwest/southeast. The slight difference in orientation of metagreywacke and argillite foliations on the regional

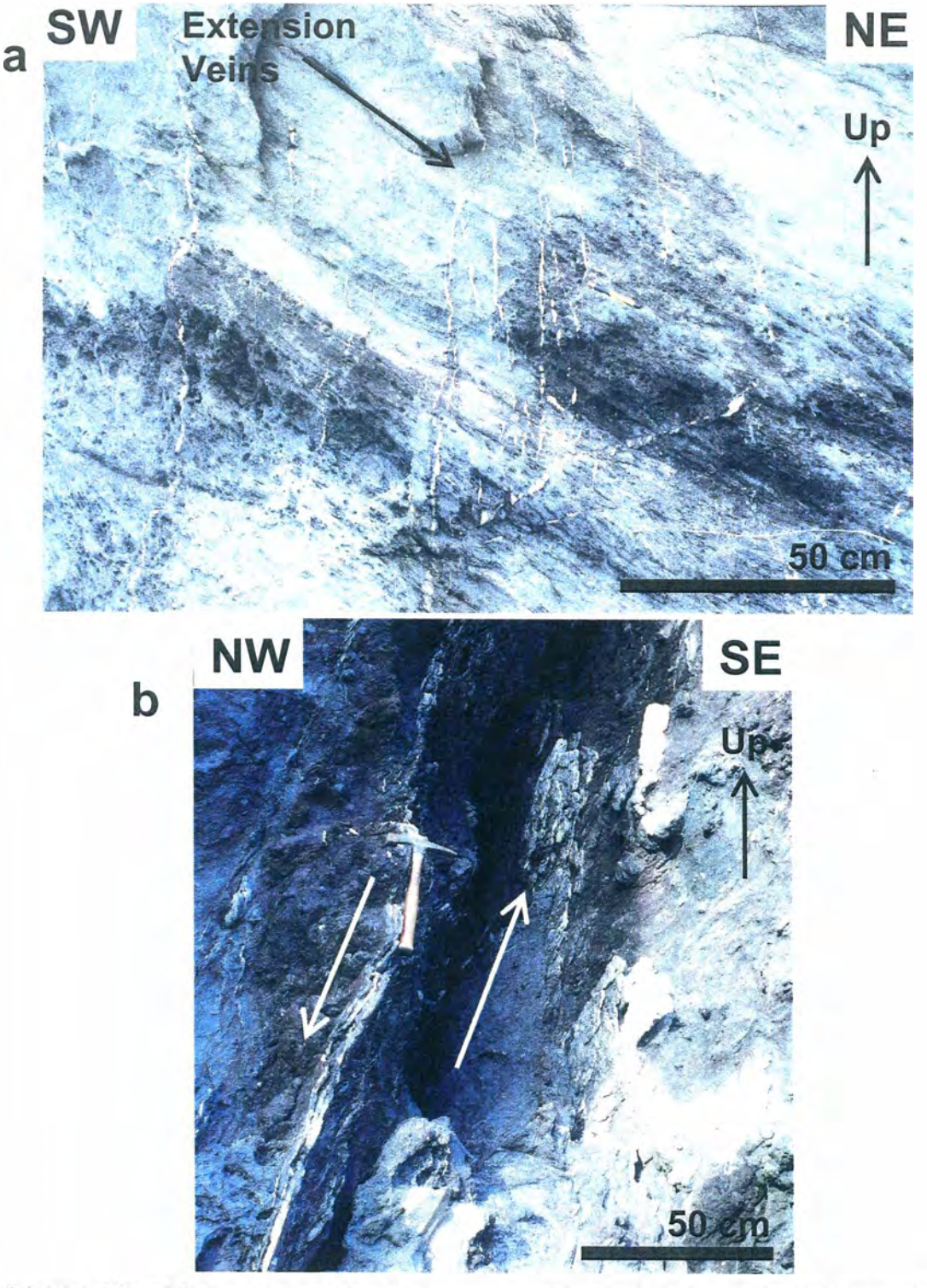

Figure 18: Brittle veins and faults crosscut cataclastic foliation at Davis Head. (a) A carbonate extension vein set in cataclasite. Yellow pencil for scale is parallel to the trace of fabric on the steep face. (b) A normal fault in cataclasite with top down-to-the-NW sense of slip. Arrows show relative motion of fault blocks.

level and the discontinuity of foliation between rock types in outcrop could be attributed to cleavage refraction, although some disruption is surely caused by local deformation of the pressure solution foliation from layer-parallel shearing along lithologic contacts. Data on cataclastic fabric are too few to allow kinematic interpretation.

Brittle Structures

Brittle structures within the LSC are divided into four groups based on relative timing and structure type. The first group consists of early strike-slip structures related to northwest/southeast lateral slip. Next are thrusts related to northeast/southwest shortening. Third, northwest/southeast extension and vertical thinning are accomplished by widespread extensional veining and normal faulting. The latest faulting episode consists of conjugate strike-slip structures, which are also consistent with northwest/southeast extension. Groups are discussed below in order of relative age as understood from outcrop observations.

Early Strike-slip Structures

Layer-parallel Slip in Coarse Rocks

Layer-parallel strike-slip surfaces are locally found on bedded chert-greywacke and shale-greywacke contacts at Iceberg point and Colville point (Figure 19). Since bedding generally parallels regional pressure solution foliation, the slip planes mostly dip moderately northeast (Figure 20a). Slickensides plot subhorizontally to the northwest/southeast. Slip sense is generally not known. The timing of this slip is loosely constrained at one location; vein material with subhorizontal slickenfibers, which lies

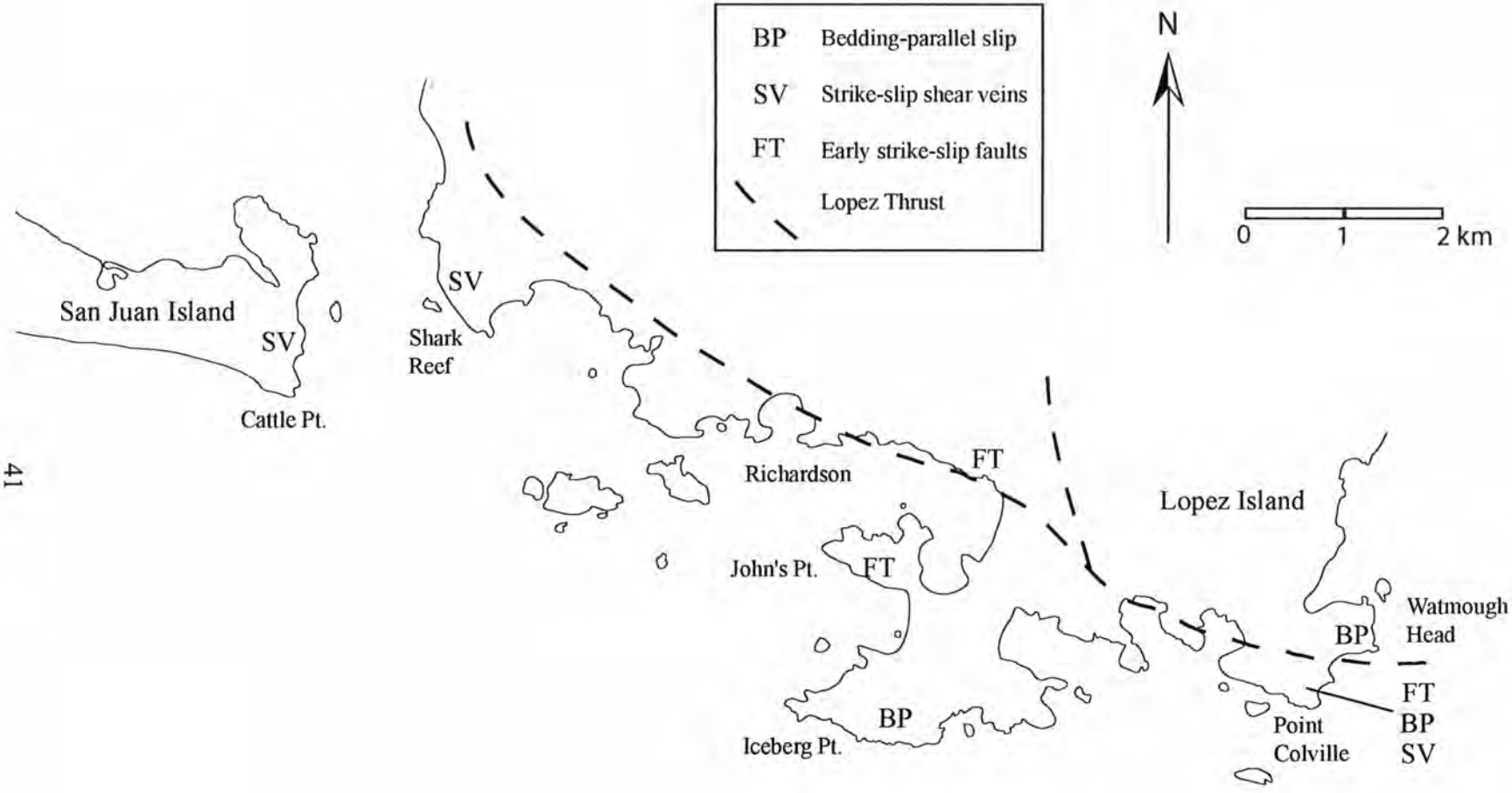

Figure 19: Map of the LSC showing major occurrence locations of localized strike-slip shear veins, bedding-parallel slip planes, and early strike-slip faults.

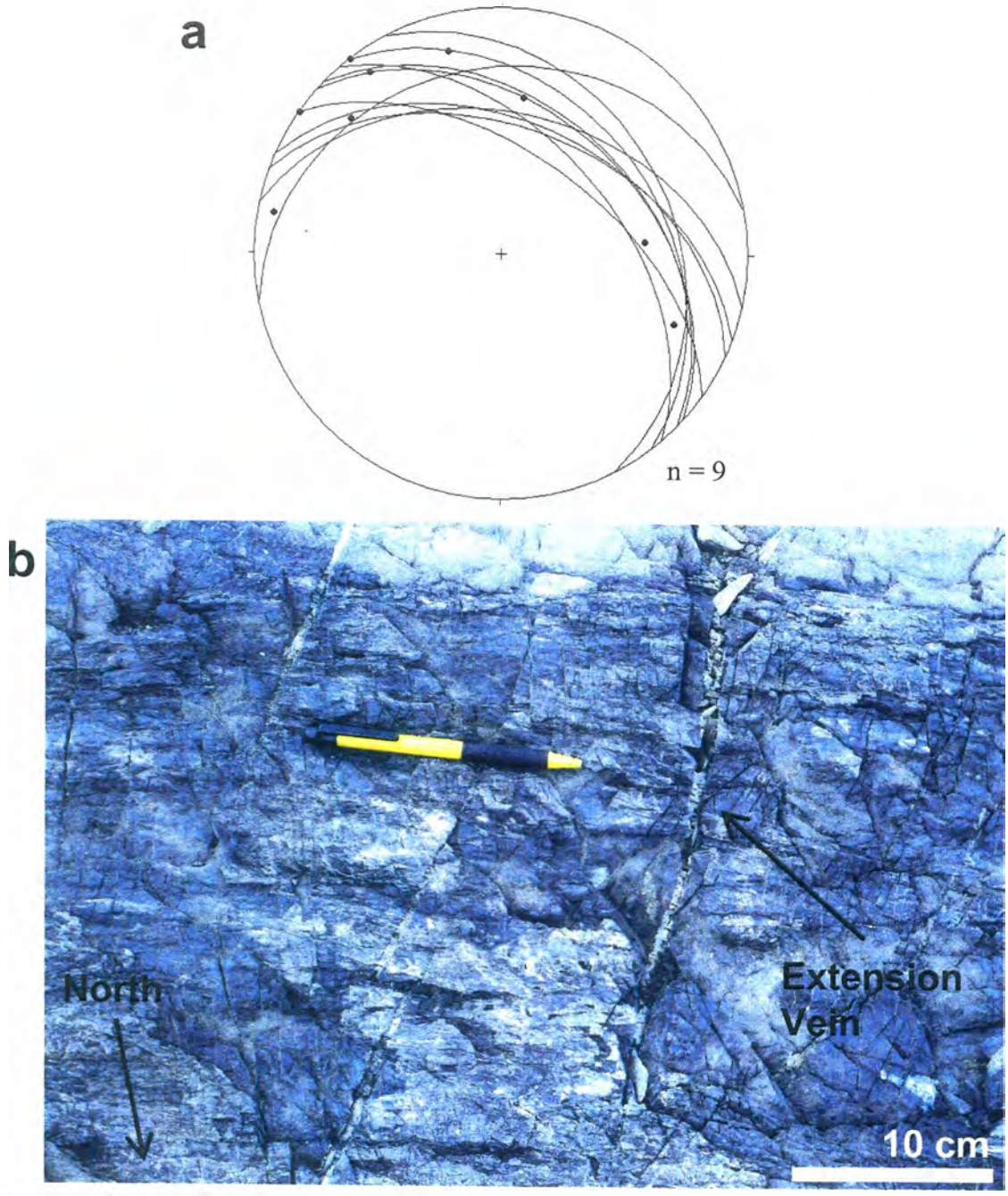

Figure 20: (a) Equal area plot of chert and shale bedding planes with slickensides at Iceberg Point and Colville Point. The majority of lineations (dots) are shallow to horizontal northwest/southeast on their respective planes. Sense of slip is not known. (b) Vein material on an exposed shale bedding plane at Iceberg Point crosscut by several small extension veins. Yellow pencil is parallel to the slickenfiber lineation. Plane of view is subhorizontal.

atop a shale layer, is crosscut by extension veins (Figure 20b). Turbidite layering in greywacke units at multiple locations outside of the LSC also show evidence of early layer-parallel subhorizontal slip (see Appendix B).

Shear Veins

Rare strike-slip shear veins are restricted to dominantly metagreywacke and metavolcanic lenses in the LSC (Figure 19). Shear veins postdate pressure solution foliation and are crosscut by extensional structures (Figure 21), but their timing relative to thrust faults is unknown. They dip moderately or steeply and strike inconsistently east/west to northwest/southeast (Figure 22). Slickenfibers on vein faces indicate strike-slip or oblique-slip motion, mostly to the northwest and southeast. Right and left-lateral shear veins are approximately equal in abundance. Shear veins typically range from 2 to 5 cm wide but occur as large as 20 cm and many trace for greater than 10 meters where exposed. The amount of offset across these features is generally not known because they occur inside large coherent blocks of relatively homogeneous metagreywacke and metavolcanic units with no reference layers. Shear veins generally contain quartz, carbonate, and prehnite, and can exhibit several layers of minerals oriented parallel to the vein walls (Figure 23). Layering is the result of several generations of fluid input and mineral growth, and therefore suggests multiple stages of dilation and shearing during vein formation.

Early Strike-slip Faults

Rare early strike-slip faults are found locally in the LSC. For this study, an early

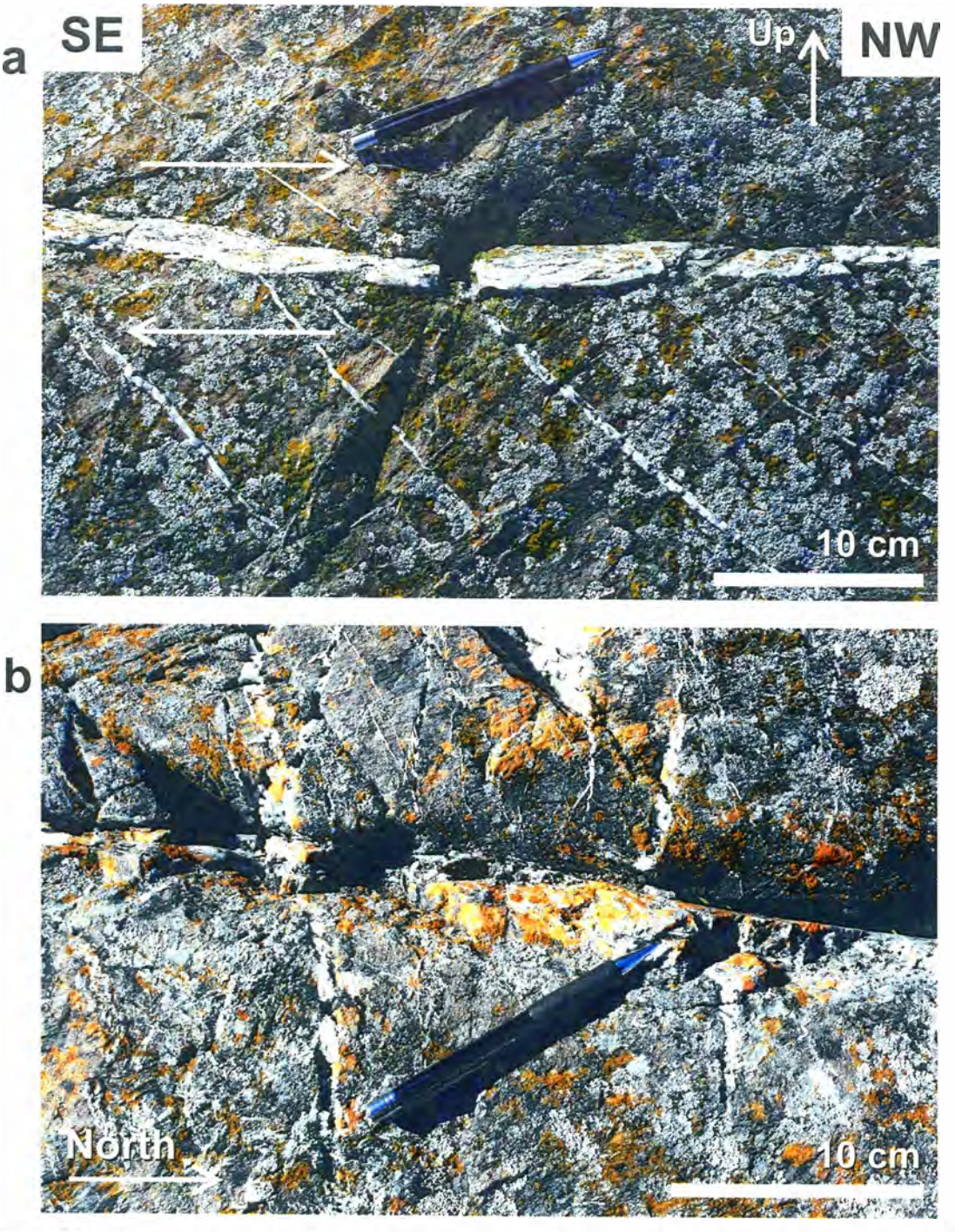

Figure 21: (a) A strike-slip shear vein crosscuts foliation in a metagreywacke outcrop at Cattle Point. Arrows show sense of motion interpreted from subsidiary en echelon veinlets. Pencil is parallel to the trace of foliation. Taken looking down to the SW. (b) An extension vein crosscuts a shear vein in metagreywacke at Cattle Point. Pencil is parallel to trace of weak foliation.

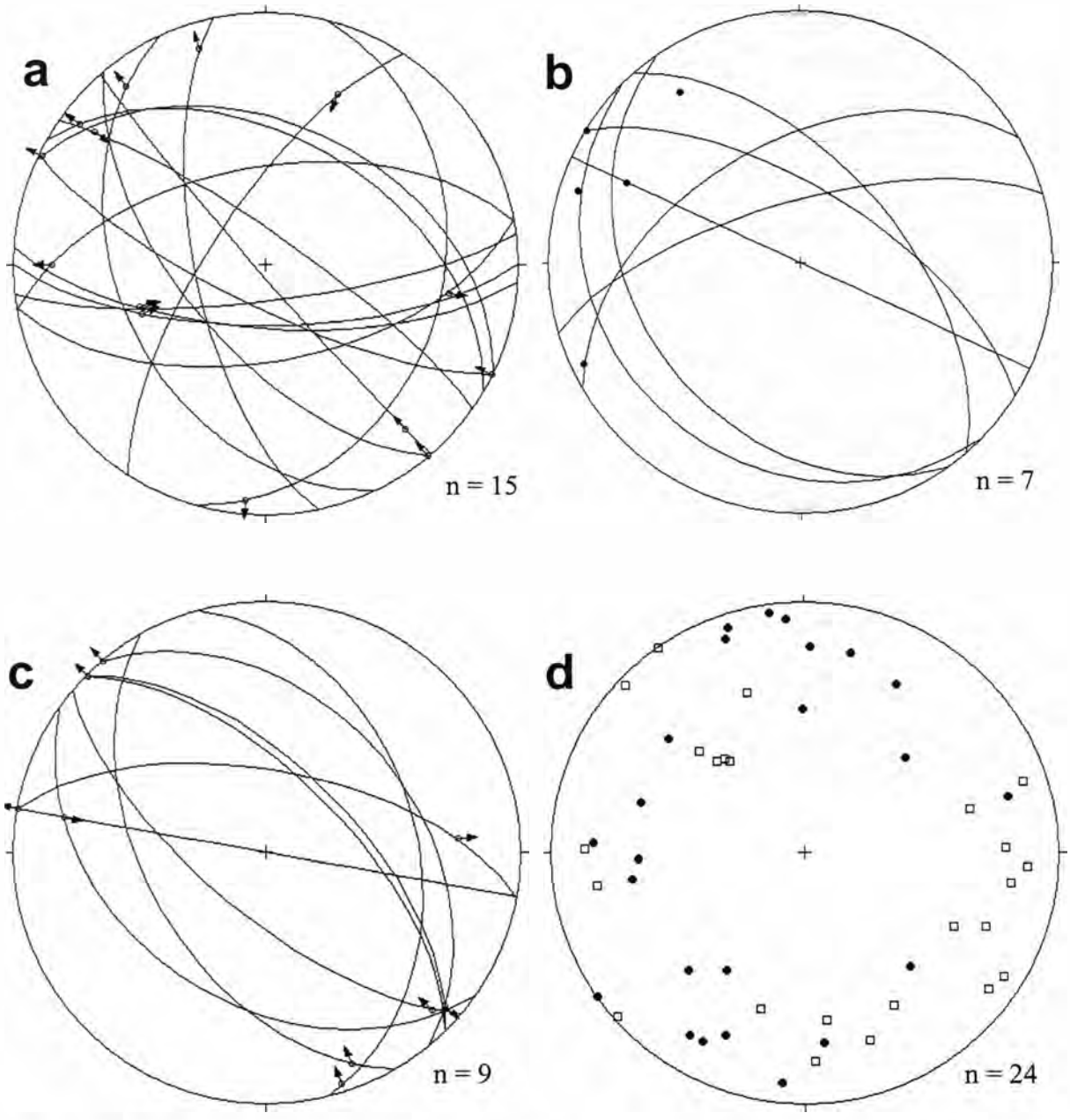

Figure 22: Equal area plots of early strike-slip structures. Arrows show sense of hanging wall motion. Right-lateral and left-lateral structures are subequal in abundance. (a) Shear veins with known slip sense. (b) Shear veins without complete kinematic information. (c) Early strike-slip faults, which generally strike northwest or southeast. (d) Kinematic axes for early strike slip structures. P axes (closed) mostly plot shallowly to the north-northeast and south-southwest. T axes (open) mostly plot shallowly northwest and southeast.

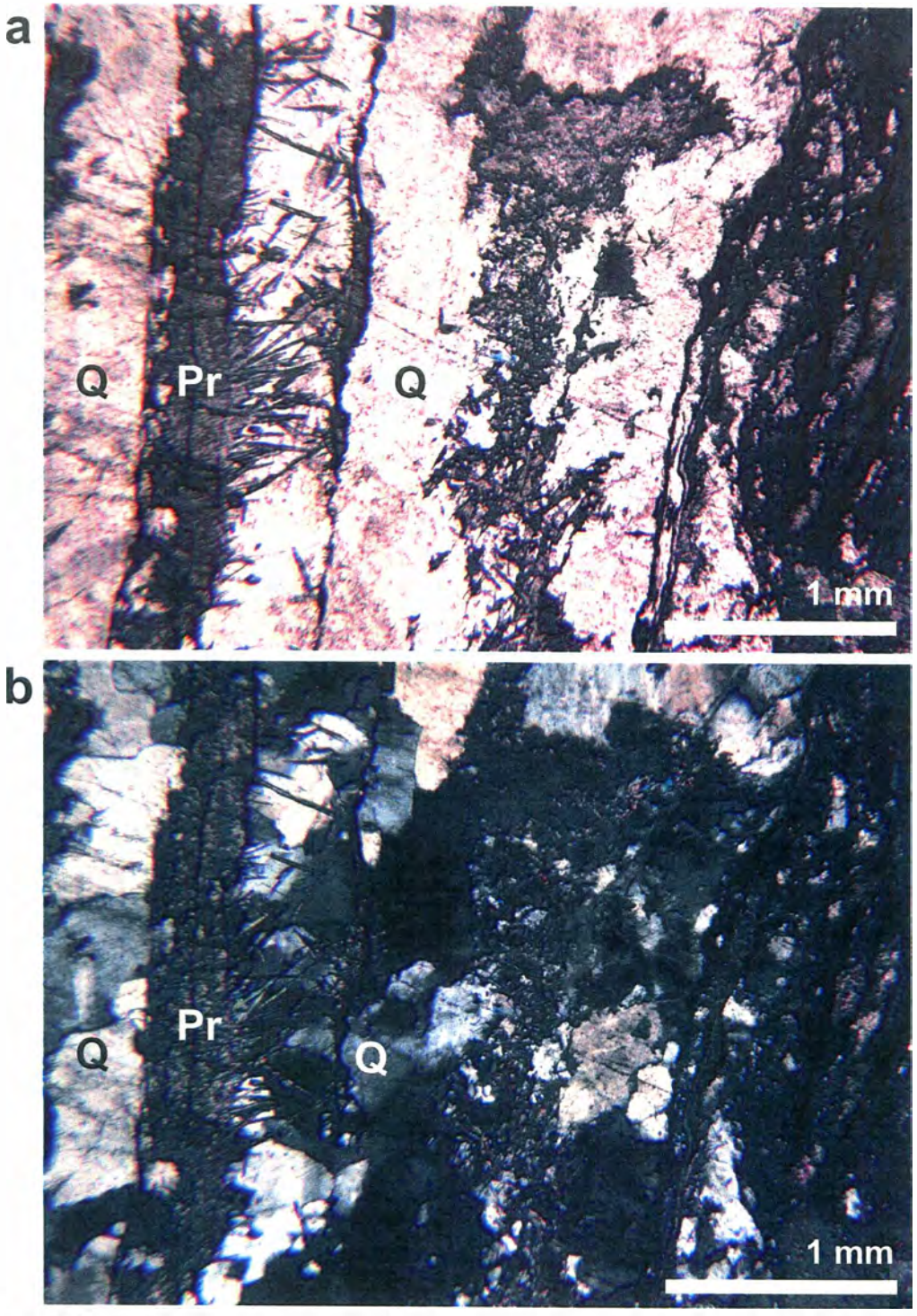

Figure 23: Thin section photograph of mineral layering in a strike-slip shear vein. The several vertical layers shown above are parallel to the vein walls. Within layers, mineral fibers grow perpendicular or parallel to vein walls. (a) Plane polarized light. Q = quartz, Pr = Prehnite. (b) Cross-polarized light.

strike-slip fault is defined as a meter-scale fault similar in length and appearance to late conjugate strike-slip faults discussed below, but with definitive crosscutting evidence in outcrop that it precedes thrust faulting and/or extensional faulting. This small fault group has an average orientation similar to other early strike-slip structures. Faults strike northwest/southeast and dip moderately to steeply northeast or southwest (Figure 22c). Occurrence is mainly limited to within greenstone outcrops near the trace of the Lopez Thrust (Figure 19). Therefore, relative timing of these faults with respect to fabric in the clastic rocks is only poorly constrained. In argillite on the south end of John's Point, an early strike-slip fault crosscuts but runs approximately parallel to the local fabric.

Kinematics of Early Strike-slip Structures

Kinematic analysis was conducted on complete data from shear veins and early strike-slip faults. Data on the small number of bedding-parallel slip surfaces were not included because they lacked a reliable slip sense. P-axes for early strike-slip structures cluster loosely to the north-northeast and south-southwest (Figure 22d). T-axes generally plot shallowly to the northwest and southeast. The subequal amount of right- and left-lateral early strike-slip structures all oriented approximately northwest/southeast suggests that these structures accommodated lateral extrusion and extension to the northwest and southeast during northeast/southwest contraction. Thus, kinematic axes of shear veins and early strike-slip faults and slip vectors of all early strike-slip structures are broadly consistent with a continuation of the northeast/southwest contractional regime as interpreted above for the kinematics of shear fabric formation.

Contractional Structures

Thrust faults are found in all major rock types throughout the LSC but are not as abundant as other brittle structures. Thrusts are mainly southwest-vergent, with a smaller northeast-vergent set (Figure 24). Most thrusts are subparallel to but crosscut or reactivate foliation and bedding (Figures 25). Slickenlines and slickenfibers range from down-dip to oblique, with more oblique slip generally occurring on shallower fault planes (Figure 24). Some thrusts contain several centimeters of gouge and fold foliation up to 2 meters on either side of the primary slip surface. Offsets are usually indeterminable, but where observed range from tens of centimeters to several meters. Some thrusts juxtapose different rock types and may accommodate greater offset (Figure 25). Thick vein deposits containing quartz, carbonate, and prehnite are common along the major slip plane. Thrust faults are seen most easily in argillaceous assemblages, where deformation is commonly distributed across a several meter wide zone with multiple slip planes and intense folding of fabric. Thrust faults in greenstone and metagreywacke outcrops generally slip on one discrete surface or within a centimeter- to decimeter-wide gouge zone.

Kinematics of Thrust Faults

The results of kinematic analysis of thrust faults show a general consistency of strain axes (Figure 24c). P-axes for thrust faults plot shallowly in the northeast and southwest quadrants. T-axes for thrusts are steeply plunging but not preferential to any one map direction and thus average to approximately subvertical.

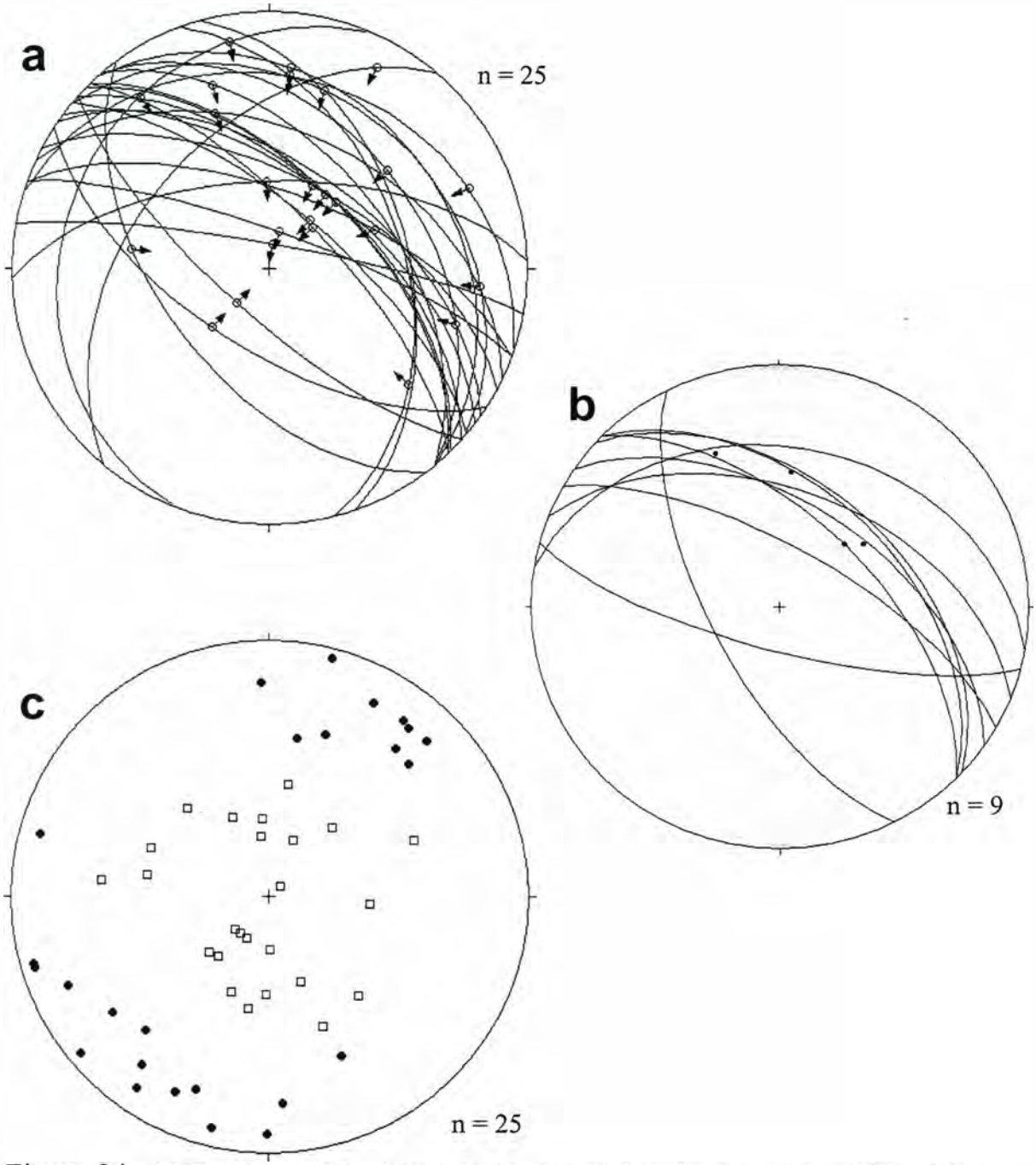

Figure 24: (a) Equal area plot of thrust faults in the LSC. Arrows show motion of the hanging wall. Most thrusts are southwest-vergent and subparallel to foliation. (b) Equal area plot of thrust sense faults with no slickenside data and faults without a reliable sense of slip but with a similar relative timing and orientation as other thrusts. (c) Equal area plot of strain axes from kinematic analysis of thrust faults in the LSC. P and T axes are filled circles and open squares, respectively. Thrusts are generally consistent with northeast/southwest shortening and subvertical extension.

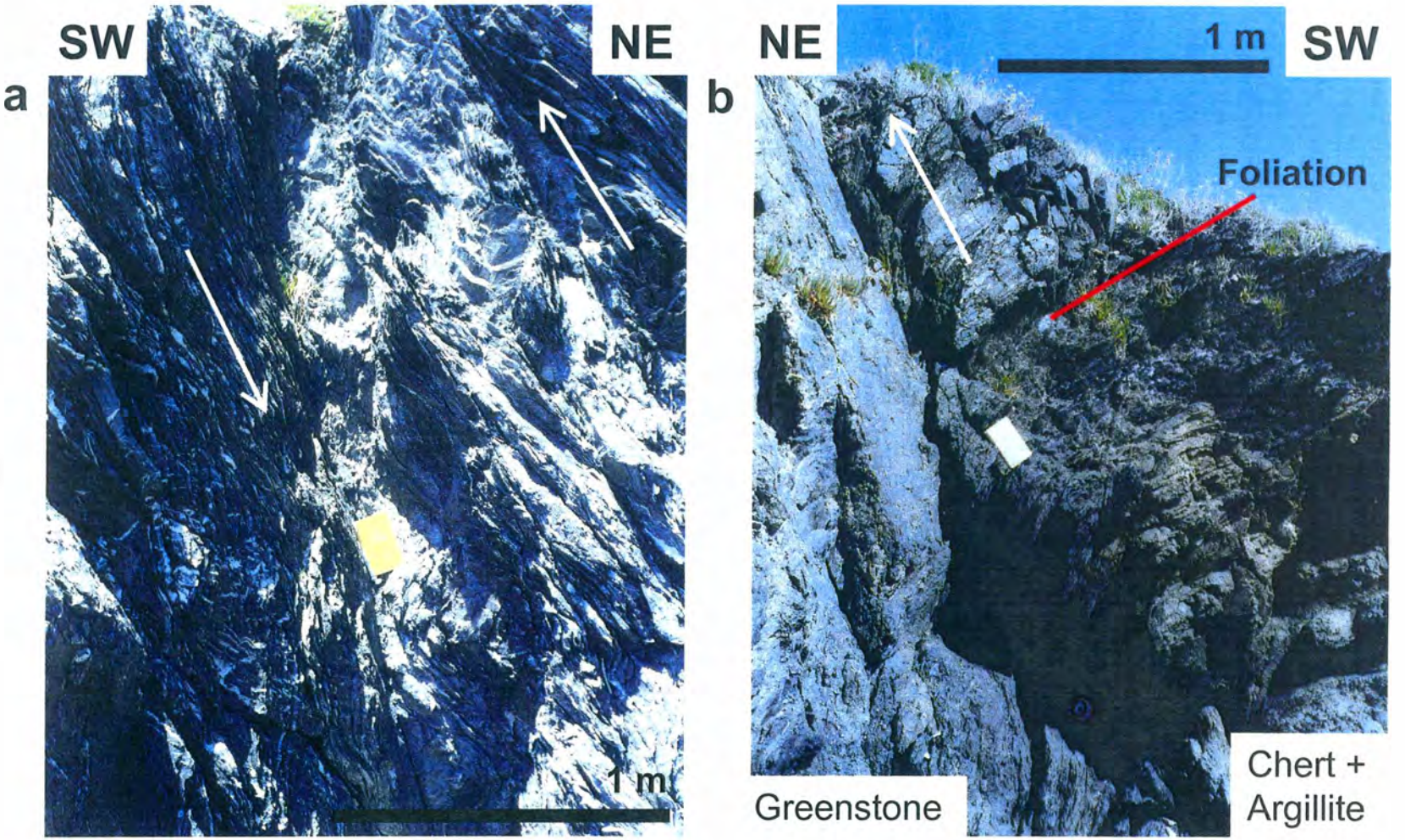

Figure 25: (a) A southwest-vergent thrust oriented subparallel to foliation in fine sandstone and argillite at Watmough Head. Field book for scale rests on main slip surface. (b) A northeast-vergent thrust at Colville Point crosscuts foliation and juxtaposes argillite-rich rocks atop a greenstone block. Arrows show sense of motion.

Extensional Structures

Extension Vein Sets

Extension vein sets are common and widespread in the LSC. These extensional structures cross-cut thrust faults (Figure 26a) and shear veins (Figure 21b). Extension veins are generally steep to subvertical and strike mostly northeast or southwest (Figure 27). Other orientations are present but much less common. Mutual cross-cutting relationships in many locations indicate all orientations were probably active at once. Veins range in size from 0.5 to 2 cm wide and 10 cm to 1 meter long, but most are approximately 1 cm wide and 0.5 meters long (Figure 26b). The majority of sets include 10 to 15 veins, but some include as few as 3 or as many as 20 veins. Extension veins are especially abundant in the metagreywacke and greenstone lenses, but are also commonly found in argillaceous units.

Vein mineralogy generally correlates with host rock composition, which suggests vein sets were at least partially filled with locally derived precipitate. Quartz-rich veins are found in metagreywacke- and chert-dominated sequences. Carbonate veins are common in greenstone blocks and argillite-rich zones. Most extension veins, however, contain at least a small amount of quartz, plagioclase feldspar, prehnite, as well as calcite and/or aragonite. Because of this association between veins and host rock chemistry, extensional vein fibers preserved near the vein walls are almost exclusively syntaxial (Figure 28). However, the fibers only rarely continue far into or through the vein. Most of the vein consists of relatively large, subequant quartz or carbonate grains that generally increase in size towards the vein center (Figure 28). This change in grain shape and the presence of relict vein boundaries within some vein interiors (Figure 28b)

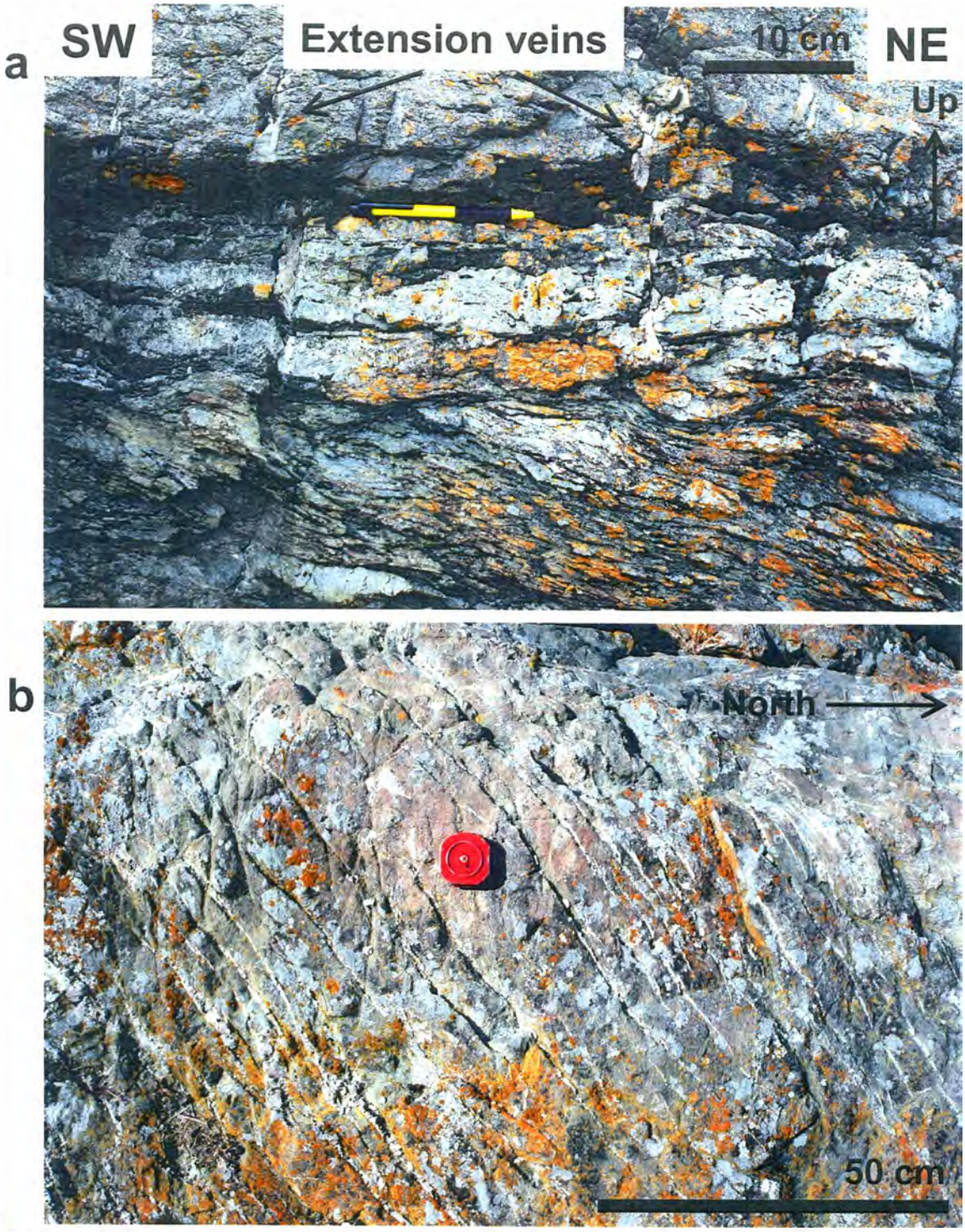

Figure 26: (a) Extension veins crosscut a thrust contact and associated fault vein at Colville Point. Pencil sits on the contact. Veins continue from the metagreywacke through the fault vein but generally end inside the fault gouge below. (b) A typical extension vein set in metagreywacke near Iceberg Point. Veins strike northeast/southwest. Outcrop surface is subhorizontal.

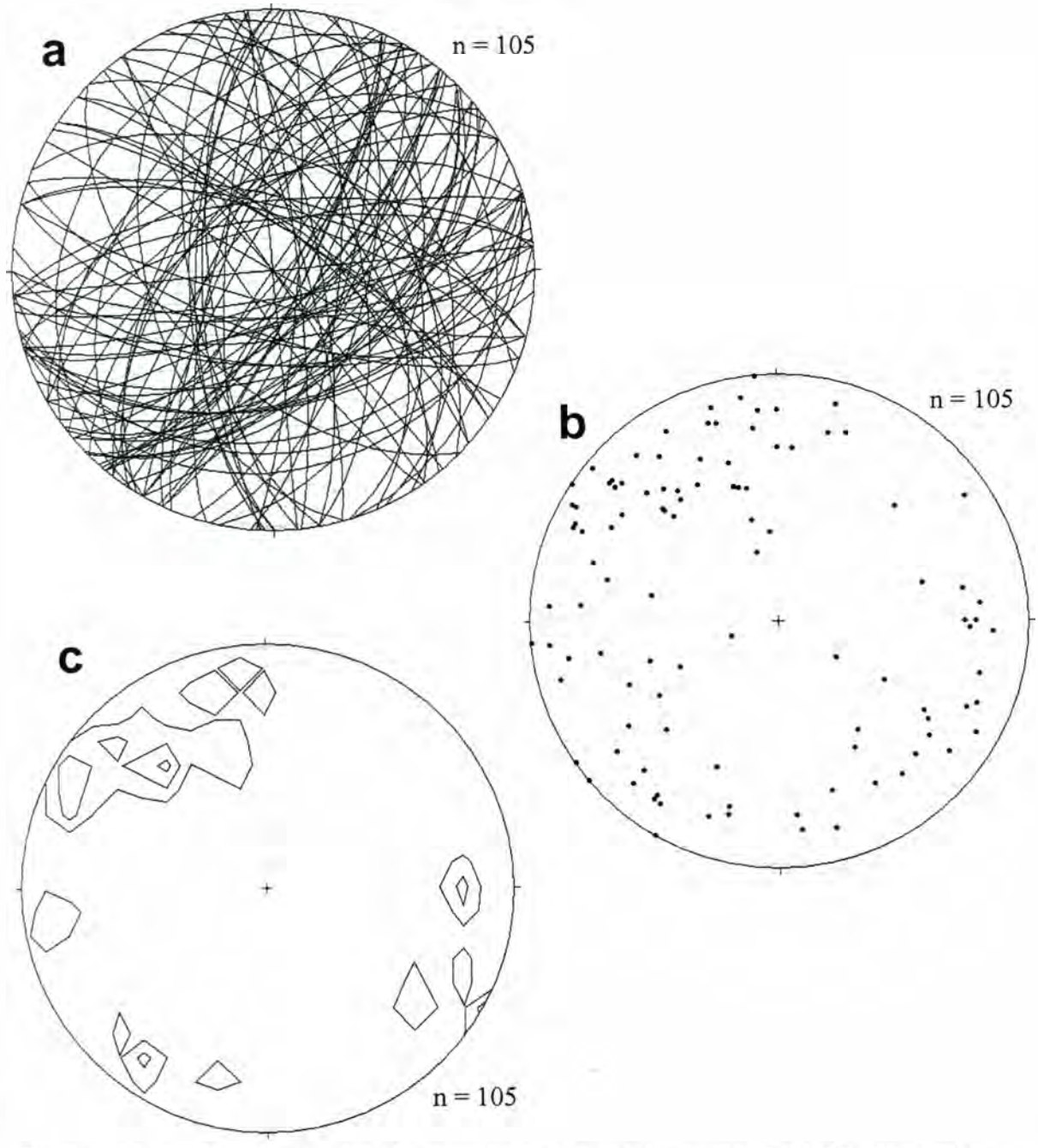

Figure 27: (a) Equal area plot of extension vein sets from across the LSC. Most veins strike northeast/southwest or north/south. (b) Poles to extension veins mostly plot shallowly in the northwest and southeast quadrants. Other poles are spread around horizontal. (c) 1% area contour plot of poles to extension veins. Contour interval is 2%. Poles are interpreted to represent the maximum extension direction for each vein set. Extension veins are generally associated with northwest/southeast extension.

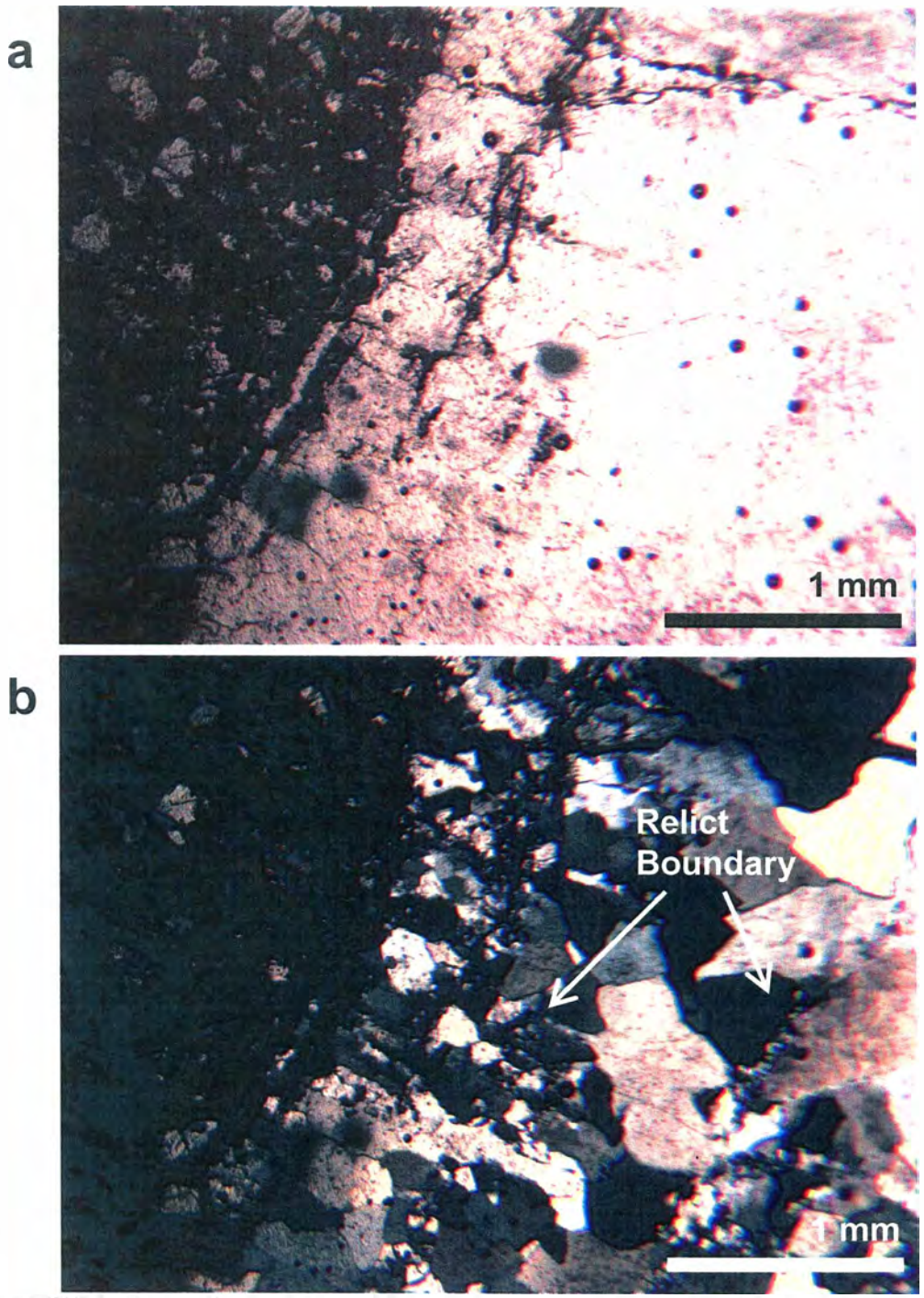

Figure 28: Thin section photographs of an extensional quartz vein from a metagreywacke outcrop. At the vein walls, small syntaxial fibers of quartz extend from the boundary towards the vein center. However, most of the vein body is composed of large, subequant quartz grains. Under cross polars, thin zones of debris are visible. These zones probably represent previous vein-wall rock contacts. Taken in (a) plane polarized light and (b) cross polarized light.

suggests that the majority of material was precipitated by crack-seal processes in one or several dilational events. The preservation of microstructures related to vein formation precludes the possibility of widespread vein recrystallization.

Normal Faults

Normal faults, while less abundant than extension vein sets in the LSC, are still very common and widespread throughout all rock types. Normal faulting post-dates thrust faulting (Figure 29a) and extension veining, but these structures also strike mostly northeast and southwest (Figure 30). Slickenlines on fault surfaces and slickenfibers in vein material within faults indicate mostly dip-slip motion, but many measured faults also accommodated a small component of lateral motion. Northeast and southwest striking faults are more common than other orientations by a ratio of approximately 4:1. There is no consistent relative timing difference between orientations, so they may have all formed contemporaneously. Normal faults occur at regularly spaced intervals of approximately 10 meters or less at many places. This spacing appears most consistent within coherent metagreywacke and greenstone lenses. Observable offsets range from decimeter to meter scale (Figure 29). Most normal faults contain carbonate or quartz-bearing vein material which is deposited along the main slip plane. Some possibly larger slip systems contain fault gouge as well and deform the surrounding foliation more significantly.

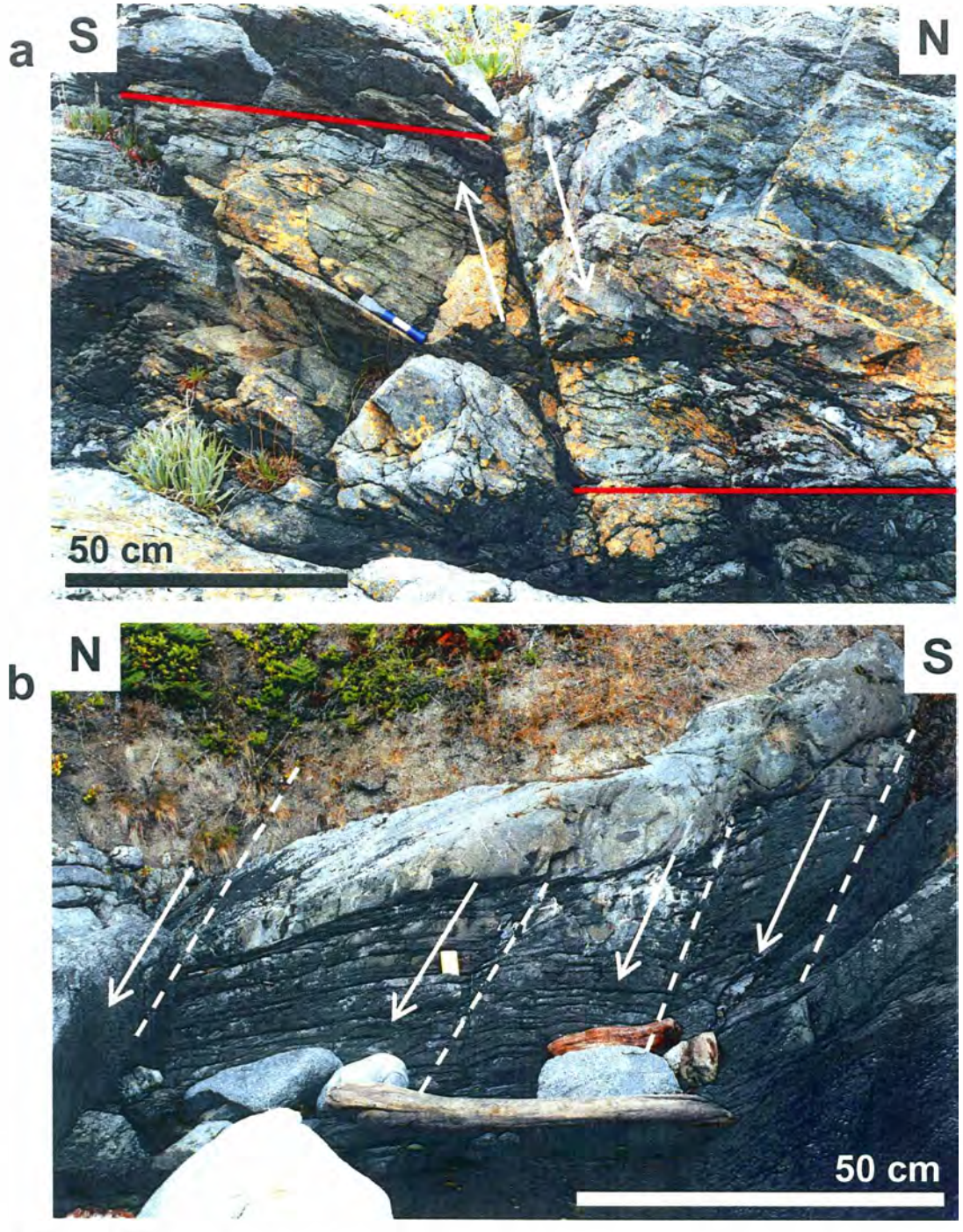

Figure 29: (a) A top-to-the-north-northeast normal fault offsets a thrust contact and associated fault vein (highlighted in red) by ~ 1 meter at Colville Point. Arrows show sense of motion. Chisel for scale. (b) A top-to-the-north normal fault system crosscuts and drags graded bedding and foliation at Shark Reef. Arrows show sense of motion along several subsidiary planes.

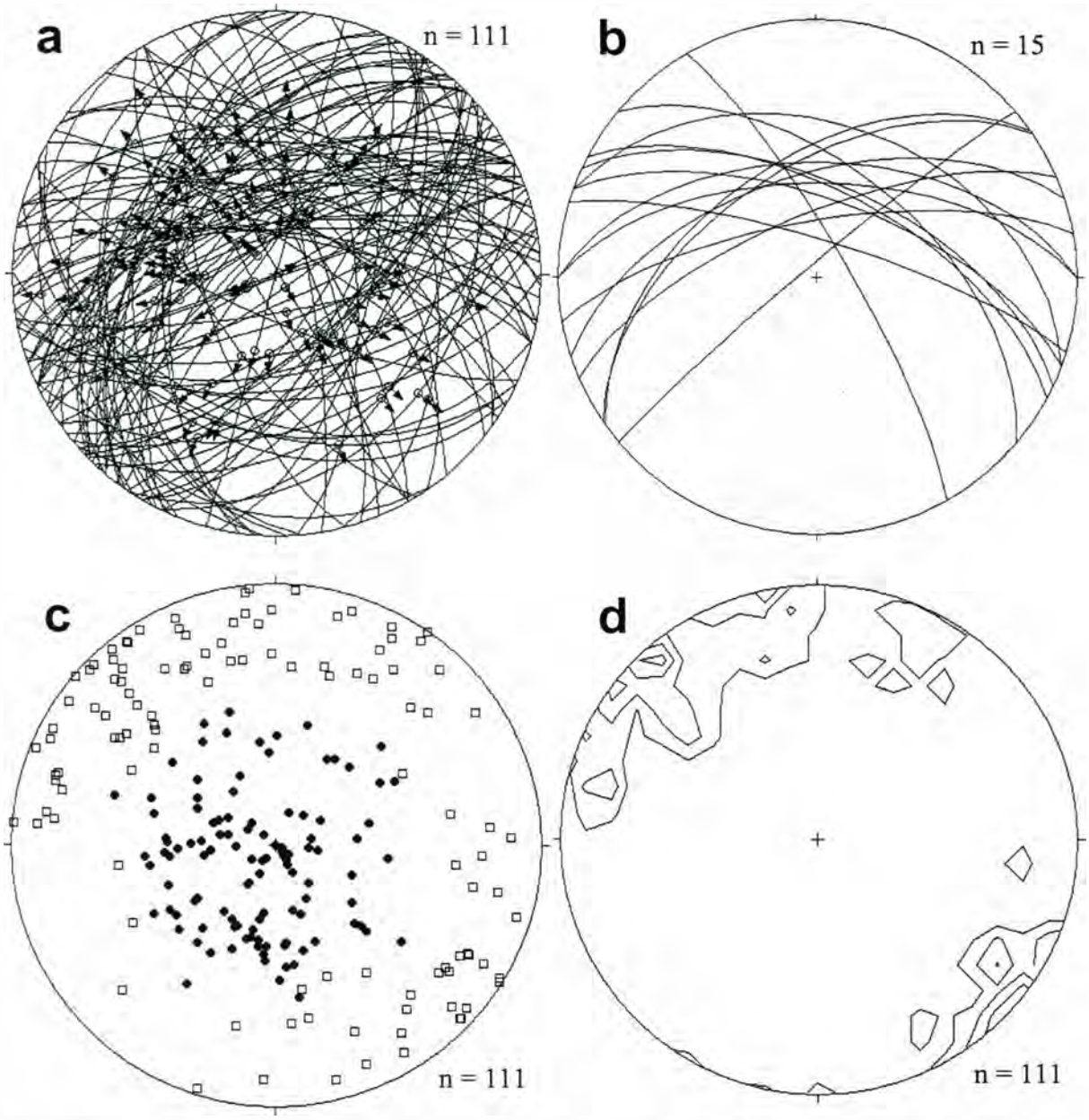

Figure 30: (a) Equal area plot of normal fault planes in the LSC. Normal faults most commonly strike northeast and southwest. Other orientations exist but are less abundant. (b) Equal area plot of probable normal faults without measurable striae. Grouping is based on a normal slip sense and similar orientation and character to other normal faults. (c) T axes of normal faults (hollow squares) cluster visibly in the northwest and southeast quadrants, but also spread around horizontal. P axes (filled circles) are subvertical. (d) 1% area contour plot of normal fault T axes. Contour interval is 2%.

Kinematics of Extensional Structures

Results of kinematic analysis of extension vein sets and normal faults suggest that the two types formed under very similar kinematic regimes. The maximum extension direction for an extension vein set is perpendicular to the vein plane (Price and Cosgrove, 1990). Poles to extension veins in the LSC trend primarily shallowly northwest/southeast (Figure 27b). The remainder of poles spread about the subhorizontal plane. Kinematic analysis of normal faults shows T-axes mostly plunge shallowly to the northwest and southeast with a smaller group spread around horizontal (Figure 30c). Thus, principal extension directions for extension veins and normal faults are approximately the same. The apparent spread of subhorizontal extension axes and overlap in timing of all orientations of veins and normal faults suggests that subvertical shortening may have been a dominant process during formation of these structures. The extensional structures would act to spread material outward horizontally with a preference to the northwest and southeast.

Conjugate Strike-slip Structures

En Echelon and Sigmoidal Vein Sets

Sigmoidal and en echelon vein sets are comparable in size to extension vein sets but are much less common, relatively younger (Figure 31a), and are observed to define shear zones. Data collection was restricted to sets observed in three dimensions in order to accurately constrain shear zone orientation. For representation and analysis of en echelon vein sets, the shear zone slip vector was calculated by plotting the orientation of

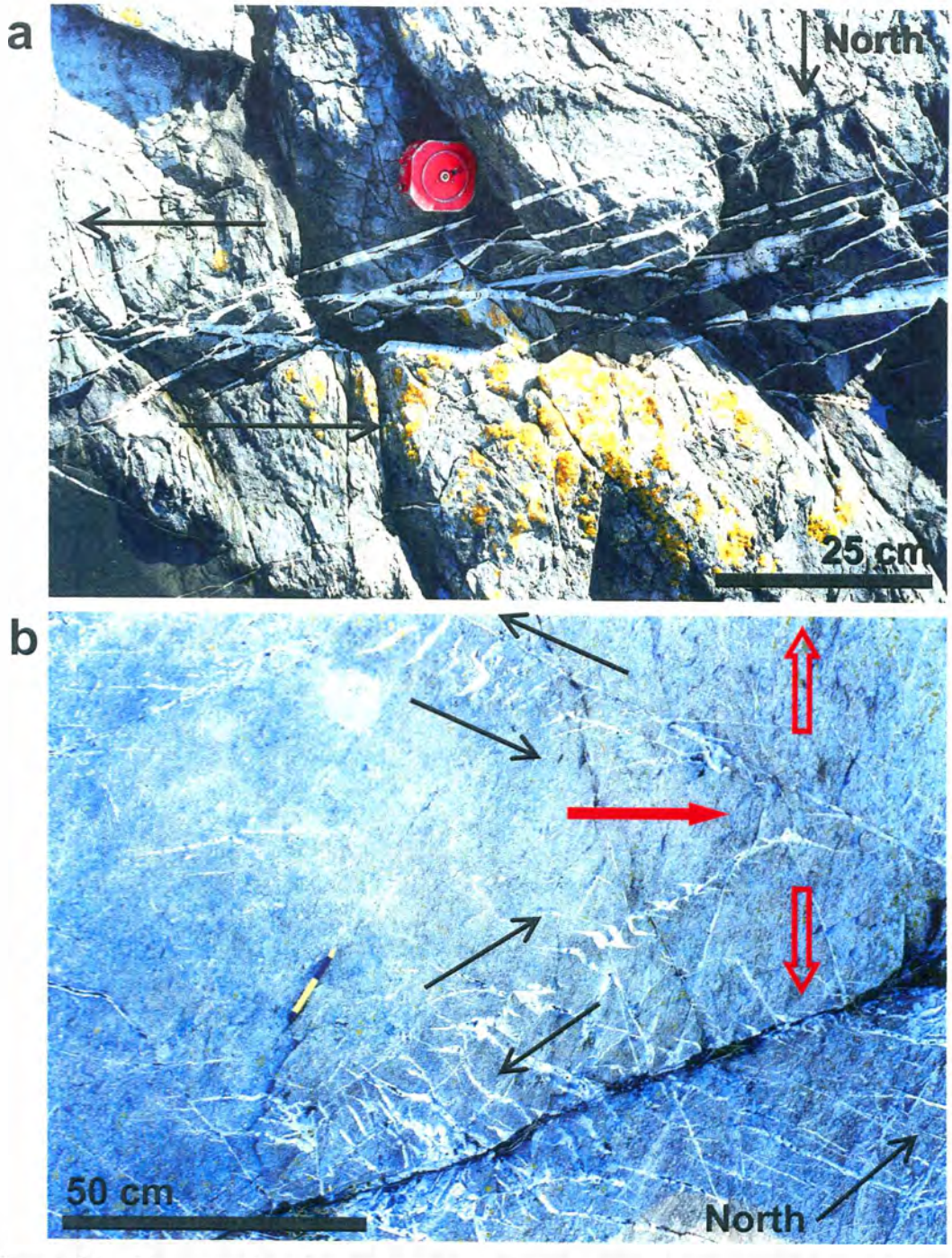

Figure 31: Photographs of en echelon and sigmoidal vein sets. (a) An en echelon set crosscuts extension veins in metagreywacke near Iceberg Point. Arrows show sense of shear. Outcrop surface is horizontal. (b) Two sets of sigmoidal veins in metagreywacke at Cattle Point. The vein sets show opposite sense (black arrows) but form a conjugate pair consistent with northwest/southeast extension (red arrows). Yellow pencil aligned with trace of fabric. Outcrop surface is horizontal.

vein tips and shear zone. The slip vector lies 90° along the great circle of the shear zone from the intersection with the vein tips. En echelon vein sets occur in two main orientations that can form subvertical conjugate sets (Figure 31b); shear zones for the right-lateral sets generally strike north/south or northeast/southwest while shear zones for the left-lateral sets strike east/west or northwest/southeast (Figure 32). However, data on these structures are sparse and relatively inconsistent. Sets usually include 5 to 10 veins which are on average 1 cm wide and 30 to 50 cm long. Measured in the horizontal plane, subvertical en echelon shear zones range in size from 25 to 50 centimeters wide and 0.5 to 2 meters long. En echelon vein sets contain primarily quartz and occur almost exclusively in metagreywacke lenses.

Strike-slip Faults

Strike-slip faults are found in all rock types throughout the LSC. They are interpreted to be the latest widespread structure because they consistently crosscut extensional structures (Figure 33a) as well as en echelon vein sets. Strike-slip faults occur in two approximately conjugate populations of steeply dipping faults. Cross-cutting relationships indicate no significant difference in relative timing of formation between the two groups, although they are not usually observed to be associated in outcrop. Left-lateral faults generally strike east/west and right-lateral faults generally strike north/south (Figure 34). Slickenlines from both groups of strike-slip faults are typically subhorizontal but can vary to 40° rake. Both dip-slip and strike-slip slickenlines

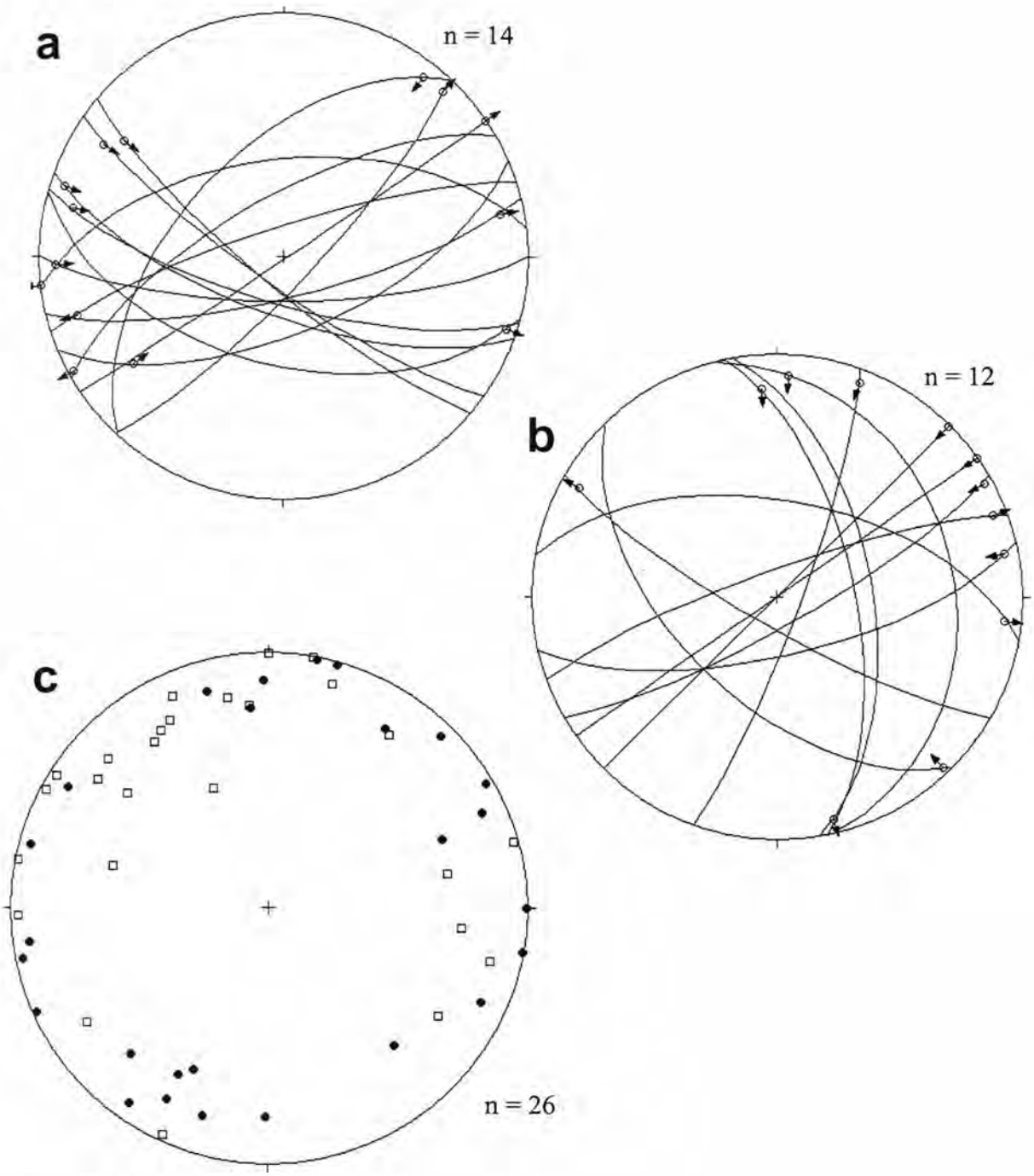

Figure 32: (a) and (b) Equal area plots of left-lateral and right-lateral en echelon vein sets. Left lateral sets most commonly strike east/west or northwest/southeast. Right-lateral sets mostly strike north/south or northeast/southwest. (c) Equal area plot of P and T axes for en echelon vein sets. T axes cluster loosely to the northwest and southeast. P axes cluster loosely to the northeast and southwest.

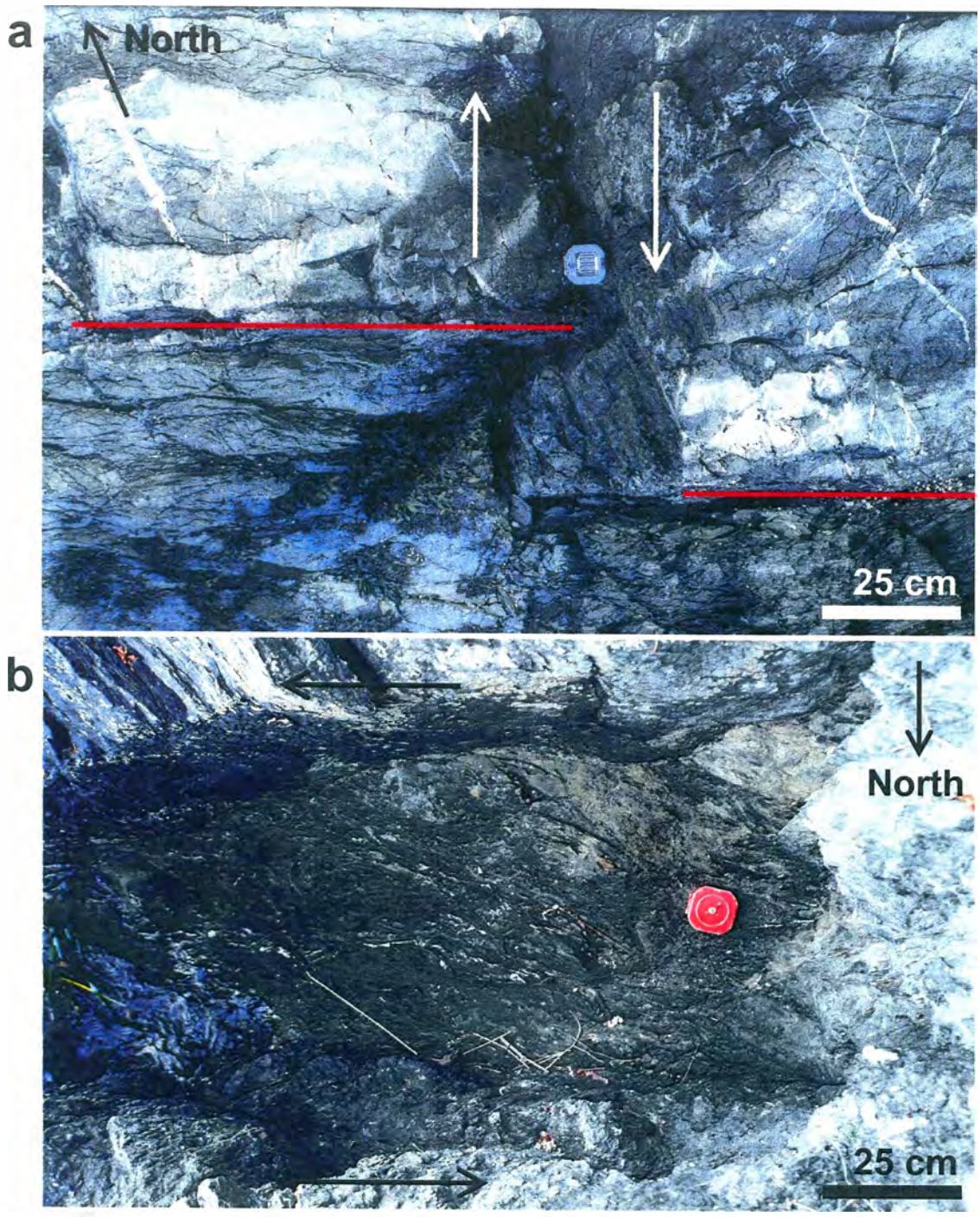

Figure 33: Photographs of strike-slip faults. (a) A discrete strike-slip fault in greenstone near Cattle Point offsets a steep normal fault (highlighted in red) surface by ~ 0.3 meters. The subvertical right-lateral fault strikes north-northeast. Outcrop surface is horizontal. (b) An example of a large strike-slip fault zone in metagreywacke at McArdle Bay with ~ 0.5 meters of gouge between two slip surfaces. Sense was interpreted as left-lateral from drag of gouge. Arrows show sense of motion. Outcrop surface is horizontal.

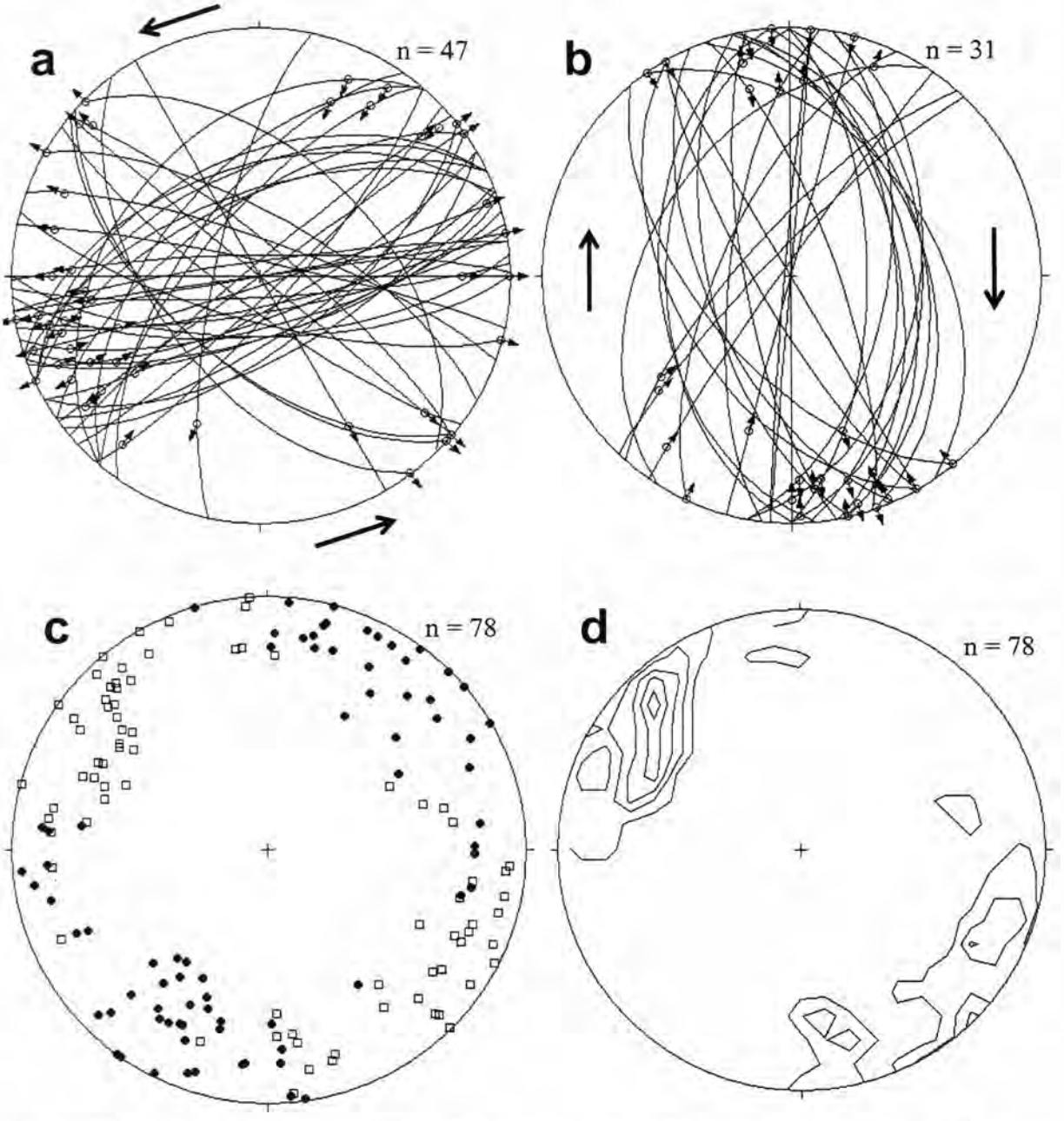

Figure 34: Equal area plots of (a) left-lateral and (b) right-lateral late strike-slip faults. Left-lateral faults on average strike approximately east/west. Right-lateral faults strike approximately north/south. Bold arrows show sense of motion. (c) Equal area plot of P and T axes for late strike-slip faults. Note both right and left-lateral faults are consistent with northwest/southeast extension and northeast/southwest shortening. (d) 1% area contour plot of T axes for late strike-slip faults. Contour interval is 2%.

can be found on many fault planes, which indicates strike-slip deformation reactivated some normal fault surfaces.

Most strike-slip fault planes are small and relatively discrete with thinner gouge zones compared to the generally more significant thrusts and normal faults. However, rare large strike-slip faults with substantial gouge do exist in the LSC (Figure 33b). Observable offsets on strike-slip faults range from ~ 10 centimeters to several meters, but a majority of offsets are approximately 0.5 - 1 meter in size. No consistent spacing of faults is observed as with normal faults, except where several adjacent normal fault planes are reactivated as strike-slip faults. Multiple faults are seen in close proximity to one another in many locations, though, especially in metagreywacke and greenstone outcrops.

Kinematics of Strike-slip Structures

Kinematic analysis verifies that strike-slip faults are regionally consistent and effectively conjugate. T-axes for right-lateral and left-lateral strike-slip faults cluster shallowly to the northwest and southeast, while P-axes cluster shallowly to the northeast and southwest (Figure 34c, d). Data on en echelon shear zones are sparse and much more inconsistent, but the two generally conjugate orientations are also kinematically compatible with approximately northwest/southeast extension. Most T-axes plot shallowly in the northwest or southeast quadrants while P-axes cluster loosely to the northeast and southwest (Figure 32c). The loose clustering of P and T axes when right and left-lateral faults and vein sets are plotted together indicates that most of these are

effectively conjugate, even if they are rarely seen as such in outcrop. Thus, late strike-slip deformation in the LSC did not accommodate unidirectional shear but is indicative of continued subhorizontal northwest/southeast extension and renewed northeast/southwest shortening of the region.

Brittle Structures in Adjacent Terranes

Structural data were collected in the three adjacent terranes for comparison with the relative timing and kinematics of deformation in the LSC. See Figure 7 for site locations. Results by location and structure are summarized in Appendix B. A comparable deformational sequence in similarly oriented meter-scale structures was observed in the Constitution terrane structurally below the LSC as well as in the Lummi Formation and Obstruction Formation, components of the Ocean Floor Complex, structurally above the LSC. At the location within the Fidalgo Complex, though, structural orientations are possibly inconsistent with the LSC. Rocks in this location may have been rotated with respect to the LSC after strike-slip faulting, but the data are too few to provide an estimate of rotation magnitude or evaluate whether the site was simply subject to localized variation during faulting. Alternatively, events that produced the structures in the Fidalgo Complex may be unrelated to the accretionary prism deformation seen in rocks of the LSC, Ocean Floor Complex, and Constitution terrane. The small amount of data available for analysis from each location prevents any significant comparison to the orientation of late structures in the LSC, but the existence of an identical structural sequence in all adjacent terranes verifies that late brittle

deformation is widespread throughout much of the San Juan Islands and is not only the result of localized deformation in the LSC.

Structural and Kinematic Summary

The relative timing, orientations, and kinematics of each structural group found in the LSC are summarized in Table 1. Preserved but folded and boudinaged structures include sedimentary and volcanic layering and early vein sets. Regional fabric was possibly formed by two deformational processes; pressure solution in coarse clastic rocks, and bi-directional foliation-parallel shearing in thin mudstone-rich zones and along boudin contacts in argillaceous rocks. Several cataclastic zones are located at major terrane boundaries. These large fault zones also predate the remainder of brittle structures. The earliest group of brittle structures includes bedding-parallel slip, rare strike-slip shear veins, and local strike-slip faults. Southwest-vergent thrusts produced in a contractional stage are crosscut by widespread extension vein sets and normal faults. Conjugate strike-slip faults and en echelon vein sets are the latest brittle structures seen in the LSC.

The change in kinematics over time records a local progression within the study area from flattening and contraction to extension-related deformation. The pervasive pressure solution fabric accommodated coaxial flattening with a maximum shortening direction that plunges moderately to the southwest. Bi-directional noncoaxial deformation in fine layers accomplished lateral northwest/southeast extrusion of material and is reasonably associated with the regional flattening event. Early strike-slip structures indicate northwest/southeast shearing by brittle deformation. Calculated P and

T axes for the remaining stages of brittle deformation show: 1) northeast/southwest shortening and subvertical extension, 2) subhorizontal extension mostly to the northwest and southeast coupled with subvertical shortening, and 3) continued northwest/southeast extension and a return to northeast/southwest subhorizontal shortening.

Stage	Structure	Orientation	Kinematics
Fabric Formation	*Coarse clastics*: Pressure solution foliation	Strikes ~ NW, dips moderately to the NE	*Flattening:* S3 plunges moderately to shallowly SW, extrusion NW/SE
	Argillite-rich rocks: Pressure solution foliation and bi-directional shear zones	Strikes ~ WNW, dips moderately to steeply NE, subhorizontal slickenlines in foliation	
	Large fault zones: Cataclastic foliation, pressure solution foliation?	Strikes ~ NW, dips moderately to the NE, variable lineation	-----
Early Strike-slip (Localized)	*Metagreywacke and Greenstone:* Strike-slip shear veins and faults, bedding slip	Strike ~ NW/SE, dips inconsistent, shallow slicks	NW/SE shearing (extrusion)
Contraction	Thrust faults	Strike ~ NW, dips moderately to steeply NE or SW	*P axes*: NE/SW *T axes*: subvertical
Extension	Extension veins	Strike ~ NE/SW, dip steep	*P axes:* subvertical
	Normal faults	Strike ~ NE/SW, dip moderate	*S1 + T axes:* NW/SE, spread subhorizontal
Conjugate Strike-slip	En-echelon veins	*Left-lat*: Strike E/W to NW/SE, *Right-lat:* Strike N/S to NE/SW	*P axes*: NE/SW
	Strike-slip faults	*Left-lat*: Strike ~ E/W, *Right-lat*: Strike ~ N/S	*T axes*: NW/SE

Table 1: Summary of structural orientations and kinematics for each stage of deformation in the LSC.

IV. P-T Conditions of Brittle Deformation

Introduction

For a tectonically complex and constantly evolving setting such as an accretionary prism, it is important to understand not only the kinematics of deformation but also the depth and temperature conditions at which this deformation occurs. By associating P-T conditions with late structures specifically, each kinematic stage can be related to an approximate depth and we can understand not only peak metamorphic conditions but also which processes are related to internal prism deformation and which occur during uplift of high pressure terranes. The significant amount of veining associated with all stages of brittle structures in the LSC provides an opportunity to study the pressure and temperature conditions related to each stage of brittle deformation.

Previous workers have documented high-pressure – low-temperature metamorphic minerals present in the fabric and in crosscutting veins in the San Juan nappes. Glassley et al. (1976) observed widespread and stably coexisting lawsonite, prehnite, pumpellyite, and aragonite in rock samples from locations across the San Juan Islands. All of these minerals are also found in deformed veins that are overprinted by foliation as well as undeformed veins that crosscut foliation (Brandon et al., 1988; Cowan and Brandon, 1994; Maekawa and Brown, 1991). However, no previous study has addressed the mineralogy in veins associated with widespread brittle faulting in the San Juan nappes.

Two techniques were used in this study to analyze the conditions of vein formation and post-vein deformation. X-ray diffraction, supplemented with petrographic observations, was used on carbonate-bearing veins to identify the high pressure polymorph aragonite as well as bulk vein mineralogy for each structural stage. Fluid inclusion analysis was performed on two inclusion populations, one water-bearing and one primarily methane-bearing, from two quartz vein samples to provide additional data on post-peak P-T conditions. The results of each technique are first discussed separately and then combined to construct a P-T path for rocks of the San Juan Islands.

Vein Mineralogy

X-ray Diffraction

Carbonate-bearing veins kinematically associated with each structural stage were collected to test for the presence of aragonite. Aragonite is generally indistinguishable from calcite in hand sample and thin section, but records a unique diffraction pattern. X-ray diffraction was performed on 69 powdered carbonate vein samples. Methods for sampling, laboratory analysis, and interpretation of diffraction patterns are provided in Appendix C.

Complete X-ray diffraction results by sample number and associated structure are shown in Table 2. Quartz and calcite are the most common minerals within veins of the San Juan Islands. Other minerals include aragonite, plagioclase, chlorite, and prehnite, in order of frequency of occurrence and approximate relative abundance estimated from diffraction patterns. Aragonite and prehnite are consistently found in deformed veins, as well as within most cross-cutting structures including thrusts, shear veins, normal faults,

	Sample #	Quartz	Calcite	Aragonite	Plagioclase	Chlorite	Prehnite
Deformed	OC06c	X	X		m	m	
Veins	**LP01b**	m	X	X			
	LP01c	m	X	m		m	
	LP09b	X	X	m		m	m
	LP10a	X	X	X		m	
	LO02a	X	X	X	m		
	LP36a	X	X	m		m	
	LP40b	X	X		X		
	SJ1c	X	X	X	m	m	
	LP45b	X	X				
	LP45c	X	X		X	m	m
	LP53e	X	X	X		m	m
Thrusts	**LP04c**	X	X	X	m		
	LP23a	X		m	m		m
	LP25a	X	X	X			
	LP34a	X	X	X	X		
	LP34b	X	X	X			
	LP53h	X	X	m	X	m	m
	LP57a	X	X			m	
Shear	**OC06b**	X	X	X	m	m	
Veins	**LP08d**	X	X	m	X		
	L001b	X	X	m	m	m	
	SJ2a	X	X	X	m	m	
	SJ3a	X	X	m	m		
	SJ4b	X			X	X	
	LP43a	X	X		m		
	LP51a	X	X	m		m	
	LP51b	X	X	X	X	X	
	LP53k	X	X	X		m	

Table 2: Full results of x-ray diffraction on carbonate-bearing veins by sample number and structure type. X = major component, m = minor component. Bold sample numbers indicate presence of aragonite.

	Sample #	Quartz	Calcite	Aragonite	Plagioclase	Chlorite	Prehnite
Extension	LP01a	X	X		X	m	m
Veins	**LP14a**	X	X	X	m		
	LP14b		X	X			
	LP16b	m	X				
	LP28b	X	X	X			
	LO02b	m	X	X			
	LP33a	X	X		m	m	
	LP34d	X	X		X		
	LP34e	X	X		m	m	
	LP38a	X	X			m	
	LP38b	X	X			m	
	SJ2b	X	X			X	
	LP42a	X	X	X			
	LP43b	X	m	X	m	X	m
	LP43c	X	X	X			
	LP52a	X	X			m	
	LP53b	X	X	X		m	X
	LP53c	X	X	X		m	m
	LP53d	m	X	X	m		
	LP19d	X	X	X		m	m
	LP25a	X	X	X			
Normal	**LP28a**	X	X	m	X		m
Faults	**LP41a**	X	X	X			
	LP48a	X	X	X		m	
	LP51c	X	X	X			
	LP52b	X	X			m	
	LP52c	X	X			m	m
	LP52d	X	X			m	
	LP53a	X	X			m	m
	SJ9a	X	X	X			
	SJ9b	X	X	X			
Strike-slip	LP09a	X	X			m	
Faults	LP31a	X	X			X	
	LP43e	X	X		X		
	LP48b	X	X			m	
	LP48c	X	X	X	m	m	m
	LP48e	X	X			m	
	LP48f	X	X			m	
	LP53i	X	X		X		

Table 2 (continued): Full results of x-ray diffraction on carbonate-bearing veins by sample number and structure type. X = major component, m = minor component. Bold sample numbers indicate presence of aragonite.

and extension veins. High pressure minerals are rare in veins associated with late strike-slip faults. The percent occurrence of aragonite in carbonate-bearing veins from each structure type is shown graphically in Figure 35. Aragonite occurrence in brittle structures is not restricted to one source terrane or rock type, but is found across the LSC (Figure 35).

Minerals in Thin Section

A petrographic survey of vein minerals was conducted to support and validate the results of x-ray diffraction. No additional minerals were found in thin section, and the relative abundances estimated from diffraction patterns are consistent with petrographic observations. As expected from preliminary field tests and diffraction results, quartz and carbonate are the major constituents in all stages of veining. It is common to observe both minerals in a given vein, though quartz is found principally in veins from metagreywacke lenses and carbonate in veins from metavolcanic lenses. Although no real attempt was made to distinguish calcite from aragonite in thin section, carbonate in some older vein sets exhibits multiple textural styles which may be associated with this mineralogical difference (Figure 36). One type occurs as anhedral carbonate mats containing many distinct grains revealed under cross-polarized light. The other type occurs as massive, euhedral to subhedral singular crystals with well defined borders and continuous twinning patterns. Because of its more chaotic appearance, smaller grain size, and sporadic occurrence within the massive grains, the first variety may represent carbonate material which was recrystallized from aragonite to calcite after re-entry into the calcite stability field during uplift. The second variety could represent the preserved

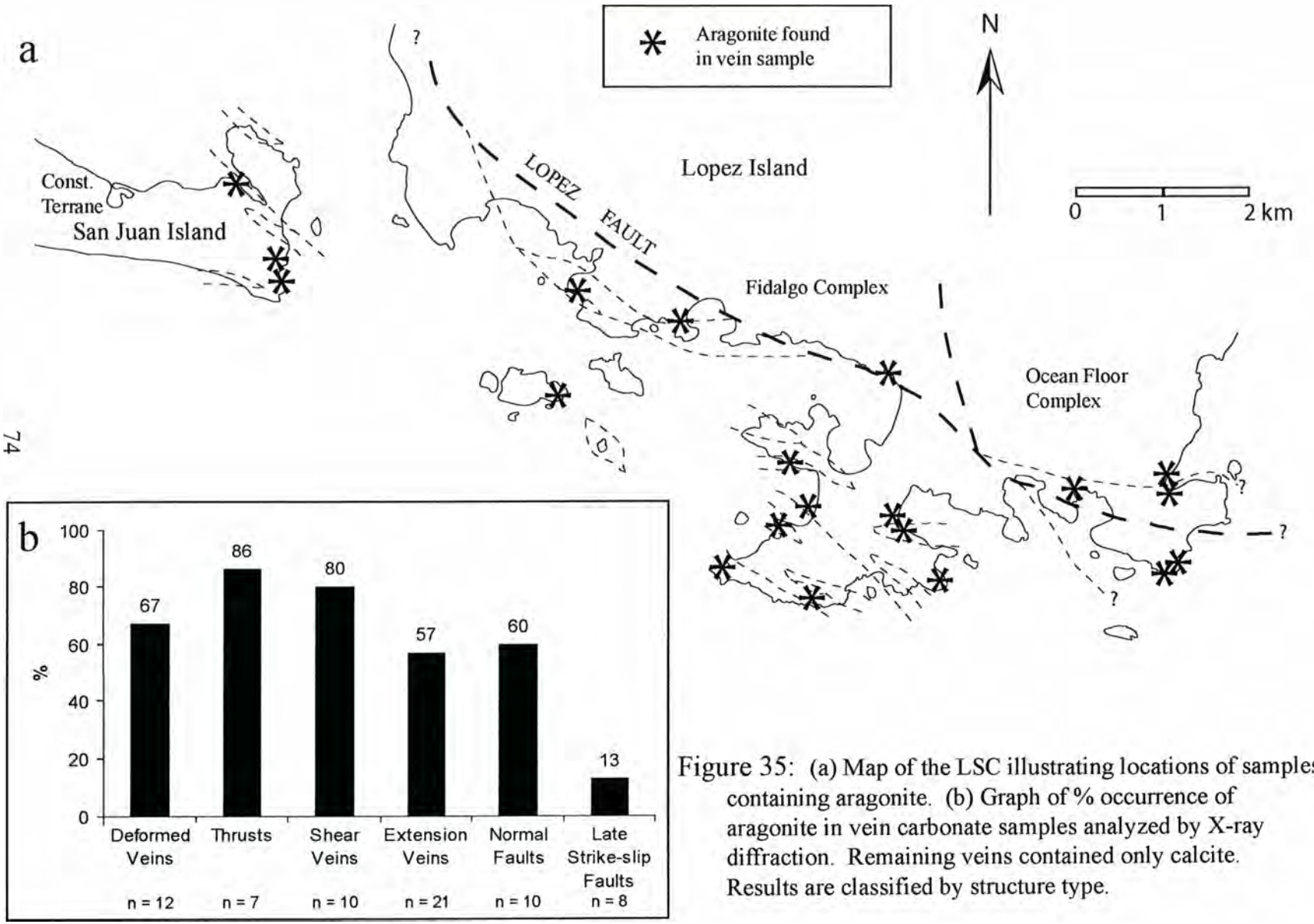

Figure 35: (a) Map of the LSC illustrating locations of samples containing aragonite. (b) Graph of % occurrence of aragonite in vein carbonate samples analyzed by X-ray diffraction. Remaining veins contained only calcite. Results are classified by structure type.

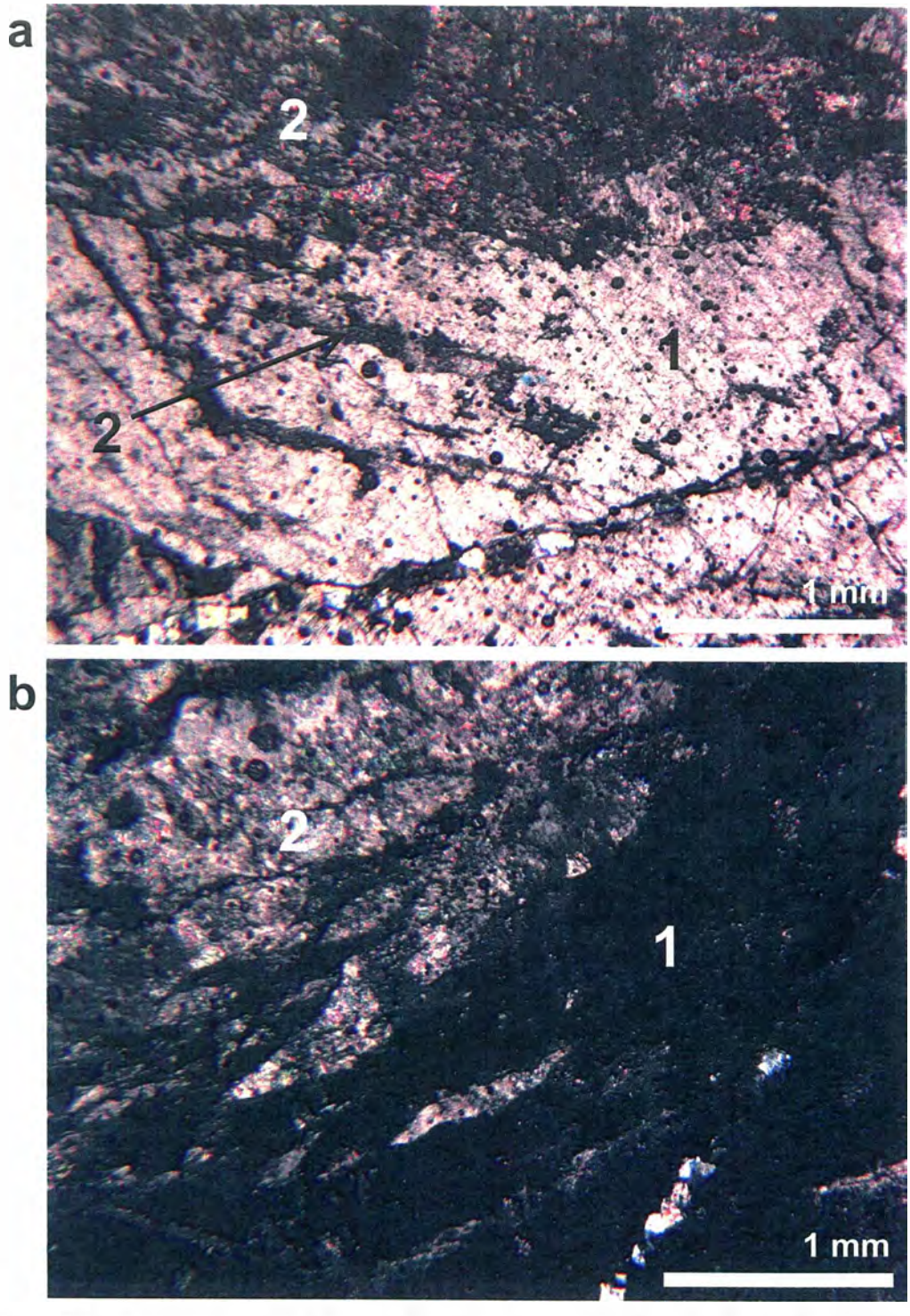

Figure 36: Two textural styles of carbonate in an aragonite-bearing vein. Taken under cross polarized light. A large single carbonate crystal ('1') at extinction in (b), is bordered by and encloses patches of carbonate mats ('2'). See text for discussion.

aragonite which is known from the results of x-ray diffraction to exist commonly in carbonate veins from the LSC.

Lesser vein constituents include feldspar, prehnite, and chlorite. Feldspar is identified to be mostly or wholly plagioclase, based on commonly observed albite twinning (Figure 37). This is consistent with diffraction results. Plagioclase is generally euhedral, relatively large grained, and almost exclusively found at vein walls, which indicates that it was precipitated early in the formation of a given vein set. Prehnite occurs as very fine grained fibrous mats or fine to coarse grained euhedral blades (Figure 37). Prehnite is thought to be a later overgrowth in previously precipitated vein material (Brandon et al., 1988). These overgrowths are generally either attached to the wall rock at vein edges or to wall rock inclusions within vein interiors.

The Significance of Aragonite

The presence and preservation of aragonite in veins of the San Juan Islands constrains pressure and temperature conditions during brittle deformation, while also restricting the P-T conditions during uplift. The pressure needed to crystallize aragonite is dependent on temperature. At temperatures of ~180 - 200° C, which correspond to peak metamorphic conditions estimated by Brandon et al. (1988), aragonite formation requires pressures greater than ~4.5 kilobars (Carlson and Rosenfeld, 1981). For structures containing aragonite, this corresponds to a depth of formation greater than or equal to ~ 18 kilometers (Figure 38). The crystallization of prehnite as an overgrowth (Brandon et al., 1988) requires lower pressures but generally higher temperatures. At its lowest possible crystallization temperature of ~200° C, prehnite occurrence in structures

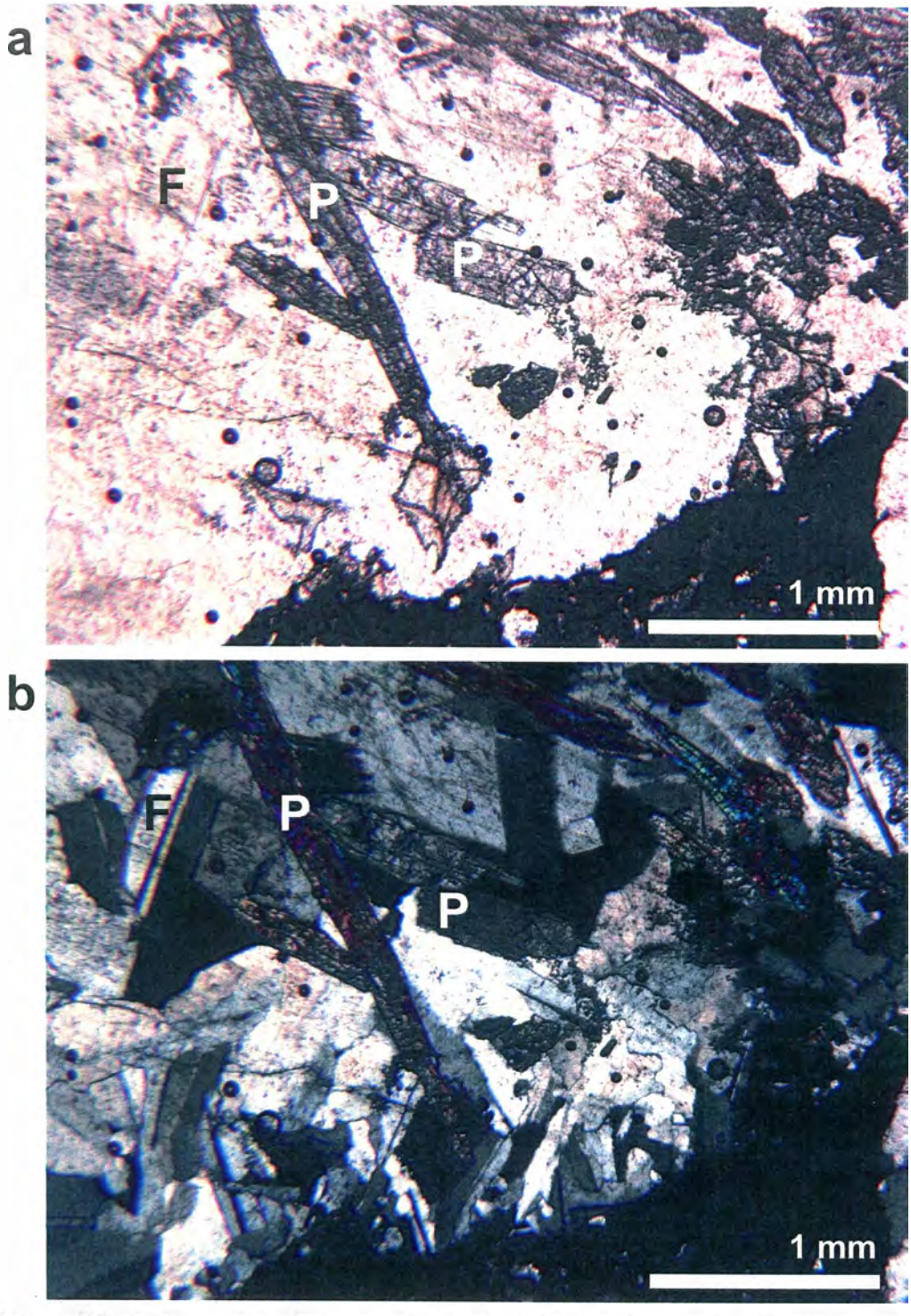

Figure 37: Thin section photographs of minerals in a shear vein. Taken under (a) plane polarized light and (b) cross polarized light. Albite twinning in plagioclase ('F') is visible under cross polarized light. Prehnite ('P') crystals are tabular and exhibit higher birefringence and relief than the surrounding quartz and feldspar.

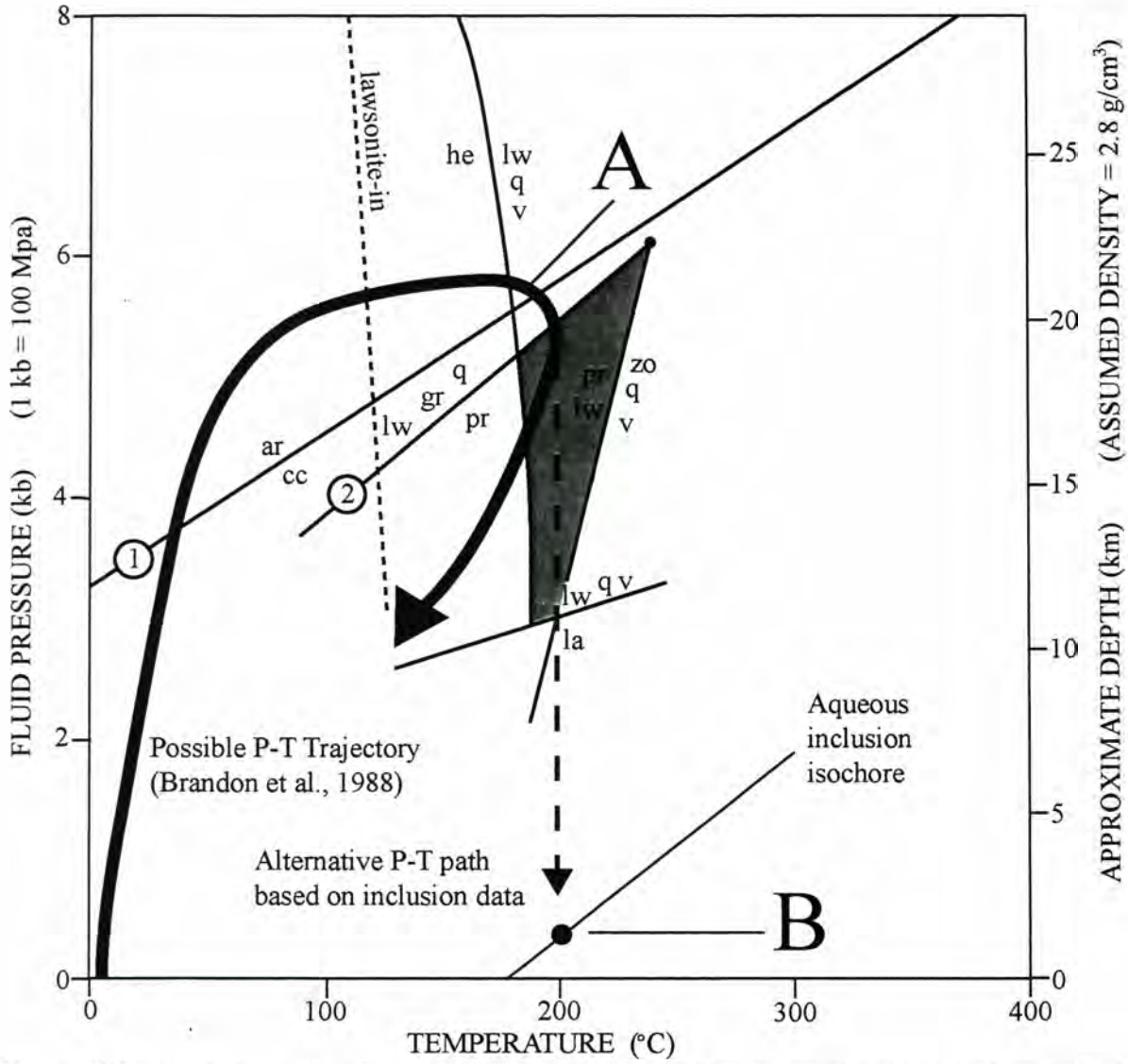

Figure 38: P-T information from the results of X-ray diffraction and fluid inclusion analysis are applied to current knowledge of the P-T path (bold line) experienced by the San Juan Nappes from Brandon et al. (1988). The shaded region corresponds to the stability range of prehnite + lawsonite + quartz. The crystallization of aragonite in brittle structures must have occurred near point 'A' above reaction 1, the aragonite/calcite transition. Prehnite overgrowth must have occurred after rocks entered the shaded zone (below reaction 2), but previous workers suspect this zone may overlap with reaction 1 (Glassley et al., 1976). Results of fluid inclusion analysis, although suspect, suggest aqueous inclusions were trapped at high temperatures but low pressures (~ point 'B') along the inclusion isochore. If accurate, the P-T path should be revised (bold dashed line) to reflect greatly reduced pressures but sustained temperatures during the majority of exhumation. Mineral abbreviations used: ar = aragonite; cc = calcite; lw = lawsonite; gr = grossular; q = quartz; he = heulandite; pr = prehnite; la = laumontite; v = vapor. Modified from Brandon et al. (1988).

of the LSC indicates formation at pressures greater than ~2 kilobars, or ~8 kilometers depth (Spear, 1993). Therefore, aragonite provides the higher pressure estimate, but the preservation of aragonite and later crystallization of prehnite in many veins has been noted by previous workers to constrain peak and post-peak temperature conditions to ~200° C (Figure 38) (Glassley et al., 1976; Brandon et al., 1988). In agreement with the low maximum temperature estimate, Carlson and Rosenfeld (1981) calculated that, for typical uplift rates of ~1 mm/year, aragonite reverts quickly to calcite if temperatures exceed ~200° - 220° C. Thus, the results of x-ray diffraction and petrographic observation indicate that most stages of faulting and veining were active at approximately peak metamorphic conditions while at a depth of at least 20 km, and that post-peak temperatures did not significantly exceed the temperature conditions present during brittle deformation at depth.

Fluid Inclusion Analysis

Introduction

A fluid inclusion is a micrometer-scale bubble of liquid and/or gas trapped within a mineral. In a vein, a fluid inclusion forms either as the mineral precipitates out of solution during initial vein formation (primary), or later as a result of localized precipitation during healing of microfractures (secondary) (Roedder, 1984). Small pockets of fluid become separated from the source liquid and are enclosed by the new mineral. The fluid inclusion represents a closed system which, if undisturbed, preserves the P-V-T relations at the time of entrapment. Therefore, two key assumptions must be adopted in order to use inclusions in determining source fluid composition and the P-T

conditions of entrapment (Roedder, 1984): 1) The inclusions were trapped from a homogeneous fluid and the portion trapped is indicative of the fluid on a larger scale. 2) Subsequent deformation has neither opened the system to leak material nor appreciably changed the volume of the inclusion. If studied correctly and within the context of a structural study, fluid inclusions provide a powerful tool to help constrain P-T conditions of deformation. They are also abundant in quartz, which makes them particularly well suited for this study.

Fluid inclusion assemblages from two quartz-bearing veins in the study area were analyzed to determine the conditions of inclusion entrapment and thus further constrain the P-T path of rocks in the San Juan Islands. Sample LP22b was taken from a steeply south-dipping extension vein set in metagreywacke at Colville Point. Sample LP07 was taken from a subvertical ~ N/S striking right-lateral sigmoidal vein set in Ocean Floor Complex metagreywacke at Hughes Bay, just north of the inferred trace of the Lopez Thrust and therefore structurally outside the LSC. Sample locations are shown on the site map in Figure A1. Procedures for selection of appropriate inclusion assemblages and heating/cooling analysis follow those discussed in Roedder (1984) and Goldstein and Reynolds (1994). Details on the methods of fluid inclusion analysis employed in this study are provided in Appendix D.

Results

Quartz grains in sample LP22b contain abundant two-phase inclusions which range from ~ 1 to 20 μm in length or diameter. Many lie along confined trails but some appear to be more isolated. A fluid inclusion assemblage is defined in this sample to

include all two-phase inclusions of varying size with similar vapor-to-liquid ratios of approximately 15 – 20% within one particularly clear quartz grain (Figure 39a). Initial observations during cooling runs indicate freezing of the liquid occurs at approximately 0° C, which is consistent with a water-dominant composition. Final melting temperatures (Tm) of ice in representative inclusions were recorded to determine actual fluid composition (Figure 39b). Melting occurs within the majority of inclusions at Tm = 0° C, and only one inclusion recorded a depressed melting temperature of Tm < -1° C. The sample was heated to determine total homogenization temperatures (Th) at which the vapor bubble dissipates completely and the inclusion becomes a single phase (Figure 39b). Homogenization temperatures range from Th = 177 to 206° C, but the majority of inclusions measured homogenize near Th = 180° C.

One quartz grain in sample LP07 contains a large number of single- and two-phase fluid inclusions of varying size and shape that were tentatively assigned to a single assemblage based solely on proximity and general appearance (Figure 40).
Initial cooling runs confirm these two types of inclusions are reasonably related. When cooled a few degrees from room temperature, vapor bubbles nucleate in the inclusions that have only one phase at room temperature and the two groups become indistinguishable. Cooling to near -200° C reveals the inclusions are methane-rich; evidence of freezing was observed below ~ -180° C and homogenization of the methane component to liquid occurred very near the pure methane phase transition temperature of Th_m = -82.6° C (Figure 41a; Goldstein and Reynolds, 1994). However, at least one additional unidentified gas component must be present, as a vapor bubble persisted through warming until total homogenization of the system was observed between

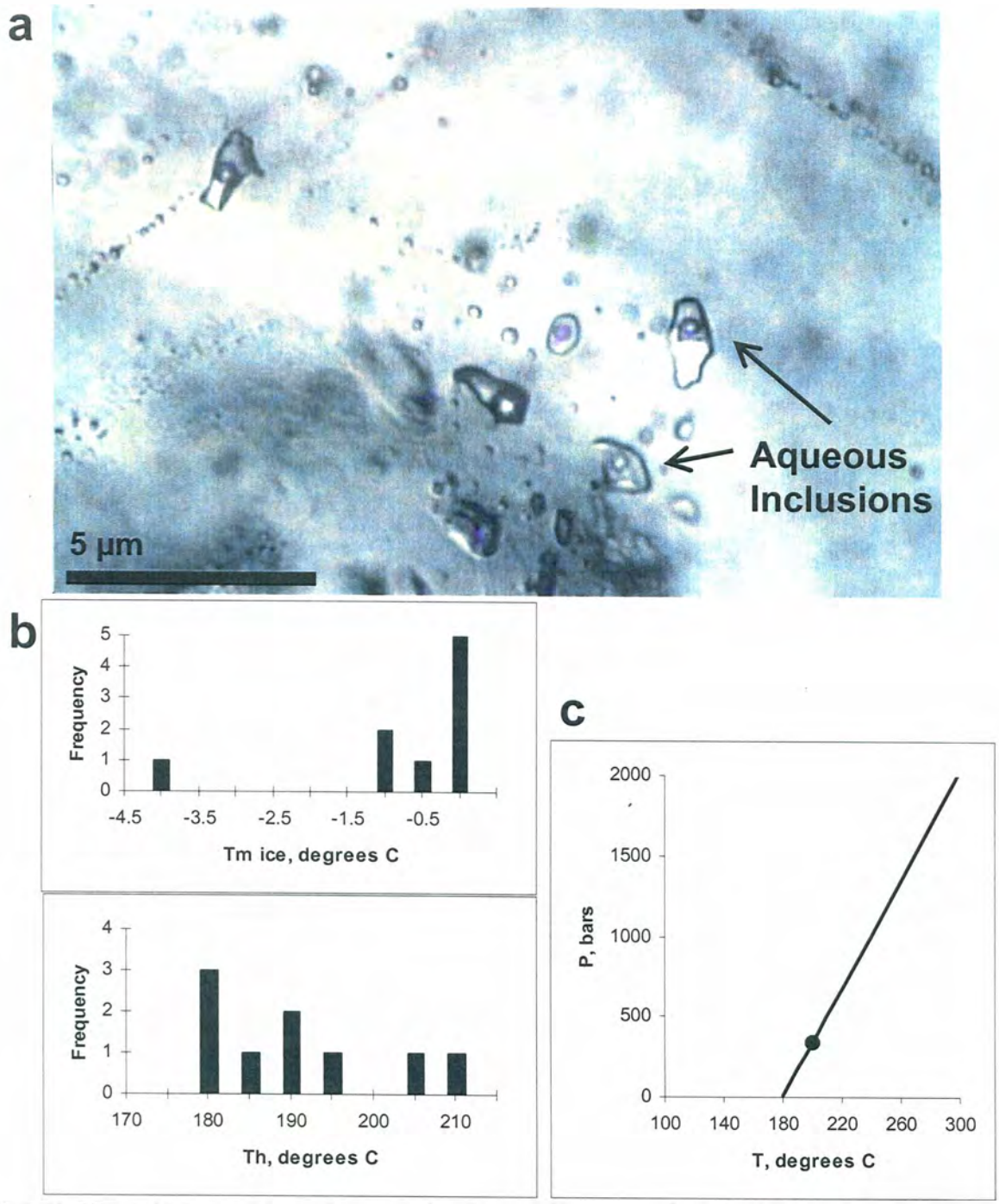

Figure 39: (a) Thin section photograph of several aqueous fluid inclusions in one quartz grain from sample LP22b. Taken at room temperature, inclusions contain a water vapor bubble that is on average 20% of the total inclusion volume. (b) Histograms showing results of freezing and heating analysis of aqueous inclusions. Tm = final melting temperature of ice. Th = total homogenization temperature. (c) P-T plot with the isochore constructed from representative homogenization data. Trapping conditions should plot along this line of constant volume. The dot marks a temperature value of ~200° C.

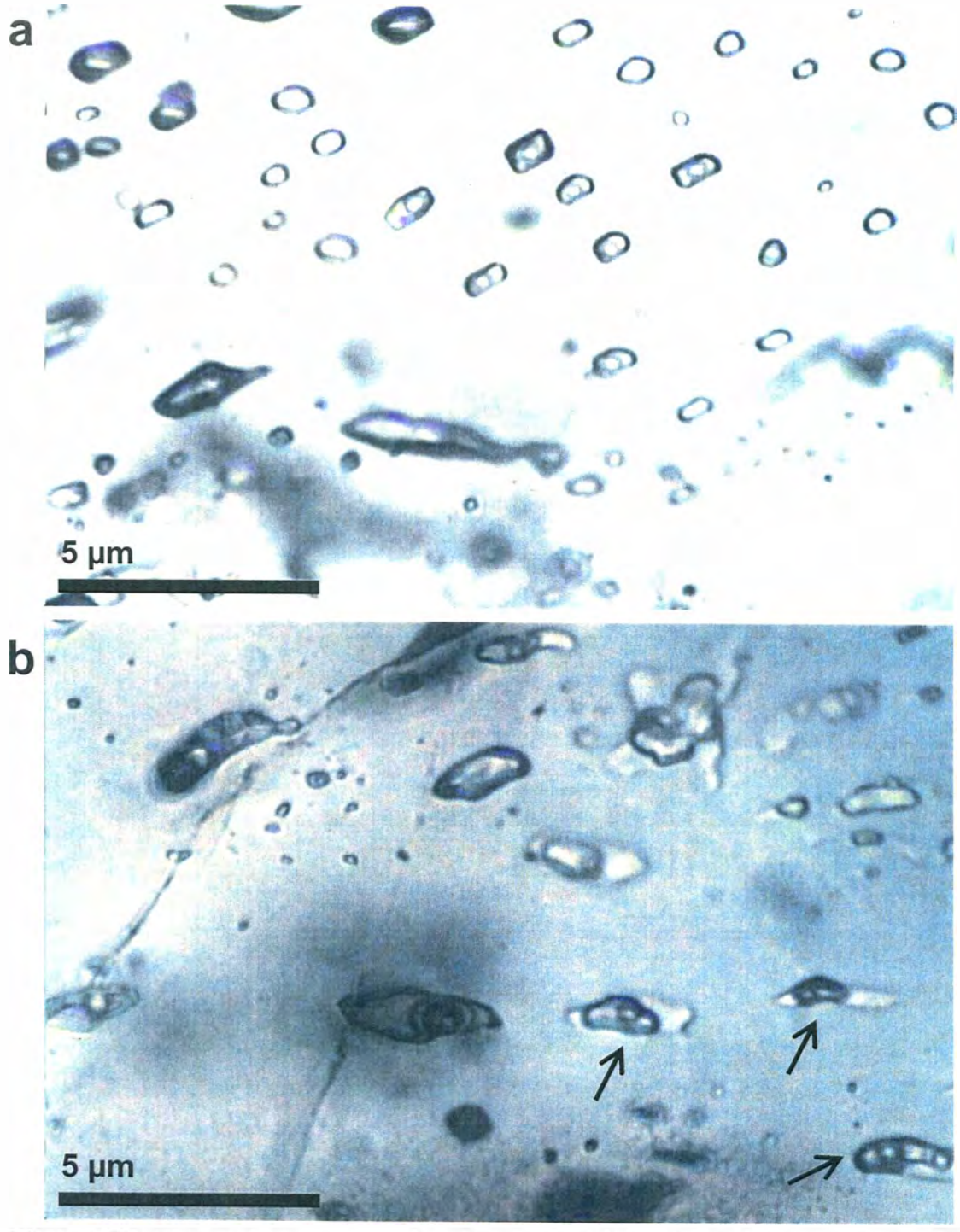

Figure 40: Thin section photographs of methane-rich inclusions in a quartz grain from sample LP07. (a) At room temperature, some inclusions contain a liquid and a gas bubble. Others contain only one phase until cooled. (b) At -90° C, methane-rich inclusions contain two bubbles, one of which contains methane gas. The inner bubble dissipates when the sample is heated to above ~ -80° C.

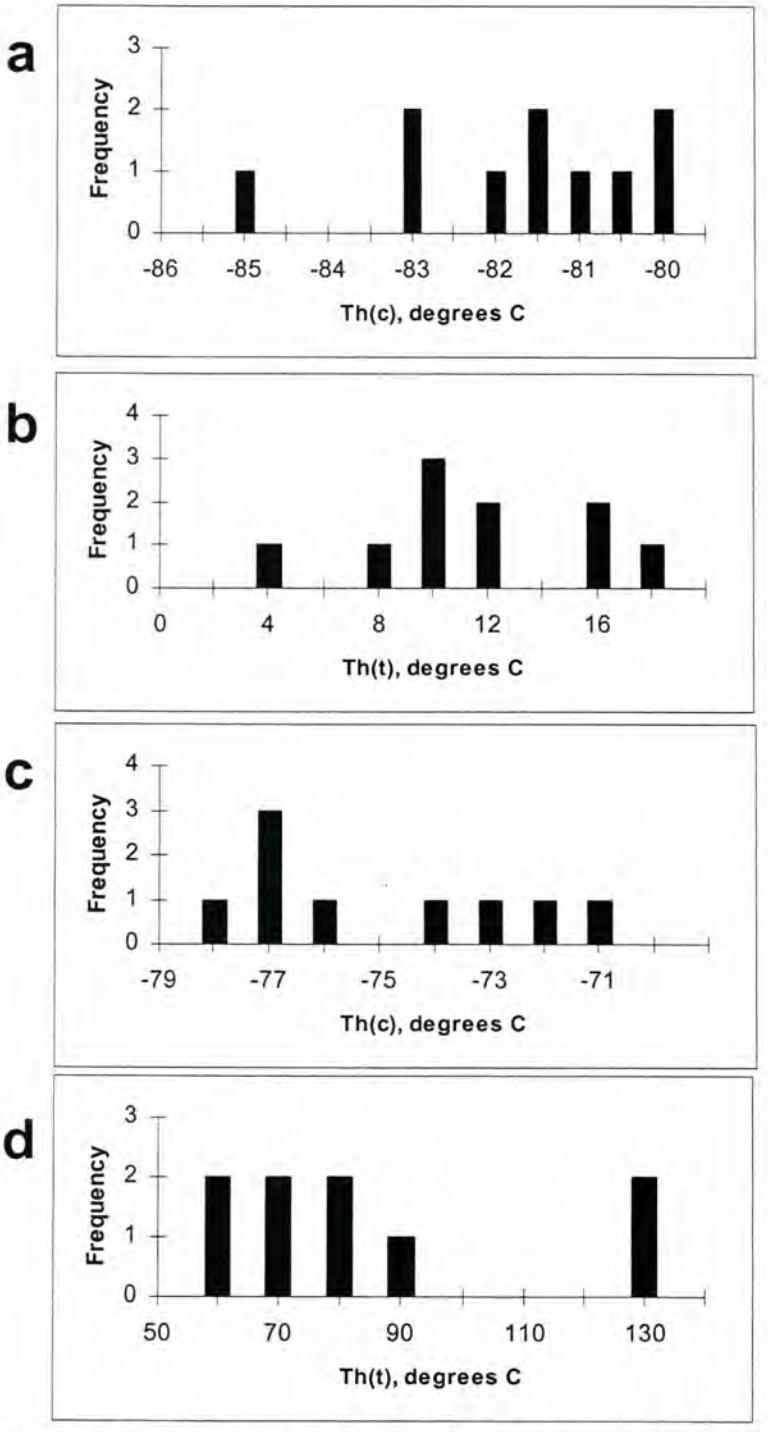

Figure 41: Results of analysis of methane-rich inclusions. (a) + (b) Freezing and heating runs conducted on 'single phase' inclusions. (c) + (d) Freezing and heating runs conducted on '2-phase' inclusions. Th(c) = carbonic homogenization temperature, at which the methane-rich gas and liquid homogenize. Th(t) = total homogenization temperature. See text for discussion.

Th_t = 2° C and 17° C (Figure 41b). The room temperature two-phase inclusions behave similarly but at different temperatures. The methane component homogenizes to liquid between Th_m = -78° C and -71° C (Figure 41c). Total homogenization occurs over a much larger range of temperatures, between Th_t = ~ 50° C and 120° C (Figure 41d).

Interpretation of Fluid Inclusion Results

Two-phase Water/Vapor Inclusions

The melting temperature of ice in a water-rich inclusion can be used to determine composition, as increasing salinity depresses the melting point of water (Goldstein and Reynolds, 1994). The assemblage in sample LP22b is interpreted to be composed of approximately pure water and water vapor because the majority of inclusions melt at 0° C. Because the vapor phase would not be present at the time of entrapment, the modal homogenization temperature of Th = 180° C is interpreted as the minimum trapping condition (Roedder, 1984). Although the homogenization data are generally consistent, the higher values recorded for some inclusions suggest trapping of this assemblage may have occurred over a period of time and could reflect decreasing or fluctuating fluid temperatures.

Assuming a pure water composition, the equation of state by Haar et al. (1984) can be used to construct an isochore, or line of constant volume, for the inclusion assemblage. The windows program FLINCOR v. 1.4 (Brown, 1989) was used to calculate isochore pressure and temperature values from homogenization data. The isochore begins at surface pressures; it intersects the temperature axis at 180° C, the representative homogenization value (Figure 39c). The trapping conditions should plot

along this line. Unfortunately, pressure and temperature conditions along the isochore may not be compatible with the P-T constraints from mineralogy discussed above. At a temperature of ~200° C, the isochore estimates a pressure of less than 0.5 kilobars when a value of several kilobars is reasonably expected (Figure 39c). Therefore, temperature values may be anomalously high. Kerrich (1976) states that even small amounts of intracrystalline strain can cause minor leakage in inclusions that in turn yield uncharacteristically high homogenization values. Although the vein samples used in analysis were not highly strained, most quartz grains display undulatory extinction so the homogenization temperatures from aqueous inclusions analyzed in sample LP22b may not accurately represent trapping conditions. Since leakage generally affects larger inclusions more drastically (Goldstein and Reynolds, 1994), minor leakage should create a spread in homogenization temperatures loosely dependent on inclusion size. A more rigorous fluid inclusion study could help determine if homogenization temperatures of Th = 180° C are truly indicative of aqueous inclusions of all sizes, and thus more reliable in determination of trapping conditions.

Methane-rich Inclusions

Total homogenization temperatures for methane-bearing inclusions also represent a minimum trapping temperature (Goldstein and Reynolds, 1994). However, the large range of homogenization temperatures recorded and coexistence of single and two-phase inclusions at room temperature indicate the composition of inclusions in this assemblage is not uniform. Inclusions with less methane and more water homogenize at a higher temperature (Kerkhof and Thiery, 1994). Therefore, they more closely represent trapping

temperature. The minimum trapping temperature for this assemblage is interpreted to be ~ 120° C. However, because no water-dominated inclusions were found in this assemblage, the above estimate may be significantly lower than the actual trapping conditions. Without accurate compositional data, it is not possible to construct an isochore for this assemblage and thus the pressure of entrapment cannot be estimated.

Coexistence of Inclusion Assemblages

After analysis of sample LP07, an assemblage of single and two-phase inclusions most likely rich in methane was also observed in sample LP22b but not analyzed because of inadequate time. The relative age of entrapment for each assemblage in reference to one another is not known, but both are probably secondary populations. Because the assemblages coexist, it is possible that they were trapped as part of the same immiscible system, in which case they would represent two end-members of composition. The minimum trapping temperature of Th = 180° C estimated from analysis of the water-rich inclusions would then apply to both assemblages. However, a more detailed fluid inclusion study is necessary to reach full interpretation. Future work should concentrate on testing the possible association and relative timing of water-rich and methane-rich inclusions. A quantitative technique, such as electron probe microanalysis, gas chromatography, or spectroscopy (Goldstein and Reynolds, 1994), should also be employed to gather compositional information on methane-bearing assemblages in order to determine the exact chemical system to use for a more exhaustive interpretation of entrapment conditions.

The P-T Path

Many previous studies have documented in detail the blueschist-facies metamorphic mineralogy present both in wall rock and veins of the San Juan Islands, but none has attempted to relate P-T conditions to any specific stage of post-fabric deformation. The conditions of peak metamorphism and the inferred prograde P-T path proposed by Brandon et al. (1988) are adopted here with the assumption, based on the relative timing of brittle structures versus the regional fabric, that the initiation of peak conditions preceded most veining and all late faulting. The results of x-ray diffraction and fluid inclusion analysis discussed above are added to the latter portion of this P-T path in Figure 38.

Structures from contractional and extensional stages of brittle deformation commonly contain aragonite and prehnite. Although these structures crosscut regional fabric, they must have formed at near peak conditions of ~20 km depth and ~200° C (Figure 38: point A). Because aragonite occurs only rarely in late strike-slip faults, these faults may have formed near the calcite-aragonite transition zone at a slightly lesser depth during uplift. The occurrence of prehnite in all late structures, coupled with the preservation of aragonite, indicates temperatures were probably consistent at ~200° C throughout brittle deformation. Aqueous fluid inclusions in quartz veins, whether primary or secondary, provide data consistent with this temperature (Figure 38: point B). The majority record minimum trapping temperatures of ~180° C, just under peak conditions, while no inclusions measured had homogenization temperatures greater than ~200° C, which is consistent with preservation of aragonite. Although the isochore constructed from these data is suspect for reasons discussed above, an alternative P-T

path is shown (Figure 38: dashed line) that considers a sustained maximum temperature but greatly reduced pressure after significant exhumation, as suggested by the aqueous inclusion isochore. This interpretation implies that uplift occurred faster than the rocks could cool. Of course, because leakage may have shifted the aqueous inclusion isochore to higher temperatures, it is possible that rocks in the San Juan Islands experienced a P-T path between that presented here (Figure 38) and that provided by Brandon et al. (1988). Methane-rich inclusions record minimum trapping temperatures of less than ~120° C. However, the lack of an independent compositional constraint prevents an estimate of true entrapment conditions at depth. If this is not a gross underestimate, methane-rich inclusions are secondary and formed under cooler conditions after a period of exhumation.

V. Discussion

The Nature of Regional Fabric

Results from this study suggest fabric in the LSC formed by a combination of two processes, pressure solution and shearing, which are both interpreted to be related to regional flattening. Pressure solution that facilitated flattening in coarse grained clastic rocks and produced an approximately axial planar foliation is kinematically related to shortening perpendicular to the foliation plane. The localized non-coaxial fabric shows flattening or rotation of large grains within the foliation and subequal evidence of right and left-lateral northwest/southeast shear along high contrast bedding planes and weak mudstone-rich zones subparallel to foliation. Price and Cosgrove (1990) state that in low grade, fine grained sedimentary rocks, shearing along foliation planes can occur late during the same deformational episode that produced the flattening fabric. Therefore, bi-directional shearing in argillaceous rocks of the LSC could indicate lateral extrusion of material late during ductile thinning. The existence of two temporally associated fabrics could be a result of strain partitioning. Because of rheological differences, pressure solution and shearing were partitioned primarily into terranes dominated by metagreywacke and argillite, respectively, but both processes contributed to ductile thinning of the San Juan nappes. These conclusions are based on a small amount of data, however, so future work should concentrate efforts on determining if there is in fact any reliable shear sense for foliation-parallel slip planes and whether there is a regionally consistent difference in relative ages of the two fabrics.

Association with Early Strike-slip Structures

Rare early strike-slip structures are tentatively thought to precede all other meter-scale brittle structures in the LSC, and are kinematically similar to the localized shear fabric. Bedding-parallel slip in coarse clastic units accommodates bi-directional shear to the northwest and southeast along planes of high layer contrast in otherwise fairly homogeneous clastic terranes. This is comparable to the discrete shear surfaces observed on some clasts in outcrops of argillite-rich rocks, and it could also be related to subhorizontal extrusion of material during regional flattening. Most early strike-slip faults and shear veins, which also show subequal evidence of right and left-lateral shear, are conceivably associated by orientation and kinematics with this event as well. Early strike-slip structures occur almost exclusively in massive metagreywacke and greenstone units and therefore crosscut flattening fabric. However, because late motion within the shear fabric is thought to locally postdate cessation of pressure solution processes, early strike-slip structures could have formed within coherent terrane blocks while the shear fabric was still active within argillaceous zones.

Comparison to Previous Studies

The Controversy over Late Cretaceous Kinematics

Models of large-scale Late Cretaceous faulting in the San Juan nappes proposed by previous workers can be evaluated with structural data collected in this study. The model proposed by Brandon et al. (1988) suggests that the Lopez Structural Complex is an imbricate thrust zone created during top-to-the-southwest motion, with offset confined to terrane-bounding cataclastic zones that were later overprinted by a solution mass

transfer flattening fabric. The dip-slip slickensides measured on boudinaged, foliation-parallel vein material at Davis Head provide tentative support for northeast/southwest motion. However, because the vein material is discontinuous and relatively minor compared to most fault-related veins in the study area, it is unclear if the slickensides reflect major fault motion or if the vein actually crosscuts originally unoriented cataclasite (Brandon et al., 1988) and thus reflects later, minor slip along the vein surface. Meter-scale thrusts within terrane blocks and argillaceous zones are southwest-vergent, but these structures crosscut cataclastic fabric at Davis Head and consistently crosscut regional fabric. Therefore, they must post-date both large-scale faulting and the solution mass transfer fabric of Brandon et al. (1988).

Maekawa and Brown (1991) argue that Late Cretaceous thrusting was directed towards the northwest and that the thrusting imposed a kinematically related fabric in the cataclasite and argillaceous shear zones. These conclusions are based in part on a shallowly plunging northwest/southeast lineation within shear zones produced by sheared vein material, stretched rock fragments, and slickensides. The oblique stretching lineation measured in cataclastic fabric at Iceberg point plunges moderately to the northwest and is broadly consistent with lineation orientations presented in Maekawa and Brown (1991). Subhorizontal northwest/southeast slickenside lineations from argillaceous outcrops are consistent with shear zone lineations documented by Maekawa and Brown (1991), and they also note some ambiguity in the shear sense of such structures. However, evidence from this study indicates northwest/southeast subhorizontal motion continued along brittle, meter-scale structures after fabric formation. Thus, northwest/southeast shear is not restricted to have occurred only during

major faulting but may be a more continuous process than proposed by Maekawa and Brown (1991).

Support is found for the linked faulting model of Bergh (2002), which states that orogen-normal contraction led to isoclinal folding of bedding and production of a regional axial planar cleavage. Southwest-directed thrusting during the same deformational episode was followed by strike-slip reactivation of fault zones. The southwest-vergent thrusts oriented subparallel to but crosscutting foliation documented in this study are consistent in relative timing and kinematics with this model, and some are reactivated as strike-slip faults. Evidence was also found for early northwest/southeast strike-slip motion, both within localized shear fabric and along structures that crosscut foliation. A detailed comparison with the results of Bergh (2002) is provided below.

Shear Fabric

The existence of a steeply west-northwest-striking shear-related fabric in argillaceous rocks of the LSC is documented by Bergh (2002). The D2 shear foliation of Bergh (2002) post-dates and reactivates an axial planar D1 flattening fabric along the steep limbs of kilometer-scale folds of bedding in the Lopez Structural Complex. Bergh (2002) suggests this reactivation is caused by left-lateral subhorizontal shearing concentrated within the weaker, mudstone-rich zones. It is manifested as a composite fabric with synthetic, left-lateral faults parallel to foliation and antithetic right-lateral faults oriented approximately orthogonal to the foliation.

The observations of shear foliation in argillaceous rocks and the early strike-slip structures documented in this study are also consistent with an early subhorizontal

northwest/southeast shearing event. However, the relative timing relationships between the flattening fabric and shear fabric, as well as the overall sense of shear, are ambiguous. An approximately equal number of early right- and left-lateral foliation-parallel faults were recorded. More data on foliation and bedding-parallel slip were collected, but usually the sense of slip was indeterminable. Ample evidence was also found for right-lateral strike-slip faults similar in orientation to the antithetic faults of Bergh (2002), although these faults occurred not only in argillite but were widespread in greenstone and metagreywacke lenses as well. These north/south striking right-lateral faults were interpreted to be late structures because they clearly crosscut regional fabric and extensional structures, so they could not be associated with the earlier, foliation-parallel shearing.

Post-fabric Deformation

Common Structural Sequence

Brittle structures are widespread throughout the San Juan Islands. The relative timing of structures documented within the Lopez Structural Complex is identical to the sequence found elsewhere in the San Juan nappes. Ocean Floor Complex and Fidalgo Complex rocks exposed in the eastern San Juan Islands are deformed by meter-scale thrusts, extensional structures, and conjugate strike-slip structures, in order of relative age (Lamb, 2000; Lamb and Schermer, 2003). Because the same sequence of post-fabric structures exists across terrane boundaries in the San Juan Islands, this deformation is interpreted to have occurred after terrane juxtaposition. Orientations among late structures may have once been regionally consistent. At present, however, the

orientations of structures and the kinematics of deformation, although consistent within the LSC, vary regionally depending on geographic location. The results of kinematic analyses from structures in the LSC are illustrated in map view in Figure 42 for comparison with generalized kinematic results of Lamb (2000).

The Question of Reorientation

Burmester et al. (2000) have discussed the likelihood of late structural reorientation and the problems associated with assuming that kinematic interpretations of earlier structures in present day coordinates are directly applicable to deformation in Cretaceous time. While orientations of brittle structures and paleomagnetic directions are consistent within the LSC, Lamb (2000) documented significant variation in the eastern San Juan Islands. Although brittle structures may be partly responsible for locally reorienting fabric, it is clear from the regional disparity in orientations of late structures that at least some differential reorientation post-dates all of the structural sequence described in this study. Broad regional folding about a shallowly southwest-plunging axis (Feehan and Brandon, 1999; Lamb, 2000) after conjugate strike-slip faulting probably contributes to some of the observed discrepancy. However, Burmester et al. (2000) were unable to restore consistency in paleomagnetic directions simply by removing the effects of late folding. Also, kinematic axes for thrusts, normal faults, and strike-slip faults in the eastern San Juan Islands are not systematically folded or rotated with respect to those in the LSC. For example, thrusts in each location are subparallel to local foliation and record similar contraction directions but have opposite vergence (Figure 42). In each study location, extension directions are parallel for normal faults and

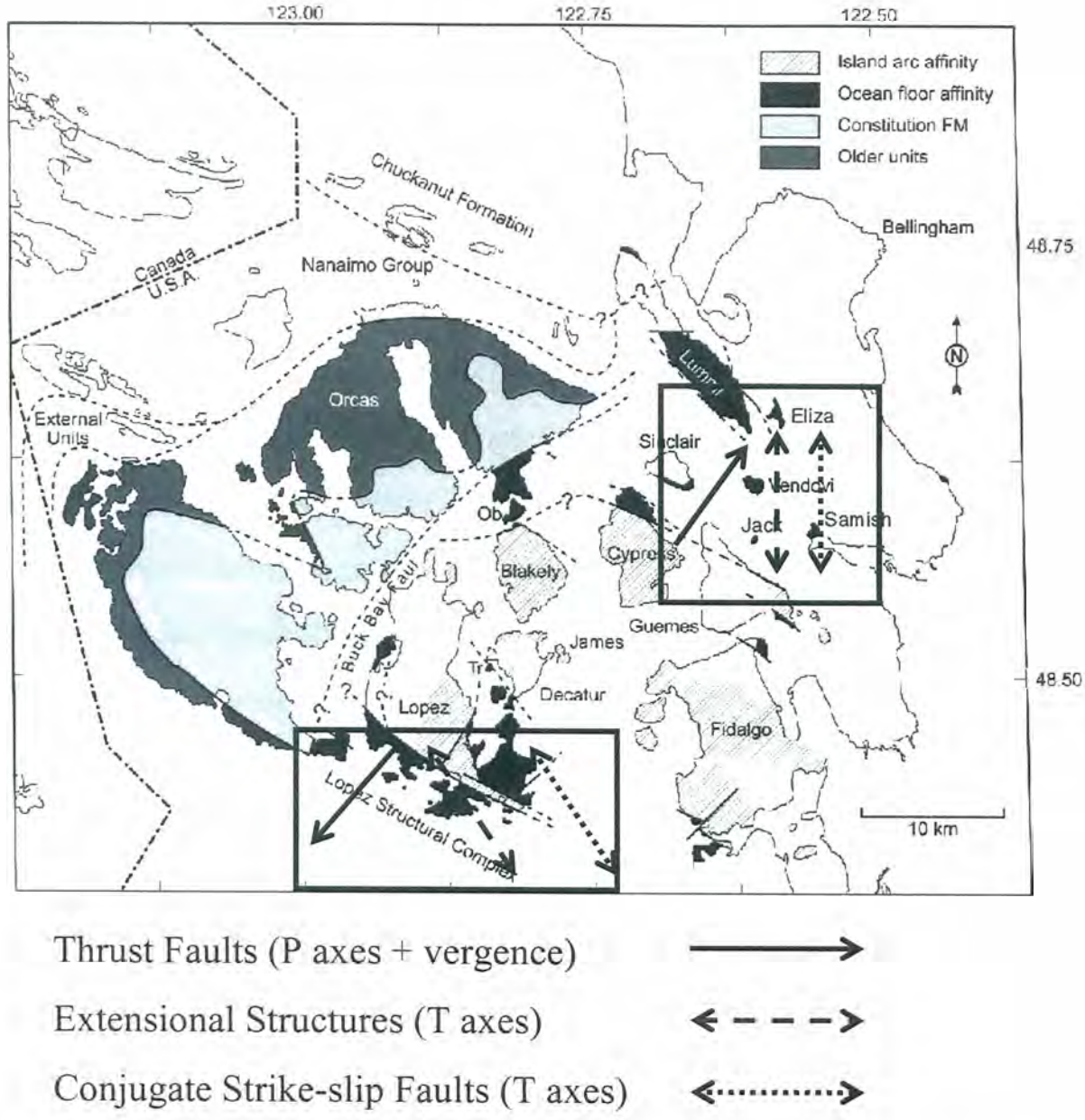

Thrust Faults (P axes + vergence) ——→

Extensional Structures (T axes) ←– – –→

Conjugate Strike-slip Faults (T axes) ←·····→

Figure 42: Regional comparison of kinematic axes from analysis of brittle structures. Results from the Lopez Structural Complex (bottom of figure) and generalized results from the eastern San Juan Islands (Lamb, 2000) differ. Thrust vergence is approximately opposite but P axis trends are similar. While T axes for extensional and strike-slip structures consistently trend northwest/southeast in the LSC, T axes in the eastern San Juan Islands trend approximately north/south. Base map from Burmester et al. (2000).

conjugate strike-slip faults but the relation of late extension directions to thrust vergence and foliation is noticeably dissimilar.

Because of these complexities, restoration of paleomagnetic directions and structural orientations is not trivial and cannot be accomplished by a simple rotation. A combination of mechanisms, including structures that are not currently exposed on land, must contribute to the reorientation of paleomagnetic and structural data. Additional data on late structures in other areas of the San Juan Islands may help constrain the magnitude of local variations. Coupled with the published paleomagnetic data from Burmester et al. (2000), further comparison of late structural orientations should lead to a more complete understanding of the timing and local mechanisms of reorientation. Until restoration can be accomplished, the orientations and kinematics of structures in the San Juan Islands are best considered in terms of present day coordinates.

The Timing of High-pressure Conditions and Deformation

Recent Ar/Ar geochronology in the San Juan Islands indicates high pressure metamorphism and the crystallization of metamorphic minerals was not caused by thrust stacking during Late Cretaceous faulting but began sometime in the Early Cretaceous (Brown and Lapen, 2003; Brown et al., in press; Lamb and Schermer, 2003). The linked structural and P-T results presented in this study reveal high pressure, low temperature conditions in the Lopez Structural Complex persisted through and after terrane juxtaposition as well. The formation of high pressure minerals in veins did not cease during ductile thinning, as was proposed by Brandon et al. (1988) and Feehan and Brandon (1999). Pervasive crosscutting extensional structures associated with

either subduction-related deformation at depth or early uplift of the San Juan terranes contain the high pressure minerals aragonite and prehnite. This high pressure signature is consistent throughout all but the latest stages of brittle deformation. Therefore, in order to maintain the low temperatures and high pressures required to crystallize and preserve aragonite through several stages of late deformation, the structures discussed herein could only have formed at depth within an accretionary prism during active subduction.

This conclusion is in disagreement with relative geochronology in the translational model of San Juan thrusting proposed by Maekawa and Brown (1991). Based on fault zone kinematics and the observed synchronicity of thrust-related fabric and high-pressure mineralogy, Maekawa and Brown (1991) states blueschist-facies metamorphism did not occur within a subduction zone but resulted from thrust stacking at a step-over bend in the North American margin. In contrast, sustained high-pressure – low-temperature metamorphism is generally consistent with the interpretation of Ar/Ar results by Brown et al. (in press) that states subduction-related metamorphism initiated in the Early Cretaceous and is unrelated to emplacement onto the continental margin.

Deformation in an Accretionary Prism

Ductile Thinning

The high pressure metamorphic signature and several stages of brittle faulting and veining in the San Juan nappes are indicative of structures seen in rocks that were deformed at depth after being underplated in an accretionary prism setting. Each

structural stage should be related to a prism process such as accretion, internal wedge adjustment, or exhumation. Feehan and Brandon (1999) have proposed that the pressure solution fabric is related to vertical ductile thinning after assembly of the San Juan terranes at the base of an accretionary prism. This is based on their conclusion that fabric in metagreywacke units is entirely coaxial at the regional scale, and the observation of Brandon et al. (1988) that pressure solution fabric overprints fault zones in the San Juan nappes. Feehan and Brandon (1999) interpret ductile thinning coupled with erosion as the main method of exhumation which is active from depths greater than 20 km to within a few kilometers of the surface. The discovery of aragonite within contractional and extensional structures that crosscut the regional pressure solution foliation contradicts this model because the crosscutting structures must have formed at a depth of at least ~ 20 km. Ductile vertical thinning and lateral extrusion by fabric formation in the San Juan nappes must have been a less continuous process that was active at depth after underplating but ceased long before exhumation was complete. Instead, this mode of deformation was replaced by brittle faulting and veining prior to the majority of uplift. Because P-T conditions probably did not vary appreciably at depth during active subduction, the switch from ductile to brittle deformation more likely reflects a change in material behavior due to substantial fluid loss by pressure solution processes and/or an increase in strain rate in response to externally driven changes in wedge geometry.

Brittle Faulting

The faulting seen in accretionary environments, with the possible exception of near-surface deformation, can generally be attributed to internal adjustments that

maintain wedge shape in response to external influences such as erosion, additional accretion, or changes in subduction conditions (e.g., Davis et al., 1983; Platt, 1986). Late thrusts in the Lopez Structural Complex are most likely a result of orogen-normal contraction and internal wedge adjustment. If the regional fabric in an underplated terrane is reasonably assumed to have formed approximately parallel to the boundary with the subducting plate, synthetic thrusts exploiting the weak foliation and bedding planes would also form parallel to the subduction horizon (Figure 43a). These are accompanied by a smaller number of antithetic thrusts. Late or out-of-sequence thrusts can occur as post-accretionary structures and are a common occurrence within accretionary prism environments, accommodating and resulting in internal thickening of the wedge after additional accretion of material (Platt, 1986). Silver et al. (1985) suggest that for turbidite sequences found in ancient accretionary complexes, small late thrusts can be common and provide an important mechanism for stratal disruption and steepening of local dips without appreciably disturbing surrounding material.

The prevalent extension vein sets and normal faults in the LSC signal a kinematic shift from contraction to subhorizontal extension and subvertical shortening that initiated at depths of at least ~ 20 km. Normal faults accommodated mostly orogen-parallel extension with a smaller amount related to orogen-normal and orogen-oblique extension (Figure 43b). Extensional structures would have acted to spread material outward laterally with an along-strike bias presumably because of continued subduction with no lateral buttress. This deformation could be a result of internal wedge adjustment after overthickening of the prism center due to the previous thrusting, additional underplating, or a combination of both. Platt (1986) predicts subduction-related extension to be

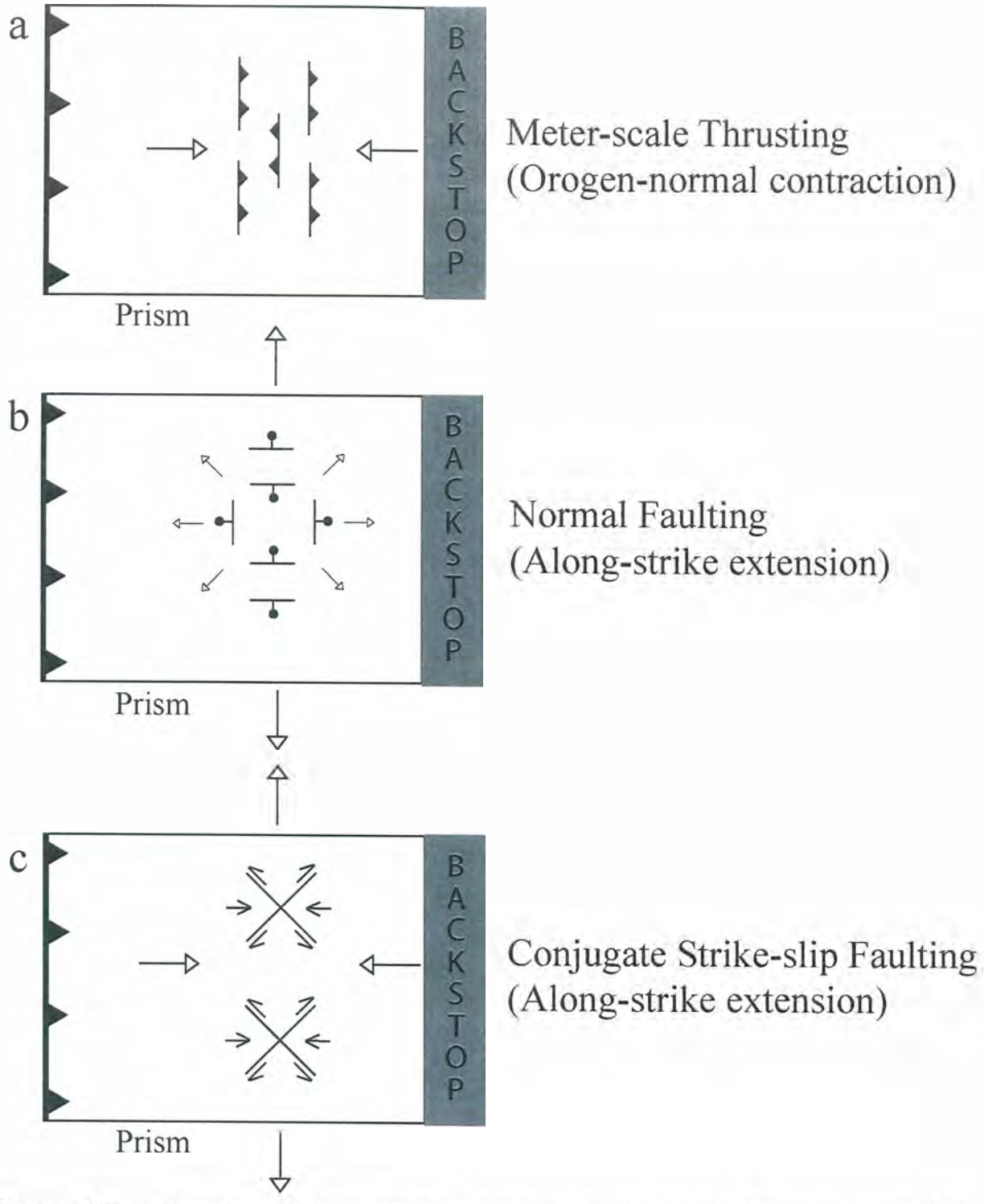

Figure 43: Schematic cartoon illustrating the tectonic interpretation of three stages of brittle structures. Shown in map view at ~ 20 km depth within an accretionary prism. Arrows show approximate kinematic regimes inferred from the results of structural analysis. See text for discussion.

accomplished mainly along large offset kilometer-scale listric faults which begin at the surface and initially extend to ~ 12-15 km depth, at which point the deformation typically becomes ductile in nature. Small-scale extensional deformation in the LSC could conceivably be a brittle but more evenly distributed version of Platt's (1986) large discrete faulting that would have produced the same result of vertically thinning and exhuming the high pressure rocks. The ~20 kilometer depth at which the San Juan nappes were located may have prevented such major structures from penetrating down to the LSC, while low temperatures and a possibly high strain rate dictated brittle faulting as opposed to ductile deformation. It is feasible that large extensional structures did exist structurally above the rocks now exposed, or do exist in the San Juan Islands but are not currently exposed.

Conjugate strike-slip deformation continued the along-strike extrusion of accreted material during sustained subduction (Figure 43c). The change from normal faulting to strike-slip faulting, however, signals a shift in importance from vertical thinning and horizontal extension to orogen-parallel extrusion and possibly a renewed greater influence of orogen-normal contraction. One likely cause of this change is simply the reduction in wedge thickness by extension to the point at which the maximum compressive stress ceases to be vertical and once again is shallow and orthogonal to the orogen. This would not necessarily be true for the entire wedge; the effective vertical load on a given region such as the LSC would be continuously reduced during along-strike extrusion and/or uplift and erosion. If a comparable orogen-normal compressive stress were maintained throughout brittle deformation, at a certain reduced overburden the mode of faulting would change to provide a better mechanism for both lateral orogen-

parallel extrusion and orogen-normal contraction. If subduction continued, extensional faulting and veining might still be active at depth during conjugate strike-slip faulting at shallower levels.

The model presented here for the sequence and orientations of brittle structures relative to a Cretaceous subduction zone (Figure 43) may not be entirely applicable to rocks deformed in other locations on strike within the same accretionary prism. The prevalence of orogen-parallel extension in virtually every stage of deformation requires a lack of along-strike buttressing to allow extrusion to occur. It is also likely that the San Juan nappes, when at depth, were located within a zone of higher accretion relative to other areas in the subduction complex. This discrepancy in accumulation, and thus wedge thickness, would encourage the along-strike redistribution of material after accretion, as suggested by persistent orogen-parallel extension in the structural sequence.

Plate-scale Influences on Deformation

A plate-scale external change that requires a responsive adjustment in wedge geometry could cause the shift from the relatively slow process of ductile thinning to brittle faulting in the San Juan nappes. Ductile deformation at low temperatures by pressure solution may deform rocks too slowly to contribute effectively to wedge stability (Ring and Brandon, 1999). Platt (1986) states that, if subjected to a period of higher stress, intrawedge deformation may simply occur at a higher rate. Therefore, it is appropriate to discuss plate tectonic changes as a likely cause for meter-scale brittle deformation in the San Juan Islands. Likely causes include a significant frontal accretion episode of which we have no currently observable evidence, a shift in the plate

convergence rate or direction, or a large underplating event possibly related to the arrival of a sediment pile or even the collision of Wrangellia with the Cretaceous prism.

North American and Farallon Plate Interaction

Changes in plate boundary conditions between the North American and oceanic Farallon plate could facilitate intrawedge contraction, assuming the San Juan nappes were part of a Cordilleran accretionary prism and not some other subduction complex located elsewhere. Since meter-scale brittle structures crosscut foliation that overprints major fault zones (Brandon et al., 1988), the timeframe of interest must postdate earliest faulting constraints in the LSC of 112 Ma (Brown et al., in press) and predate exposure of the San Juan nappes by 84 Ma (Brandon et al., 1988). If ductile thinning reflects a period of relative wedge stability (Ring and Brandon, 1999) and low strain rates, an increase in the plate convergence rate could cause late thrusting. The orogen-normal component of convergence for North American subduction is thought to have increased at ~100 Ma, from 50 km/m.y. to over 100 km/m.y. (Engebretson et al., 1985). This change could raise basal shear stress on the wedge at the plate boundary and lead to internal thickening (Dahlen, 1984). The sense of oblique convergence between the Farallon and North American plates also changed at ~100 Ma, from left-lateral to right-lateral (Engebretson et al., 1985). It is plausible that during this switch the convergence vector was for a short time approximately orthogonal to North America, which would increase the orogen-normal component and cause internal contraction. When convergence became more oblique again, the wedge may have collapsed laterally into a new geometry appropriate

for the revised plate boundary conditions, assuming there was no lateral buttress to prevent the along-strike extrusion of excess material.

Influence of Wrangellia

A major underplating or subduction event could also reasonably initiate the sequence of late thrusting followed by extension at depth. Any passage or addition of material at the base of the wedge would result in contraction before and during accretion, then lateral extrusion above the added material to maintain appropriate wedge thickness (Platt, 1986). Recent structural investigation of the Chugach Complex revealed a similar sequence of thrusting followed by normal and conjugate strike-slip faulting associated with oblique extension, which some workers have attributed to the passage of the Kula/Farallon ridge (Kusky et al., 1997).

The collision and possible partial underthrusting of the margin of Wrangellia beneath the Cretaceous prism could overthicken the wedge. Silver et al. (1985) suggest that, although high pressure metamorphism may occur in all subduction zones, the uplift and preservation of blueschist terranes is not due to steady-state accretionary prism processes but can only be facilitated by the collision of buoyant material. The margin of Wrangellia could not subduct and would effectively be underplated to the base of the wedge, which would thicken, then elevate the previously stable material and lead to a lateral collapse. This scenario could involve either of two events; the actual arrival of Wrangellia in the Late Cretaceous and collision with the fore-arc of North America (e.g. Brandon et al., 1988), or the northward translation of an active fore-arc sliver, as suggested by Brown (submitted), which could collide with and be thrust atop the

previously accreted Wrangellia. Brown and Lapen (2003) and Brown et al. (in press) show that the onset of metamorphism predates major faulting in the LSC. Results of this study indicate high pressure conditions persisted after major faulting in the Late Cretaceous. If assembly of the LSC and emplacement atop Wrangellia occurred as part of the same faulting episode (Brandon et al., 1988) during active subduction but after underplating and metamorphism of the San Juan nappes, it is likely that the late brittle deformation followed soon after emplacement and reflects contraction and rapid uplift of the San Juan nappes caused by this collision. If metamorphism and assembly of the LSC occurred to the south near the Klamath Mountains (Brown, submitted) but during active subduction, late brittle structures could either be related to the initiation of emplacement from an active forearc sliver to atop Wrangellia after translation, or to internal wedge deformation caused by changing plate motions and terrane translation in an overall transpressive environment.

Unfortunately, it is not realistic to distinguish by kinematics whether the small-scale brittle deformation in the San Juan nappes is a result of changing plate boundary conditions and translation or rapid uplift after emplacement atop Wrangellia. However, if brittle deformation occurred during translation and not emplacement, the structures described in this study must predate and be overprinted by emplacement-related structures. Therefore, knowledge of the relative timing of emplacement structures would help determine which event caused the brittle deformation. A future study in the San Juan Islands could focus attention on the relative timing and kinematics associated with a possible emplacement structure, the structurally lowest fault contact in the San Juan nappes that defines the boundary with the external Nanaimo Formation and Wrangellia.

VI. Conclusions

Based on a primarily oceanic origin of material, a complex ductile and brittle deformational history, and the widespread preservation of high pressure-low temperature mineralogy, terranes in the San Juan Islands were most likely underplated and deformed deep within a Cretaceous accretionary prism. While the kinematics of major faulting and the age of blueschist-facies mineral growth for the San Juan nappes remain controversial, results presented in this study help constrain the kinematics, relative timing, and P-T conditions of late stage deformation. Pressure solution foliation in coarse clastic rocks provides evidence for regional flattening during ductile deformation. There is some evidence for generally synchronous northwest/southeast bi-lateral shearing partitioned into thin mudstone-rich zones and along high-contrast contacts in argillaceous terranes of the LSC. Also indicative of lateral northwest/southeast motion, the earliest brittle structures include rare northwest and southeast striking bedding-parallel slip surfaces, shear veins, and early strike-slip faults. Three stages of widespread brittle structures post-date fabric formation and early northwest/southeast shearing. Southwest-vergent thrusts subparallel to fabric are crosscut by abundant extension veins and normal faults that mostly strike northeast and southwest. Late strike-slip faults are effectively conjugate; right-lateral faults strike ~ north/south and left-lateral faults strike ~ east/west.

Kinematic analysis of the deformational sequence recorded by rocks in the LSC shows a progression within the study area from flattening and contraction to extension-related deformation. Pressure solution foliation formed under a principal contraction

direction that plunges moderately to the southwest. The localized shear fabric and early strike-slip structures are consistent with continued northeast/southwest contraction, and they accommodated lateral extrusion of material to the northwest and southeast. Meter-scale thrusts also show northeast/southwest contraction after ductile deformation was replaced by brittle faulting. Prevalent extension veins and normal faults indicate a period of vertical thinning and subhorizontal extension, mostly to the northwest and southeast. Late conjugate strike-slip faulting is also related to northwest/southeast extension but shows a renewed significance of northeast/southwest contraction. Therefore, the entire structural sequence documented here is generally consistent with northeast/southwest contraction and northwest/southeast extension, with periods of enhanced emphasis on vertical thinning. Results of structural investigation in adjacent terranes are comparable, which suggests late brittle deformation is common throughout the San Juan nappes. Unfortunately, because of poorly constrained differential rotation throughout the San Juan Islands due to late regional folding and other less understood mechanisms, it is not presently possible to restore structural orientations and kinematic axes to their Cretaceous directions.

High pressure minerals in structures constrain brittle deformation to have occurred at greater than ~ 20 km depth and at most ~ 200° C, near peak metamorphic conditions and above the calcite/aragonite transition. These P-T conditions and the preservation of widespread aragonite are only possible if the brittle structures formed within an accretionary prism during active subduction. Reconnaissance fluid inclusion results substantiate the continuation of low temperature conditions after vein formation and during uplift. Therefore, meter-scale brittle structures in rocks of the LSC preserve a

record of internal wedge deformation at depth and/or early during uplift of the San Juan nappes. The sequence observed is consistent with internal orogen-normal contraction and vertical thickening followed by lateral along-strike extension and vertical thinning. For brittle faulting to replace ductile thinning as the dominant mechanism of deformation at depth, an external influence on wedge geometry may be necessary. Some possibilities include a change in the orientation or magnitude of plate convergence vectors, a large underplating or accretion event, or the collision of the Cretaceous prism with the margin of Wrangellia. By combining detailed, outcrop-scale structural analysis of brittle features with multiple techniques for determining the pressure and temperature conditions of vein deposits associated with deformation, this study contributes to greater knowledge of the tectonic history of terranes deformed in an active Cretaceous accretionary prism and provides a basis for future structural study of the San Juan Islands.

VII. APPENDICES

Appendix A: Methods of Structural Study

Field Work

Field work was focused within the Lopez Structural Complex, exposed on southern Lopez Island and southeastern San Juan Island (Figure 2), during 2003 and 2004. Terranes adjacent to the LSC were studied on eastern San Juan and northern Lopez Islands, as well as to the northeast on Orcas and Lummi Islands. Transportation to sites was primarily by ferry, car, and foot, but the WWU Geology department inflatable boat was used for small island study and exploration of otherwise inaccessible coastlines. Field sites were selected in order to distribute data collection and sampling among the several rock types in the LSC, as well as to provide coverage through the complex (Figure A1).

Detailed outcrop analysis for each site included measuring and interpreting brittle structures, determining relative ages using cross-cutting relationships, and sampling rock types and vein material within the structures. First, foliation (and bedding if present) was measured. The orientation and relative timing of faults and shears was found. If possible, offset of older structures or layering was used to estimate fault sense and displacement magnitude. Drag folding of bedding or foliation and the direction of slickenside steps was also helpful in determining fault sense when offset was not apparent. Techniques using minor fault plane structures to determine sense on brittle faults without visible offset or drag, especially useful in the massive sandstones and

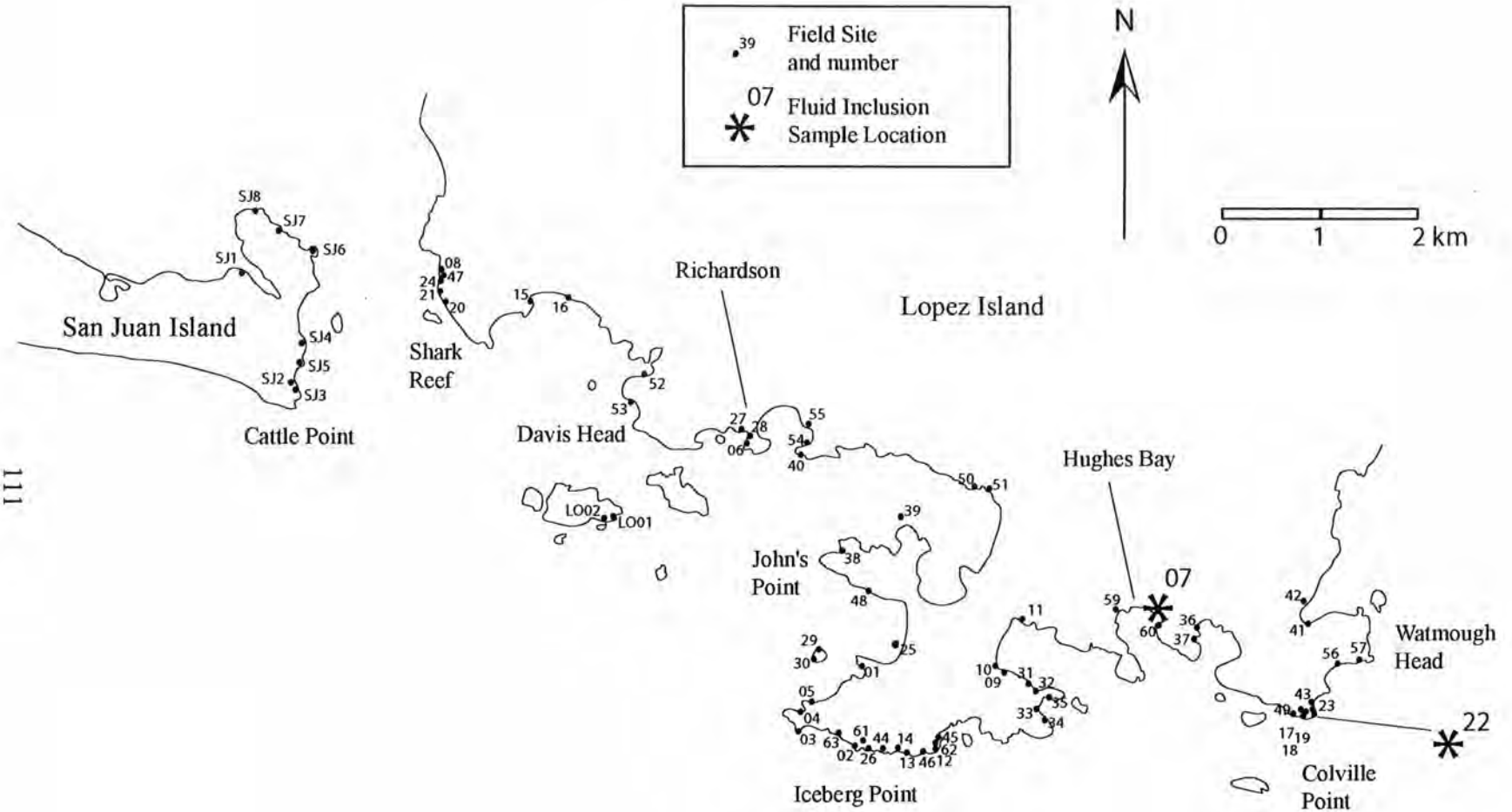

Figure A1: Map of the study area showing locations of field sites and fluid inclusion sample locations.

homogeneous basalts of the San Juan Islands, are described in Petit (1987). Of these, a common feature used in this study were localized vein deposits on fault surfaces called accretion steps which develop on the leeward side of irregularities and therefore show the relative sense of motion of the absent block. Other common minor structures are generally oriented at a low angle to the main fault surface and include vacant or vein-filled en-echelon tensile fractures with no displacement, and small synthetic 'R' and 'P' fractures which show the same sense of relative motion as would the fault plane. The trend and plunge or rake of slickensides was measured to constrain the direction of fault movement. Several features of vein sets were documented, including: variety – extensional, shear, en echelon, or sigmoidal; pattern of fiber growth – syntaxial, antitaxial, or layered parallel to the vein wall; size of veins and spacing of array; shear sense and slickenfiber orientation if applicable.

Definition of Structures

Structural data were tentatively assigned to one of several groups in the field and groups were verified later during analysis. Faults are grouped according to relative age, slickenside rake, and sense of slip. Many faults in the field area contain slickensides with rakes $> 10°$ or $< 80°$ and are thus technically oblique-slip (van der Pluijm and Marshak, 1997). However, because most slickensides rake $< 30°$ or $> 60°$, it is most useful in this study to classify faults as either primarily dip-slip or strike-slip. Dip-slip faults of either normal or reverse sense are defined to contain slickensides with a rake of $\sim 45°$ or greater. Slickensides on strike-slip fault surfaces rake $\sim 45°$ or less. Vein sets are divided into three groups by vein type. Shear veins are defined as continuous planar

fissures in which the displacement across the vein is parallel to the vein walls (Ramsay and Huber, 1983). Mineral layering also parallel to the vein walls is typically visible in outcrop, and slickenfibers are generally seen on the vein walls. They are separated from faults in this study because of the large amount of vein material and lack of deformation in the nearby wallrock associated with these features. Extension and en echelon veins display growth fibers approximately perpendicular to the vein wall (Ramsay and Huber, 1983). Veins are assumed to be extensional in this study if there is no visible shear zone defined by the vein set. En echelon and sigmoidal vein sets lie within and at an angle to a measurable shear zone (van der Pluijm and Marshak, 1997). They are appropriately grouped together in this study because the process of formation for each is diagnostically similar and there is no observed difference of relative timing in the LSC.

Data Representation and Analysis

Structural data was plotted using the StereoWin v 1.2 and FaultKinWin v 1.2.2 programs (Allmendinger, 2003). Lower hemisphere projections and equal area stereonets were used exclusively for all data plots. Contour plots of large data sets were constructed using 1% area contours with contour intervals appropriate to the amount and spread of data for each plot. The average orientation of fabric was calculated in StereoWin v 1.2 by finding the mean trend and plunge of poles.

Fault data with complete information (fault orientation, sense of slip, and slickenside rake or trend and plunge) was analyzed in FaultKinWin v 1.2.2 to find the principal strain axes corresponding to each fault. The program calculates P and T axes that represent the maximum shortening direction and maximum extension direction,

respectively (Marrett and Allmendinger, 1990). For each fault, a great circle is constructed that contains the slickenside data point and the pole to the fault plane. Both the P and T axis are plotted along this great circle at 90° from one another and 45° from the pole to the fault plane. Each fault, then, is represented by strain axes which can be visually compared to other data and interpreted kinematically. The program also allows for weighting of data by fault magnitude, but because offset on faults in the LSC was generally not found construction of the contour plots assumes all data are weighted equally. Although it is not possible to verify this assumption without comparing results to a weighted analysis of the same data, Marrett and Allmendinger (1990) state that the kinematics of most fault populations they have observed are scale-invariant, so contouring of data by uniform weighting is an acceptable proxy for weighted analysis.

Other assumptions inherent in the P and T axis calculations of FaultKinWin v 1.2.2 are less easily dismissed for rocks in the San Juan Islands. Local or regional reorientation of structures, a likely problem for this study, would obviously change the orientation of strain axes as well and could lead to scattering of data and even kinematic misinterpretation if reorientation is severe enough. Since the possible effects have not been quantified on a local or regional level in the San Juan Islands, this study must accept the assumption that reorientation is minor and the kinematics of structures are interpreted directly. Other assumptions necessary for interpreting the kinematics of a fault population include homogeneous strain and representative sampling. Field observations reveal no major variation in the scale, amount, or orientation of structures on the outcrop or kilometer scale within the study area, and care was taken during field work to measure

all types of structures in major rock types across the study area to ensure a representative data set.

Appendix B: Brittle Deformation in Adjacent Terranes

The Constitution Terrane – Eastern San Juan Island

Greenstone and metagreywacke of the Constitution terrane at Friday Harbor Peninsula on eastern San Juan Island is highly dissected by normal faults and strike-slip faults. Local foliation strikes northwest and dips moderately northeast. Cross-cutting relationships show that northeast striking normal faults are followed by northwest striking normal faults. This is potentially reversed from the relative timing pattern documented in the LSC but the orientations of normal faults are generally consistent with faults in the LSC (Figure B1). Strike-slip faults cut normal faults and form a conjugate pattern of approximately north striking right-lateral faults and northwest or southeast striking left-lateral faults (Figure B1). Kinematic analysis shows T axes for normal faults in the Constitution terrane plot shallowly to the southeast or northeast/southwest, while P axes are subvertical (Figure B2). T axes for strike-slip faults mostly plot shallowly to the southeast, while P axes plot shallowly to the northeast and southwest.

The Fidalgo Complex – Northern Lopez Island

Metaconglomerates at northeastern Upright Head on northern Lopez Island are deformed by normal and strike-slip faults as well as abundant extension vein sets. These sedimentary rocks are mapped as arc-related and belonging to the Fidalgo complex (Burmester et al., 2000; Blake et al., in preparation). Local foliation strikes north-

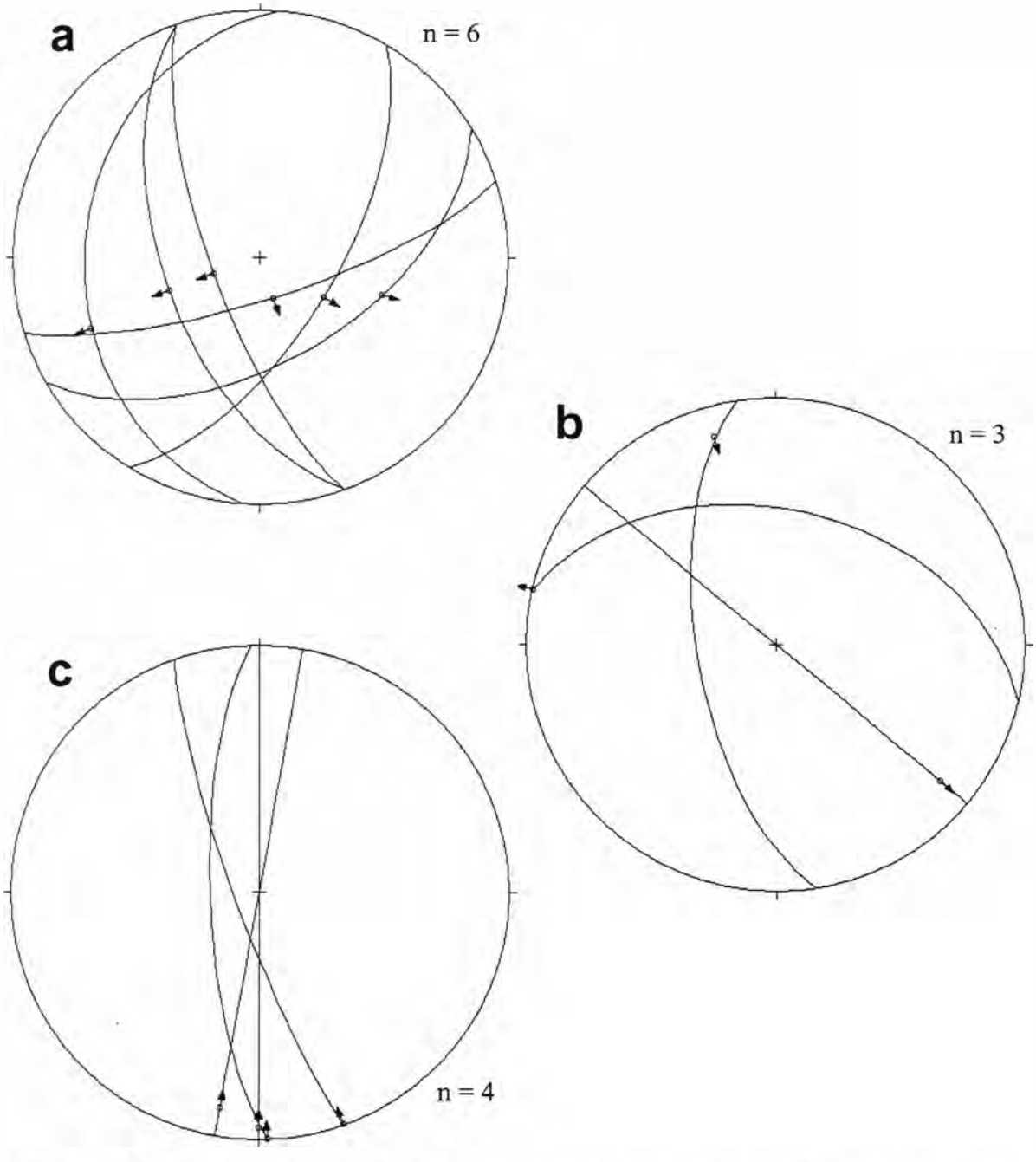

Figure B1: Equal area plots of brittle structures in the Constitution Terrane on eastern San Juan Island. (a) Normal faults. (b) Left-lateral strike-slip faults. (c) Right-lateral strike-slip faults. Arrows show direction of hanging wall movement.

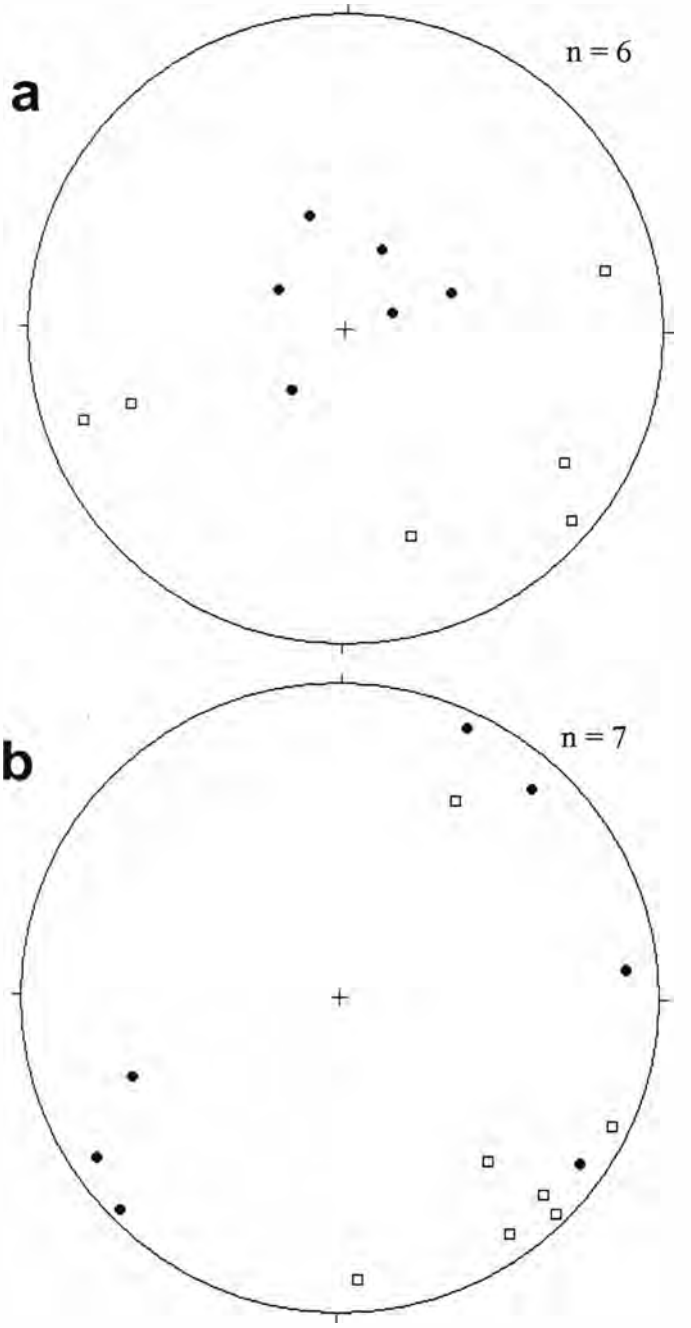

Figure B2: Equal area plots of kinematic axes from brittle structures in the Constitution Terrane on eastern San Juan Island. (a) Normal faults. (b) Strike-slip faults. P-axes = closed circles and T-axes = open squares.

northwest and dips shallowly to moderately towards the east-northeast but is not well defined in outcrop. Normal faults and extension veins all strike approximately east/west (Figure B3). Normal faults are mostly associated with top-to-the-northeast motion. Strike-slip faults crosscut extension vein sets and strike north-northeast/south-southwest (Figure B3). The majority are left-lateral but slip sense conflicts within this one orientation. Kinematic analysis of extensional structures shows T-axes of normal faults and poles to extension veins cluster shallowly to the north and south (Figure B4). Kinematic analysis of strike-slip faults is inconsistent for this small data set.

The Lummi Formation (Ocean Floor Complex) – Southwestern Lummi Island

Metasedimentary rocks of the Lummi Formation exposed near Mary Point on the western shore of Lummi Island are of ocean floor affinity (Burmester et al., 2000; Blake et al., in preparation). There are strong similarities in rock type and late structures with the LSC. Data on brittle structures are shown in Figure B5. Local foliation and bedding both dip moderately to the northeast. Slip surfaces along bedding contacts and exposed foliation planes indicate early northwest/southeast strike-slip motion. As in the LSC, later thrusts crosscut and drag contacts and foliation but are generally oriented subparallel to them. However, local variations in layering scatter orientations in this small data set. Extension veins crosscut foliation and strike northeast. Normal faults crosscut extension vein sets and strike northwest or northeast. Results of kinematic analysis by structure type are shown in Figure B6. T axes of thrusts are subvertical, but P axes are inconsistent. Poles to extension veins indicate a shallow to moderately plunging

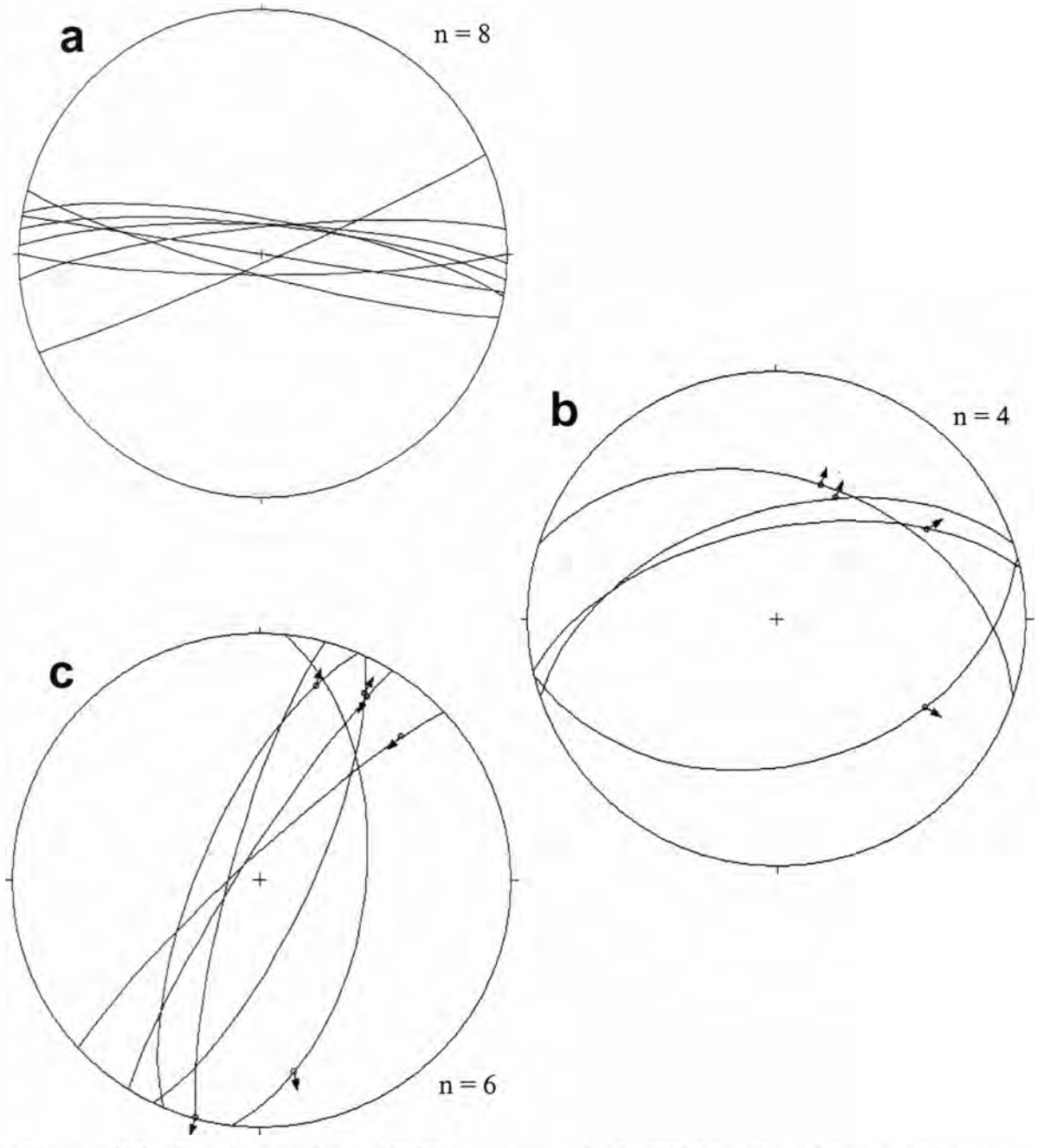

Figure B3: Equal area plots of brittle structures in the Fidalgo Complex on northern Lopez Island. (a) Extension vein sets. (b) Normal faults. (c) Strike-slip faults. Arrows show direction of hanging wall movement.

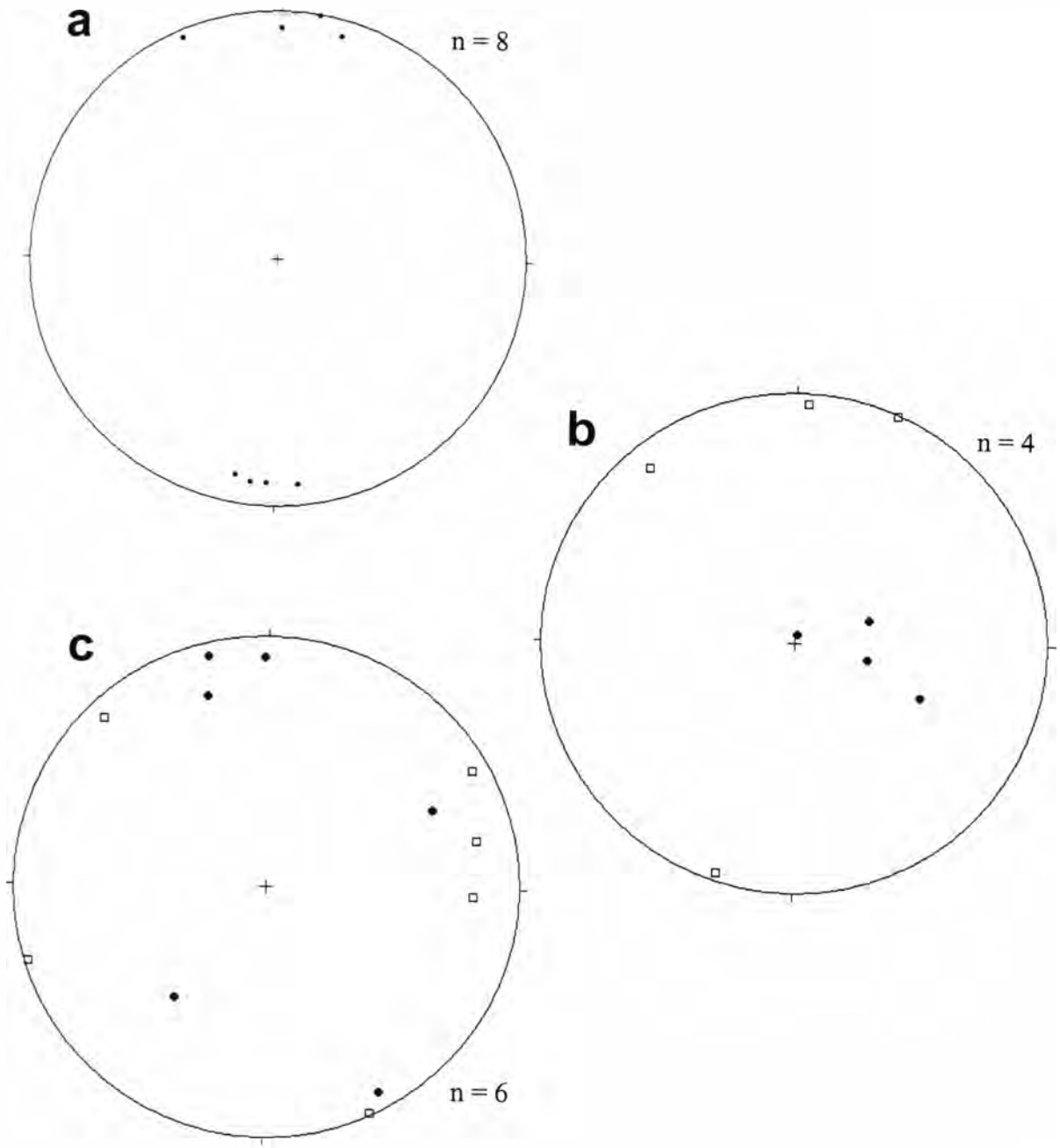

Figure B4: Equal area plots of kinematic axes from brittle structures in the Fidalgo Complex on northern Lopez Island. (a) Poles to extension vein sets. (b) Normal faults. (c) Strike-slip faults. For (b) and (c), P-axes = closed circles and T-axes = open squares.

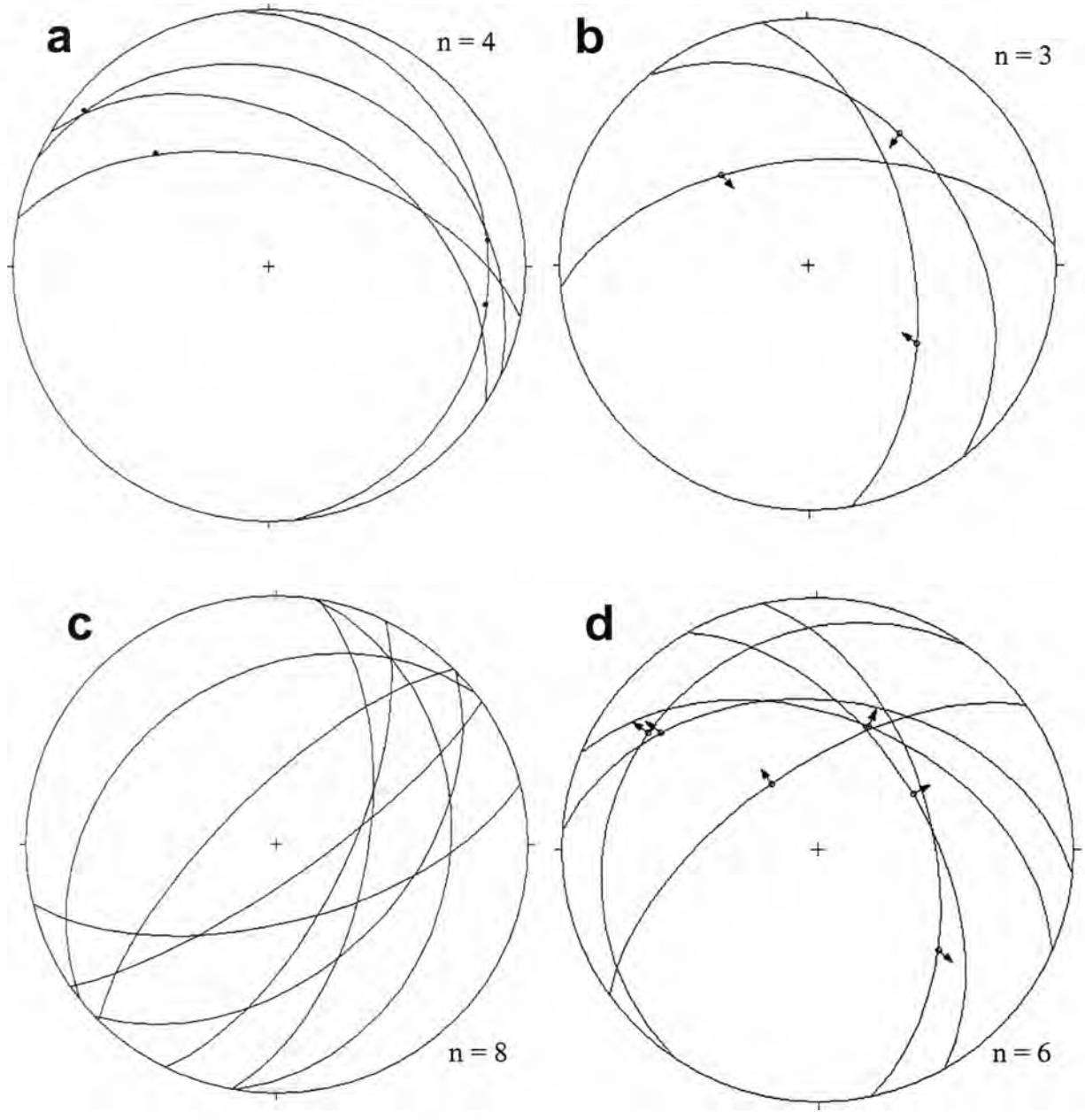

Figure B5: Equal area plots of brittle structures in the Lummi Formation on western Lummi Island. (a) Layer parallel slip surfaces. (b) Thrust faults. (c) Extension vein sets. (d) Normal faults. Arrows show direction of hanging wall movement.

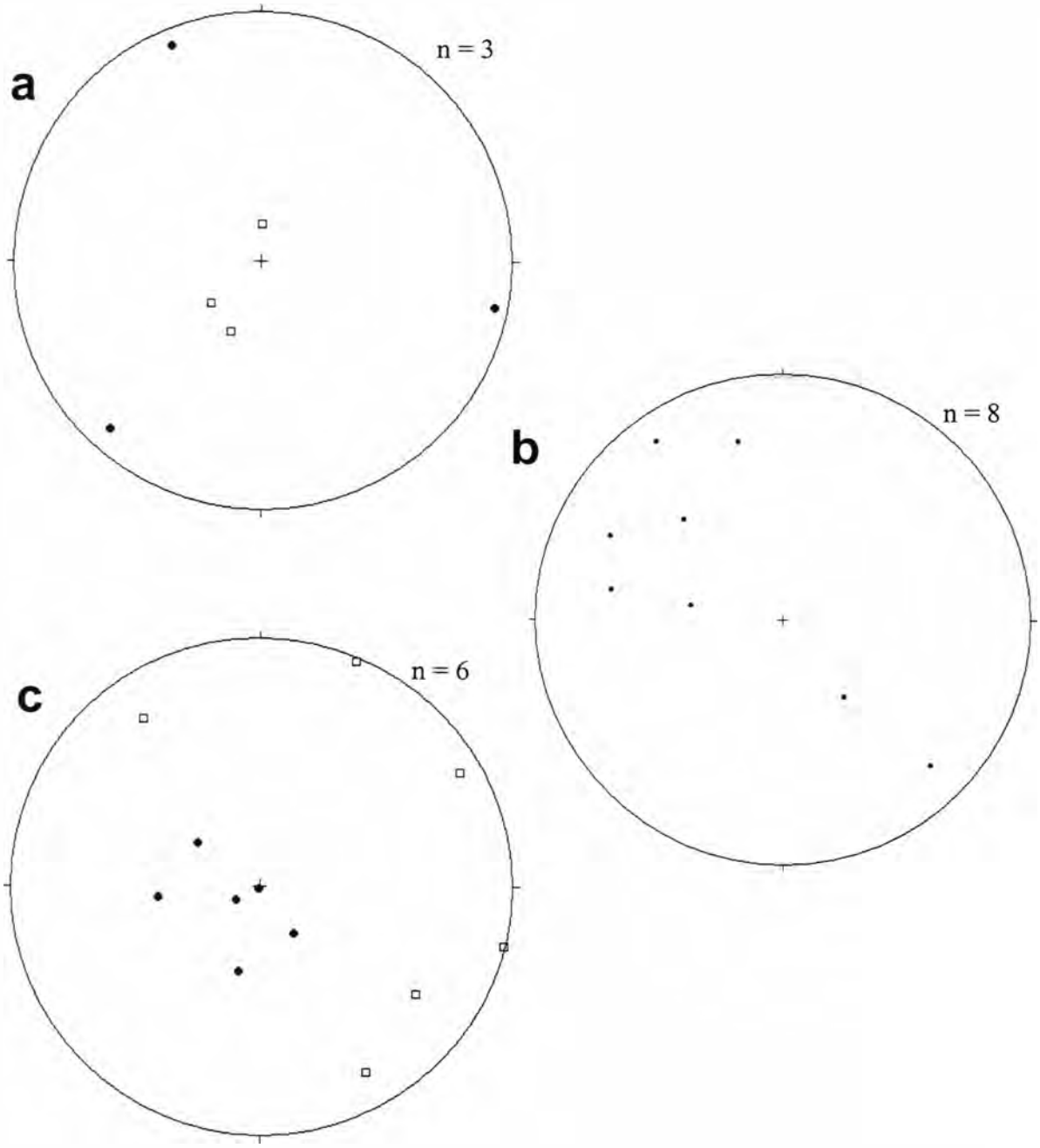

Figure B6: Equal area plots of kinematic axes from brittle structures in the Lummi Formation on western Lummi Island. (a) Thrust faults. (b) Poles to extension vein sets. (c) Normal faults. For (a) and (c), P-axes = closed circles and T-axes = open squares.

northwest/southeast extension direction. T axes of normal faults are spread horizontally but most are consistent with northwest/southeast extension.

The Obstruction Formation (Ocean Floor Complex) – Southeastern Lopez Island

Metasedimentary rocks of the Obstruction Formation exposed just north of the Lopez Thrust at Watmough Head on southeastern Lopez Island are part of the Ocean Floor Complex (Burmester et al., 2000; Blake et al., in preparation). However, brittle deformation in the turbidite sequences at this location is indistinguishable from that seen in the LSC. Data on brittle structures are shown in Figure B7. Layer-parallel strike-slip surfaces such as those seen locally in the LSC are prevalent along shale layers in well-bedded turbidite sequences at Watmough Head. Slip is subhorizontal to the west-northwest/east-southeast, and right and left-lateral faults are subequal in abundance. Thrust faults deform foliation, but most are south or southwest-vergent and oriented subparallel to local layering. Normal faults and extension veins occur in several orientations but many strike northeast and southwest as in the LSC. Results of kinematic analysis by structure type are shown in Figure B8. Layer-parallel slip data is excluded from analysis because the conflicting shear sense on similarly oriented planes yields inconsistent kinematic data. T axes of thrusts are subvertical and P axes are consistent with approximately north/south contraction. Poles to extension vein sets and T axes of normal faults indicate shallow to moderately plunging extension, but directions are inconsistent so extension is spread about horizontal.

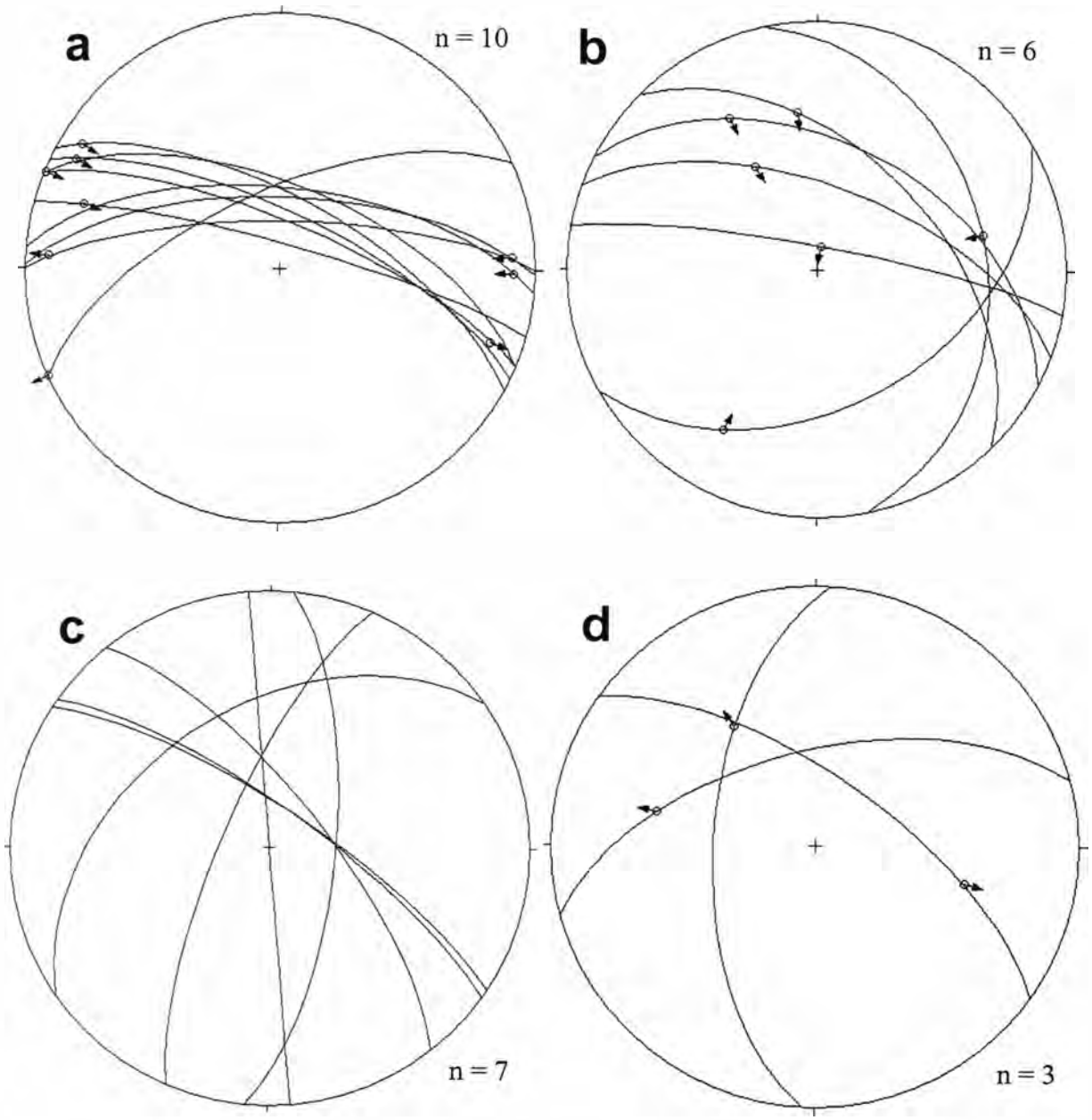

Figure B7: Equal area plots of brittle structures in turbidites of the Obstruction Formation at Watmough Head on southeastern Lopez Island. (a) Bedding parallel slip planes. (b) Thrust faults. (c) Extension vein sets. (d) Normal faults. Arrows on striae show sense of hanging wall movement.

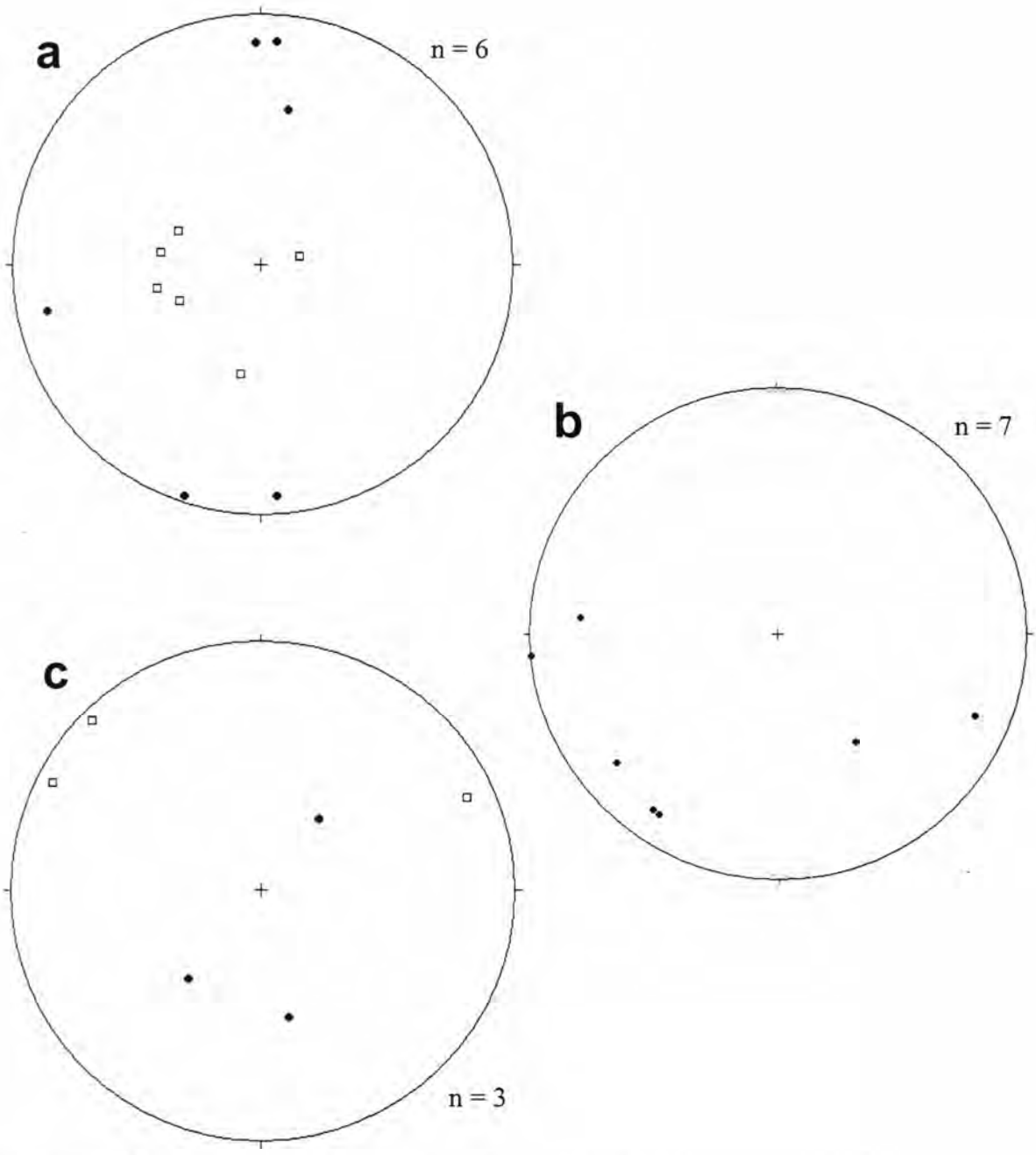

Figure B8: Equal area plots of kinematic axes from brittle structures in the Obstruction Formation at Watmough Head on southeastern Lopez Island. (a) Thrust faults. (b) Poles to extension vein sets. (c) Normal faults. For (a) and (c), P-axes = closed circles and T-axes = open squares.

Appendix C: Methods of X-ray Diffraction

Field and Laboratory Methods

Carbonate-bearing veins within each type of structure were collected in the field for use in x-ray diffraction. Care was taken to assure that veins sampled from faults were kinematically associated with that faulting episode, and not an artifact of previous veining or faulting incorporated into the fault plane. Thus, sampling was restricted to veins that were continuous, undeformed, relatively planar features found on the fault plane and veins that contained slickenfibers associated with vein growth during faulting. Veins from faults with evidence of reactivation were excluded from testing to reduce the possibility of vein preservation from a previous faulting event.

Laboratory work was conducted at WWU. Vein samples were first separated from any remaining wall rock and crushed by hand, then pulverized for approximately 2 - 5 minutes to a fine powder in the Spex Mixer Mill with steel grinding container and ¼" steel grinding balls. X-ray diffraction on the powdered sample was performed using a General Electric XRD-5 Diffractometer with motorized rotating goniometer and nickel-filtered X-ray tube operated at 35 KeV/15 mA. Diffraction patterns were recorded at a rate of 2°/minute for 2θ values of 18° - 52°, which covers the peak signatures of common vein forming minerals.

Analysis of Diffraction Patterns

X-ray diffraction patterns were interpreted manually using the Mineral Powder Diffraction File (JCPDS, 1980) as a reference for 2θ values. The 2θ angle and relative magnitude of each peak in a pattern was first identified. Angles were then compared to

the documented major peaks of several vein forming minerals: quartz, calcite, aragonite, plagioclase feldspar, prehnite, and chlorite. Significant 2θ values used in this study to identify each of these minerals are listed in Table C1.

Appendix D: Methods of Fluid Inclusion Research

Field and Laboratory Methods

During field work, quartz-rich veins from each stage of structures were collected in order to conduct a fluid inclusion study. An initial search in thin sections for undeformed and definitively primary inclusions was unsuccessful. Most samples are too filled with small inclusions to identify distinct populations. Four of the clearest samples that contain larger inclusions were selected and doubly polished fluid inclusion sections were ordered from Vancouver Petrographics. From two of the samples, two suitable and consistent groups of inclusions were identified during preliminary petrographic investigation. Prior to analysis, the polished sample plates were soaked overnight in acetone to remove them from the glass slides.

The remainder of laboratory work was completed with the help of Assistant Professor Dan Marshall at Simon Fraser University in Vancouver, BC. Analysis was conducted on an Olympus BX51 long objective petrographic microscope with an attached Linkam heating/cooling stage and digital temperature gauge accurate to 0.1° C. Liquid nitrogen pumped through the stage was used to cool the sample. To reduce the risk of inclusion destruction, freezing runs were conducted first (Roedder, 1984). Water-rich inclusions were cooled quickly to ~ -40° C and then reheated at a slow rate of 1°/minute to observe the melting temperature of ice. Because this phase transition was

Quartz	**20.9**	**26.6**	36.5	39.5	50.2
Calcite	23.1	**29.4**	36.0	47.5	48.4
Aragonite	26.2	**27.3**	33.2	37.9	45.8
Plagioclase	22.1	23.8	**27.8**	30.6	33.8
Prehnite	**25.6**	27.2	**29.0**	31.8	35.2
Chlorite	**18.8**	25.2	31.5	40.0	

Table C1: 2θ values used in identification of minerals during manual interpretation of x-ray diffraction patterns. Key values are shown in bold. Values provided by the Mineral Powder Diffraction File (JCPDS, 1980).

usually difficult to observe, freezing runs were duplicated to ensure accuracy. Methane-rich inclusions were cooled to ~ -100° C and slowly reheated to record methane homogenization temperatures. Heating runs were conducted on both inclusion assemblages to record total homogenization temperatures at a rate of 2-3°/minute. Homogenization values were taken when the vapor bubble completely dissipated and the inclusion became entirely one phase.

References

Allmendinger, R. W., 2003. StereoWin v 1.2.0, FaultKinWin v 1.2.2: Downloaded from Rick Allmendinger's home page, November 2003: http://www.geo.cornell.edu/geology/faculty/RWA/RWA.html.

Armstrong, R. L., 1988. Mesozoic and early Cenozoic magmatic evolution of the Canadian Cordillera: Geological Society of America Special Paper, vol.218, pp.55-91.

Bergh, S. G., 2002. Linked thrust and strike-slip faulting during Late Cretaceous terrane accretion in the San Juan thrust system, Northwest Cascades orogen, Washington: Geological Society of America Bulletin, v. 114, p. 934-949.

Brandon, M. T., 1980. Structural geology of middle Cretaceous thrust faulting on southern San Juan Island, Washington: M.S. Thesis, University of Washington, 130 p.

Brandon, M. T., Cowan, D. S. and Vance, J. A., 1988. The Late Cretaceous San Juan thrust system, San Juan Islands, Washington: Geological Society of America Special Paper, 221, 81 p.

Brandon, M. T., Roden-Tice, M. K., Garver, J. I., 1998. Late Cenozoic exhumation of the Cascadia accretionary wedge in the Olympic Mountains, Northwest Washington State: Geological Society of America Bulletin, vol.110, p.985-1009.

Brown, E. H., 1977. Ophiolite on Fidalgo Island, Washington: in Coleman, R. G., and Irwin, W. P., eds., North American ophiolites: Oregon Department of Geology and Mineral Industries Bulletin, v. 95, p. 67-73.

Brown, E. H., 1987. Structural geology and accretionary history of the Northwest Cascades system, Washington and British Columbia: Geological Society of America Bulletin, v. 99, p. 201-214.

E.H. Brown. Large-scale orogen-parallel thrusting along the Cretaceous continental margin in northwest Washington: submitted to Tectonics.

Brown, E. H. and Lapen, T. J., 2003. Revised metamorphic history of the San Juan Islands: Geological Society of America Abstracts with Programs, v. 35, p. 113.

Brown, E. H., Lapen, T. J., Leckie, R. M., Silva, I. P., Verga, D., and Singer, B. S., in press. Revised ages of blueschist metamorphism and the youngest pre-thrusting rocks in the San Juan Islands, Washington: Canadian Journal of Earth Sciences.

Brown, P., 1989. FlinCor: A microcomputer program for the reduction and investigation of fluid-inclusion data: American Mineralogist, v. 74, p. 1390-1989.

Burmester, R.F., Blake, M.C. Jr. and Engebretson, D.C., 2000. Remagnetization during Cretaceous Normal Superchron in Eastern San Juan Islands, WA: implications for tectonic history: Tectonophysics, v. 326, p. 73-92.

Butler, R. F., Gehrels, G. E., and Kodama, K. P., 2001. A moderate translation alternative to the Baja British Columbia hypothesis: GSA Today, v. 11, p. 4-9.

Carlson, W. D. and Rosenfeld, J. L., 1981. Optical determination of topotactic aragonite-calcite growth kinetics: Metamorphic implications: Journal of Geology, v. 89, p. 615-638.

Cowan, D. S. and Brandon, M.T., 1994. A symmetry-based method for kinematic analysis of large-slip brittle fault zones: American Journal of Science, v. 294, p. 257-306.

Dahlen, F. A., 1984. Noncohesive critical Coulomb wedges: An exact solution: Journal of Geophysical Research, v. 89, p. 10125-10133.

Davis, D., Suppe, J., and Dahlen, F. A., 1983. Mechanics of fold-and-thrust belts and accretionary wedges: Journal of Geophysical Research, v. 88, p. 1153-1172.

Dewey, J. F., 1988. Extensional collapse of orogens: Tectonics, v. 7, p. 1123-1139.

Engebretsen, D. C., Gordon, R. G., and Cox, A., 1985. Relative motions between oceanic and continental plates in the Pacific basin: Geological Society of America Special Paper, 206, 59 p.

Fassoulas, C., Kilias, A., and Mountrakis, D., 1994. Postnappe stacking extension and exhumation of high-pressure/low-temperature rocks in the island of Crete, Greece: Tectonics, v. 13, p. 127-138.

Feehan, J. G. and Brandon, M. T., 1999. Contribution of ductile flow to exhumation of low-temperature, high-pressure metamorphic rocks: San Juan-Cascade nappes, NW Washington State: Journal of Geophysical Research, v. 104, p. 10883-10902.

Glassley, W. E., Whetten, J. T., Cowan, D. S., and Vance, J. A., 1976. Significance of coexisting lawsonite, prehnite, and aragonite in the San Juan Islands, Washington: Geology, v. 4, p. 301-302.

Goldstein, R. H., and Reynolds, T. J., 1994. Systematics of fluid inclusions in diagenetic minerals: Short course 31: Society of Economic Paleontologists and Mineralogists, Denver, Colorado, 184 p.

Haar, L., Gallagher, J. S., and Kell, G. S., 1984. NBS/NRC steam tables: Thermodynamic and transport properties and computer programs for vapor and liquid states of water in SI units: Hemisphere Publishing Corp., Washington, 320 pp.

Harms, T. A., Jayko, A. S., and Blake, M. C., 1992. Kinematic evidence for extensional unroofing of the Franciscan Complex along the Coast Range Fault, northern Diablo Range, California: Tectonics, v. 11, p. 228-241.

Haugerud, R. A., 1989. Geology of the metamorphic core of the North Cascades: in Joseph, N. L. and others, eds., Geologic guidebook for Washington and adjacent areas: Washington Division of Geology and Earth Resources information circular 86, p. 119-136.

Housen, B. A., and Beck, M. E. J., 1999. Testing terrane transport: An inclusive approach to the Baja B.C. controversy: Geology, v. 27, p. 1143-1146.

Irving, E., Wynne, P. J., Thorkelson, D. J., and Schiarizza, P., 1996. Large (1000 to 4000 km) northward movements of tectonic domains in the northern Cordillera, 83 to 45 Ma: Journal of Geophysical Research, v. 101, p. 17901-17916.

Johnson, S. Y., Zimmerman, R. A., and Naeser, C. W., 1986. Fission-track dating of the tectonic development of the San Juan Islands, Washington: Canadian Journal of Earth Sciences, v. 23, p. 1318-1330.

Jones, D. L., Silberling, N. J., and Hillhouse, J., 1977. Wrangellia; A displaced terrane in northwestern North America: Canadian Journal of Earth Sciences, v. 14, p. 2565-2577.

Joint Committee on Powder Diffraction Standards, 1980. Mineral powder diffraction file – data book: JCPDS International Centre for Diffraction Data, Swarthmore, Pennsylvania, 1168 pp.

Kerkhof, F. van den and Thiery, R., 1994. Phase transitions and density calculation in the CO_2-CH_4-N_2 system: in Benedetto, D. V. and Frezzotti, M. L. eds, Fluid inclusions in minerals: Methods and applications: Blacksburg, Virginia Tech, 377 pp.

Kerrich, R., 1976. Some effects of tectonic recrystallization on fluid inclusions in vein quartz: Contributions to Mineralogy and Petrology, v. 59, p. 195-202.

Kusky, T. M., Bradley, D. C., Haeussler, P. J., 1997. Progressive deformation of the Chugach accretionary complex, Alaska, during a Paleogene ridge-trench encounter: Journal of Structural Geology, v. 19, p. 139-157.

Lamb, Rynn, 2000. Structural and tectonic history of the eastern San Juan Islands, Washington: MS Thesis, Western Washington University, 236 p.

Lamb, R. and Schermer, E., 2003. Metamorphism and deformation in the eastern San Juan Islands: Geological Society of America Abstracts with Programs, v. 35, p. 114.

Maekawa, H. and Brown, E.H., 1991. Kinematic analysis of the San Juan thrust system, Washington: Geological Society of America Bulletin, v. 103, p. 1007-1016.

Mahoney, J. B., Mustard, P. S., Haggart, J. W., Friedman, R. M., Fanning, C. M., and McNicoll, V. J., 1999. Archaean zircons in Cretaceous strata of the western Canadian Cordillera: the Baja B. C. hypothesis fails a "crucial test": Geology, v. 27, p. 195-198.

Marrett, R. and Allmendinger, R. W., 1990. Kinematic analysis of fault-slip data: Journal of Structural Geology, v. 12, p. 973-986.

Misch, P., 1988. Tectonic and metamorphic evolution of the North Cascades; an overview: in Ernst, W. G. ed., Metamorphism and crustal evolution of the Western United States: Rubey Volume, v. 7, p. 179-195.

Monger, J. W. H., and Price, R. A., 1996. Paleomagnetism of the Upper Cretaceous strata of Mount Tatlow: evidence for 3000 km of northward displacement of the eastern Coast Belt, British Columbia, by P. J. Wynne et al., and Paleomagnetism of the Spences Bridge Group and northward displacement of the Intermontaine Belt, British Columbia: A second look by E. Irving et al.: Discussion and reply: Journal of Geophysical Research, v. 101, p. 13,773-13,800.

Petit, J. P., 1987. Criteria for the sense of movement on fault surfaces in brittle rocks: Journal of Structural Geology, v. 9, p. 597-608.

Platt, J. P., 1986. Dynamics of orogenic wedges and the uplift of high-pressure metamorphic rocks: Geological Society of America Bulletin, v. 97, p. 1037-1053.

Platt, J. P., 1987. The uplift of high-pressure - low-temperature metamorphic rocks: Philosophical Transactions of the Royal Society of London, v. 321, p. 87-103.

Platt, J. P., 1993. Exhumation of high-pressure rocks; a review of concepts and processes: Terra Nova, v. 5, p. 119-133.

van der Pluijm, B. A. and Marshak, S., 1997. Earth structure: An introduction to structural geology and tectonics: WCB/McGraw-Hill, US, 495 pp.

Price, N. J. and Cosgrove, J. W., 1990. Analysis of geologic structures: Cambridge University Press, Cambridge, Great Britain, 502 pp.

Ramsay, J. G. and Huber, M. I., 1983. The techniques of modern structural geology; Volume 1: Strain Analysis: Academic Press, London, 307 pp.

Ring, U. and Brandon, M. T., 1999. Ductile deformation and mass loss in the Franciscan Subduction Complex: implications for exhumation processes in accretionary wedges: in Ring, U., Brandon, M. T., Lister, G. S., and Willett, S. D., eds, Exhumation processes: Normal faulting, ductile flow and erosion: Geological Society of London Special Publications, v. 154, p. 55-86.

Roedder, E., 1984. Fluid inclusions: Mineralogical Society of America Reviews in Mineralogy, v. 12, 644 pp.

Silver, E. A., Ellis, M. J., Breen, N. A., and Shipley, T. H., 1985. Comments on the growth of accretionary wedges: Geology, v. 13, p. 6-9.

Spear, F., 1993. Metamorphic Phase Equilibria and Pressure-Temperature-Time Paths: Mineralogical Society of America – Monograph, Washington, D. C., 799 pp.

Vance, J. A., 1975. Bedrock geology of San Juan County: in Russell, R. H., ed., Geology and water resources of the San Juan Islands: Washington Department of Ecology Water Supply Bulletin 46, p. 3-19.

Vance, J. A., 1977. The stratigraphy and structure of Orcas Island, San Juan Islands: in Brown, E. H., and Ellis, R. C., eds., Geological excursions in the Pacific Northwest: Bellingham, Western Washington University, p. 170-203.

Ward, P. D., 1978. Revisions to the stratigraphy and biochronology of the Upper Cretaceous Nanaimo Group, British Columbia and Washington State: Canadian Journal of Earth Sciences, v. 15, p. 405-423.